Micro-mechanical predictive modelling as an aid to CAD based analysis of composite sporting equipment

A thesis submitted in partial
fulfilment of the requirements for
the degree of

Master of Science and Technology

in

Materials Engineering

at

The University of Waikato

by

Paul Ewart

Hamilton, New Zealand 2008

Abstract

The sport and leisure industry in New Zealand (NZ) has the potential to become a major user of composite materials. Given the size of NZ industry, design and manufacturing strategies based on virtual engineering should be developed to suit NZ requirements. Virtual methods use computer aided engineering capabilities to find faults, explore alternatives and optimise product performance before detailed design or prototyping.

When doing computer aided simulation the required mechanical properties of individual reinforcement and matrix components are well documented. However, the mechanical properties of composite materials are not as simple to obtain. Micro-mechanical modelling could therefore be used to aid the design and development of composite equipment, where mechanical properties are unknown.

In this study, solids modelling was used to produce an analog model of a composite, and it was found that it lead to reductions in file size and simulation time. Representing a composite with an analog model implies that the behavioural characteristics are modelled, but not the physical characteristics of the individual components.

Three micro-mechanical models were developed to predict the flexural modulus of composite materials, based on perfect, partial and no adhesion. It was found that the partial adhesion model was both practical and consistently accurate. The partial adhesion model accounted for adhesion between components by considering an ‘effective shear value’ at the interface. Validation of the models was done by flexural testing injection moulded samples of glass, wood and carbon fibre reinforced polyethylene. It was shown that the adhesion coefficient range was 0.1 for carbon fibre, 0.5 for glass fibre and 0.9 for the wood fibre composites. It was concluded that the adhesion coefficient is crucial and it is recommended that further work is done to validate effective shear values by empirical means.

The predicted flexural modulus values were used to enable finite element simulation of modelled analog beams as well as commercial kayak paddles. It was determined that accurate simulation is possible for composite equipment using the partial adhesion model.

Keywords

CAD, flexural modulus, FEA, material design, mechanical properties, micro-mechanical modelling, NZ industry, polymer composite, simulation, sports equipment, solids modelling.

Acknowledgements

In combining my ambitions as an engineer and my prowess as an athlete I joined the emerging field of ‘Sports Engineering’. In conjunction with Dr Johan Verbeek a project was developed that became not just an interest but a passion culminating in several published technical papers and this Masters thesis.

I wish to acknowledge the following:

The unconditional support of my wife, Michelle, and my daughters, Abbie and Petra, without their understanding, patience and love I would not have been able to complete this work.

Those within the School of Science and especially the Department of Engineering who have supported me as a student and colleague while I balanced my teaching and research duties with my study.

Thanks also to the small group of industry partners who were kind enough to provide the project materials at little or no cost.

Last and by no means least, thanks to Gods’ grace.

Contents

List of Figures

List of Tables

List of symbols

Symbols that have not been annotated in the text will be referenced here.

General symbols

A	Cross sectional area [mm^2]
a	Layer thickness [mm]
B, b	Width of section [mm]
CA	Coefficient of adhesion [-]
d	Fibre diameter, depth of section [mm]
E	Elastic modulus [MPa]
F	Force [N], (may be tensile, compressive or shear.)
FS	frictionless stack
G	Shear modulus [MPa]
h	distance to section neutral axis [mm]
H	height [mm]
I	second moment of area [mm^4]
k	Number of plies
L, l	Support distance, length [mm]
M	Bending moment [MPa], mass 1 [g]
m	Mass 2 [g]
NA	No adhesion
n	Number of layers
OD	Outer diameter [mm]
PA	Partial adhesion
PB	Perfect bonding
R	Modulae ratio [-]
R_c	Radius of curvature [mm]
S	Load support
r	Fibre radius [µm]
s	Transverse strain [mm]
t	Thickness [mm]
V	Volume [mm^3]
V_f	Volume fraction [-]
ν	Poisson ratio [-]
x	Cartesian coordinate, longitudinal strain, deformation [mm]
y	Cartesian coordinate, distance from neutral axis to outer layer [mm]
z	Cartesian coordinate [mm]

Greek characters

Δ	Deflection, displacement [mm]
ε	Direct strain [mm]
ϕ	Shear strain [mm]
θ	Angle of arc [^{o}]
ρ	Density [g/mm^3]
σ	Direct stress [MPa]
τ	Shear stress [MPa]
Ψ	Load [N]
∞	Infinity

Subscripts

m	Matrix [mm]
f	Reinforcement, fibre
C	Composite
c	Compressive
i	Interfacial, reinforcement layer term
j	Matrix layer term
max	Maximum
rein	Reinforcement
tr	Tennis racket

1 Introduction

Polymer matrix composites (PMCs) have historically enabled design and production of lighter more ridged components. They are naturally corrosion resistant and easily manufactured compared to metals. Sporting equipment benefits from the reduced density and greater stiffness as a means to reduce section sizes and overall weight as part of the design process [1, 2].

When designing equipment, mechanical properties of the materials to be used are required. For example sporting equipment is often subjected to flexural loading, which makes flexural properties very important. This is shown in studies of equipment performance for bicycles, fishing rods and golf clubs [1, 3-5]. The properties of individual reinforcement and matrix components are well documented, either in general literature or from manufacturers' data. However, due to infinite variations of matrix and reinforcement fractions possible for composite materials their properties are not well documented. A simple mixture rule, based on a weighted average between components, can be used to determine material properties, although these values can be highly inaccurate [6].

Considering the relative newness of PMCs, as structural components, use of testing methods which represent end use should reduce errors. Errors can be associated with assumptions of linear elasticity, isotropy and homogeneity for reinforced polymers that may be highly anisotropic [7]. These errors, and the time and cost required for prototyping and testing, could be further reduced with the use of virtual engineering where analysis and simulation of equipment under in-use conditions becomes part of the design phase. Virtual engineering uses computer aided design (CAD), finite element analysis (FEA) and simulation in conjunction with rapid prototyping and computer aided manufacturing to improve the design and manufacture of products. However, in New Zealand, many equipment manufactures do not have the expertise or resources to utilise specialised simulation software.

The aim of this project is to present a design system that can improve the capabilities of NZ industry given the current level of technology and expertise [8]. This involves the development of a methodology to represent composite materials using simplified geometries, by solids' modelling, in combination with accurate,

yet simple, micro-mechanical models to predict composite properties. The objective is to present an accurate simulation, for composite materials and products, using analysis functionality built into standard CAD packages.

The models are verified by comparing flexural modulus values obtained from three point bend testing with predicted values. Test samples included thermoplastic and thermoset resins reinforced with natural and synthetic fibres, as well as commercially manufactured kayak paddles.

2 Background

The sports and leisure industry in New Zealand (NZ) has the potential to become a major user of composite materials. In this chapter the industry is discussed with regard to the equipment designer, the manufacturer and the end user.

2.1 Sport and leisure in New Zealand

The sport and leisure industry in New Zealand has grown considerably over the last twenty years, partly due to economic reforms of the 1980s [9]. This has been aided by the dramatic rise in adventure tourism and recognition of high profile sportspeople such as our rowing elite, the All Blacks and adventurers such as Steve Gurney and Graham Dingle [9]. The general public have also become more aware of health benefits gained from participation in sport and leisure activities by initiatives such as Push Play, Activator and Green Prescription championed by SPARC, the governing agency for sport and recreation in NZ. Table 1 shows data, ranked by participation, of the top ten physical activities and the top ten sports for adults (18+yrs) [10]. Of these at least half are reliant on manufactured equipment.

Table 1. New Zealand participation rankings for given activities.

1	Walking	Golf
2	Gardening	Tennis
3	Swimming	Touch football
4	Exercising at home	Cricket
5	Fishing	Skiing
6	Exercise class/gym	Basketball
7	Running/jogging	Motor sports
8	Tramping	Netball
9	Cycling	Yachting
10	Mountain biking	Rugby union

2.1.1 *Manufacturing for sport*

The NZ sports industry is supported by 301 sport related businesses [11], 81 sporting import and export businesses [12], and 704 sporting goods manufacturers and/or suppliers of sporting equipment [13]. These are a result of the NZ population base and ensure a thriving import market for fully developed

equipment. Annual retail sales figures for the NZ Sport and leisure industry were over NZ$2.0 Billion in 2005 [8], and is indicative of the revenue available for research and new product development [14].

Sporting equipment has developed through the use of easy to procure and machine materials, such as wood, for skis, golf clubs, cricket bats, kayaks and paddles, vaulting poles, hockey sticks and even bicycles. Skis evolved from wood, to metal, with plastics and composites, particularly fibre reinforced, used after the 1970s. Late adoption of plastics was attributed to the negative image, consumers had, that saw plastic as a cheap and practical material, not a ‘high tech’ solution [15].

High performance equipment developed for elite athletes does not need the production efficiencies of a mass market to enable production. For this reason most advanced technology is often slow to reach the mass market. Regardless of growth in the NZ manufacturing industry high performance equipment is still imported for many elite and emerging athletes. Figure 1 shows NZ made and imported equipment available to international markets.

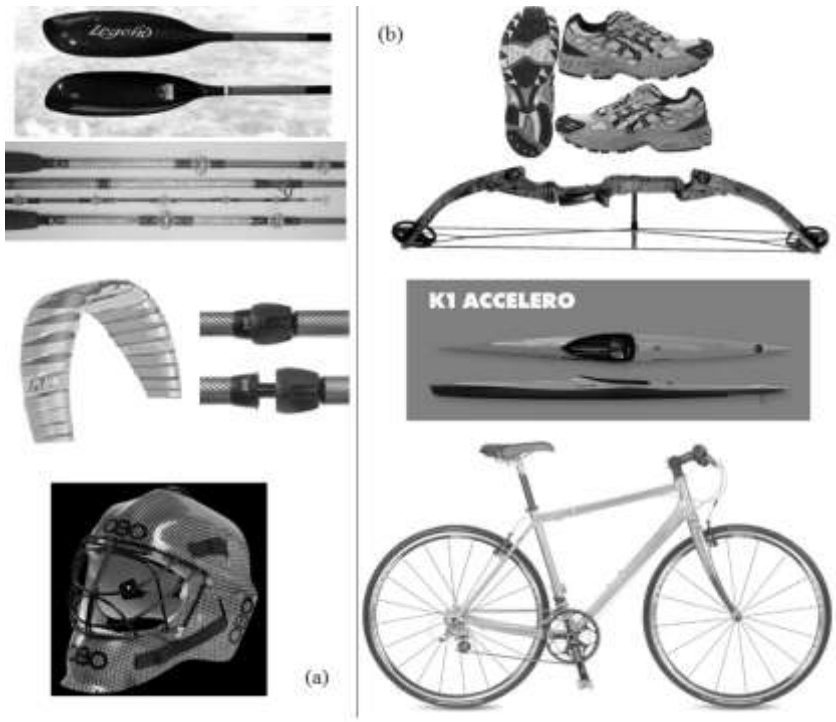

Figure 1. Sporting equipment, a) NZ manufactured, b) imported.

2.1.2 *Materials development*

Major advances in materials are evident in all sports. Many of the changes brought about by developments in polymer and fibre technologies are adapted for sporting equipment [1, 16]. McConnell stated that sporting goods represented 38% of all advanced polymer composites in use in 1999 [17]. The majority of sporting goods utilise fibre reinforced PMCs. These include continuous and short fibre reinforcement, hybridised reinforcement of various fibre types or, a layered structure of various fibre types. However, there is strong competition from metal matrix composite (MMC) materials to overcome mechanical limitations of polymers found at elevated temperature.

With PMCs having a large market share further development and innovation within the sporting goods industry is inevitable, as such; documented and published works should be a natural part of this process. This will also reduce an apparent dependence on materials data that may not be fully understood and may inadvertently lead manufacturers towards materials choices based on purely economic decisions, with few performance advantages. The majority of literature regarding sporting equipment is the result of academic work undertaken in a similar context to this report, or from research into high profile sports, such as Americas Cup yachting, or, supported by sporting brands, such as Adidas. It is likely that a large number of sports are not involved in research, or, commercial sensitivity will not allow publication of such work. And, as many NZ manufacturers do not have sufficient resources for, or direct access to research and development capabilities, development of design and manufacturing strategies to suit the NZ industry is essential for growth.

2.2 Equipment design

Traditional design methods ensure products are prototyped and built within constraints set for the required purpose [18]. Prototypes using these methods require design commitment and complete engineering prior to construction. Many companies improve conventional design protocols by investing in computer aided engineering (CAE) tools to replace 2D drafting and hardcopy data systems [19]. While CAE tools increase engineering productivity they do not offset the time and expense of reworking and multiple prototyping often required in the design-analyse-build-test approach [20].

Virtual engineering is a new approach currently being targeted by researchers and manufacturers and is depicted in Table 2. Virtual engineering encompasses simulation undertaken during the conceptual phase, to find faults, explore alternatives and optimise product performance before detailed design or prototyping [20, 21]. Functionality, geometry, and materials are then considered based on simulation results at the conceptual phase.

Table 2. Conventional and virtual design techniques [20].

Traditional techniques		
Design **Create geometry**	then	***Evaluate*** **Analyse, build and test**
-Layout drawings -CAD wireframe -Solids modelling		-Geometry layouts -Experience, management opinion -Test prototypes
Virtual techniques		
Simulate **Modify and optimise validated computer models**	then	***Design*** **Define/create geometry and materials to achieve targets**
-Parametrics -System engineering -Analysis-led design -Active target setting		-Virtual concept layouts -Multiple iterations to design -Satisfy targets

In Figure 2 it is shown that virtual engineering may reduce time to market by increasing the design in the pre-build phase of a new product. Beaumont and Sekine support the virtual engineering approach but favour physical modelling to predict material behaviour and guide optimization of micro/macro structure of materials [22]. From an academic perspective the use of standard testing needs to be mandatory, and is critical in a research environment where verification is evidence of success or failure [22].

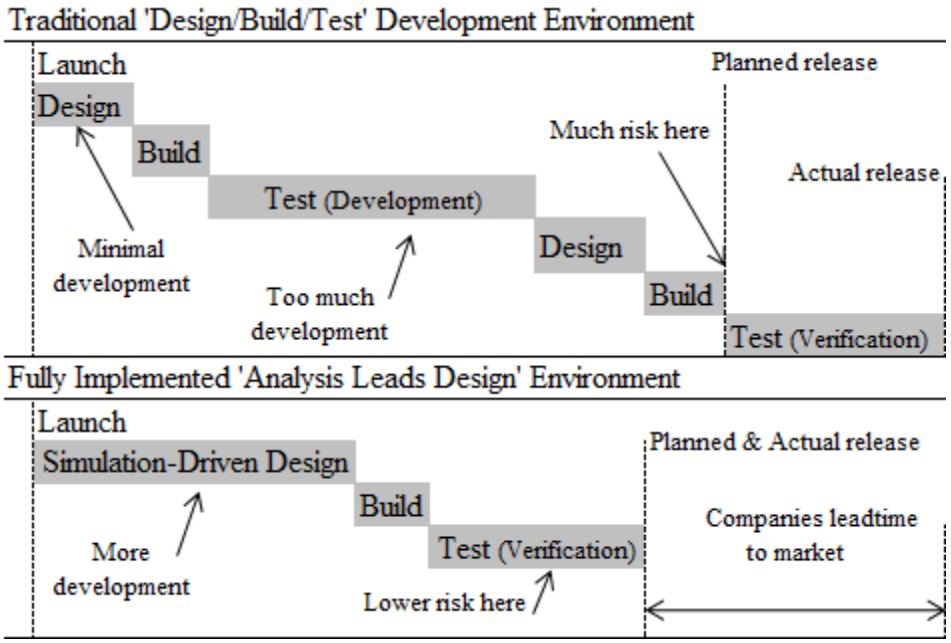

Figure 2**. Time to market reduced with virtual engineering techniques [20].**

From comparison, of various modelling techniques, McDowell found that relatively simple mathematical models that capture specified mechanisms of material behaviour can be preferred to highly complex fundamental models [23]. This is in favour of the use of micromechanical models to assist in determining materials data for use by the design engineer in CAD based design methods.

3 The mechanics of materials

To improve equipment design methodologies it is essential to understand the mechanical behaviour of materials and structures. This chapter will focus on material properties and mechanics of materials. Monolithic materials properties are discussed and include the interactions and complexities of composite materials. Composites are discussed based on reinforcement configuration, their strength and performance criteria, composite testing and how properties affect end use.

3.1 Mechanical properties

Materials are chosen for their mechanical properties and the materials reaction to loading specific to end use. The 2D loads that create reactive stresses are depicted as acting individually in Figure 3. Although they often act simultaneously during equipment usage they are essentially 2D loads.

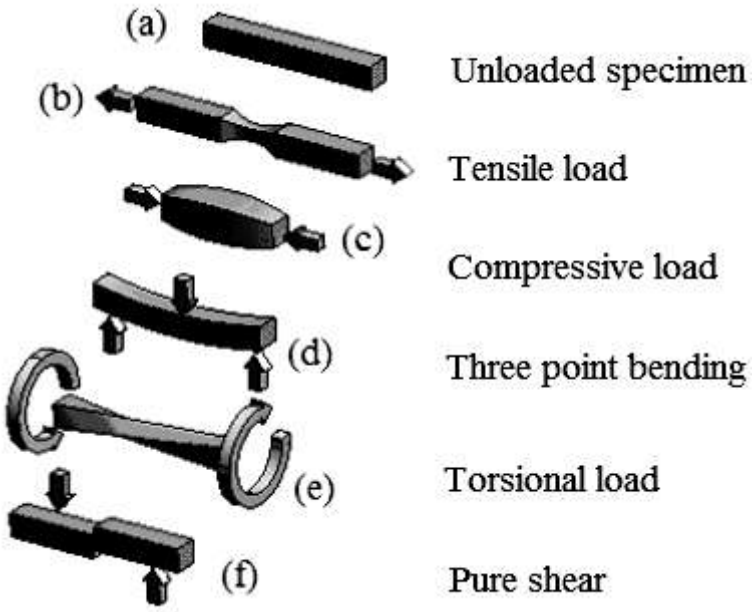

Figure 3. Material loading depicted as individual 2D loads.

Materials can be characterised in terms of their structure, scale and response to loading as [24]:

- elemental level: single molecules and crystal cells, characterised by their atomic makeup

- micro-structural level: matrices, particles and fibres, categorised by the method of interaction [25]

- macro-structural level: components and artefacts

As shown in Figure 4(a), orthotropic materials are characterised by having equal properties in all planar directions. Isotropic materials have orthotropic properties and may have equal properties in any orientation. Figure 4(b) depicts anisotropic materials where the properties in any one specific orientation are considerably different from the other planar directions.

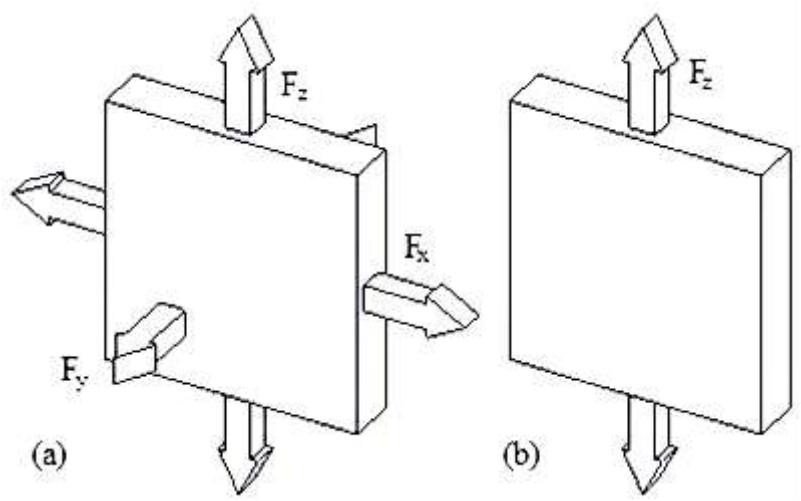

Figure 4. Elastic property definitions a) Orthotropy, b) Anisotropy.

When a material has an axial force applied to it, the force may be resolved into components normal and parallel to any plane within the material. The normal component is a tensile or compressive force, and the intensity of loading per unit area is the direct stress, σ. The parallel component is a shear force where the intensity of loading, per unit area, is the shear stress, τ. The distortion of the material due to the direct and shear forces is measured by the direct strain, ε, and the shear strain, ϕ.

3.1.1 *Direct stress and strain*

When equipment is loaded during use, forces within the materials create opposite and equal resistive forces to maintain static equilibrium.

Figure 5 shows a piece of material subjected to a tensile force *F*. If the cross-sectional area of the material is *A*, then the tensile stress on the cross-section is, $\sigma = \frac{F}{A}$.

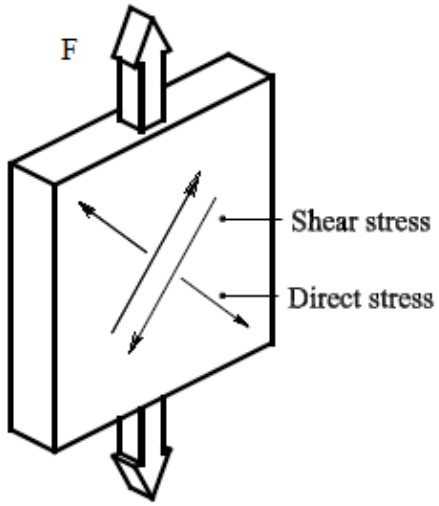

Figure 5. Component loading.

If the original length of the bar is *l* and the extension due to a tensile load is *x*, then the tensile strain is $\varepsilon = \frac{x}{l}$, since this is a ratio of lengths, it is dimensionless.

Extension in the direction of applied forces produce a contraction perpendicular to the applied force called the transverse strain. The ratio of transverse to longitudinal strain is called the Poisson ratio, *v*. The transverse strain is opposite in direction to the longitudinal strain; thus, if the longitudinal strain, x is +ve, the transverse strain, s is –ve (Figure 6).

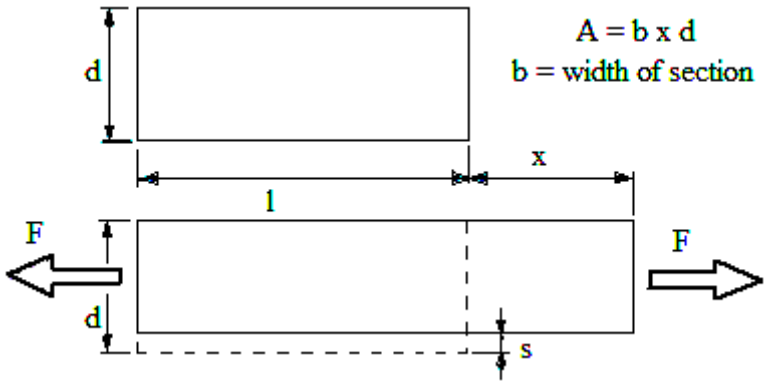

Figure 6. Direct stress and strain.

3.1.2 *Shear stress and strain*

Figure 7(a) shows a piece of material subjected to shearing forces *F*. If the cross-sectional area of the material is *A*, then the shear stress, $\tau = \frac{F}{A}$.

If the deformation in the direction of *F* is *x* and the distance between the opposite faces is *l*, then shear strain is, $\phi = \frac{x}{l}$. ϕ is the angular distortion in radians when $\frac{x}{l}$ is very small.

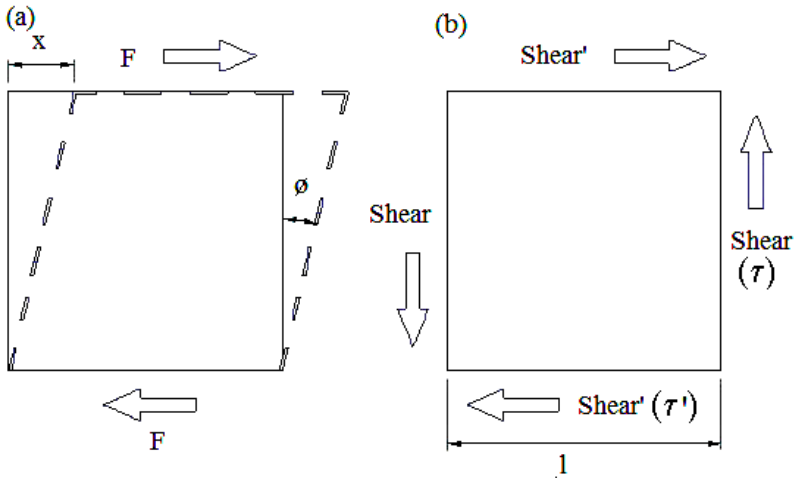

Figure 7. Shearing stresses and strains due to applied shear forces.

3.1.3 *Complementary shear stress*

Due to the shear forces shown in Figure 7(b) a clockwise couple $Fl = \tau Al$ is applied to the material. If the material is to remain in static equilibrium an equal and opposite couple must be applied by shear stresses induced on perpendicular faces. Thus for equilibrium, $\tau' A'l' = \tau Al$, but $A'l' = Al$ and therefore the induced shear stress is equal in magnitude but opposite in orientation to the applied stress giving $\tau' = \tau$ and is called the complementary shear stress.

3.1.4 *Elasticity, plasticity and Hookes' law*

If the applied load, shown in Figure 6, is removed and the bar returns to its former shape, it is said to behave elastically. If it remains deformed, it is said to behave plastically. There is also visco-elastic behaviour where the deformation is not

entirely elastic or plastic. Under ideal conditions visco-elastic materials will gradually return to their former shape when the load is removed. Linear elastic materials obey Hookes' law, where the deformation of a material is directly proportional to the load, i.e. the ratio of stress to strain is constant. For direct stress, the constant of proportionality is called the modulus of elasticity (or Young's modulus), *E*:

$$E = \frac{\sigma}{\varepsilon} = \frac{Fl}{Ax} \qquad (1)$$

3.1.5 *Flexural loading*

Many structural objects are subject to loads that produce bending (Figure 3d). For example, simply supported beams (Figure 8(a)) are held in equilibrium by fixed supports (S). Cantilevered beams (Figure 8(b)) are fixed at one end with the other end held in equilibrium by a bending moment (M) at the fixed end.

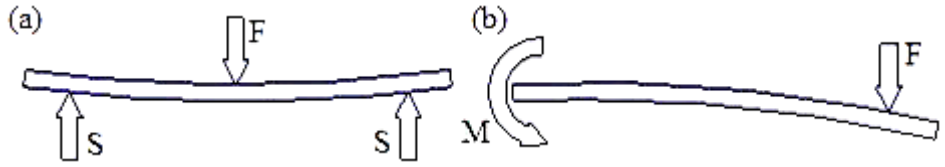

Figure 8. Materials loaded in flexure, a) three point bend, b) cantilever load.

3.1.6 *Beam theory*

Essential to the mechanics of beam theory a beam is considered to be any structure that has a length that is greater than its width and depth.

Bending a beam will produce tensile, compressive and shear stresses. A beam is considered short when the length to depth ratio is less than 16. A short beam will often be subject to direct shear acting perpendicular to the axis of the beam. Pure bending, however, is considered bending without direct shear and is a less complex form of applied mechanical loading [26].

In Figure 9 the bending moment is M. For equilibrium of any section the couple must be balanced by an equal and opposite couple exerted by forces within the beam. The bending moment is balanced by the couple represented by the pair of equal and opposite parallel forces, F. The upper force represents a compressive

force and the lower a tensile force. The parallel forces (Figure 9) balance the bending moments within a beam and produce shear stress within the beam. This shear stress can be shown to have a maximum value at the neutral axis.

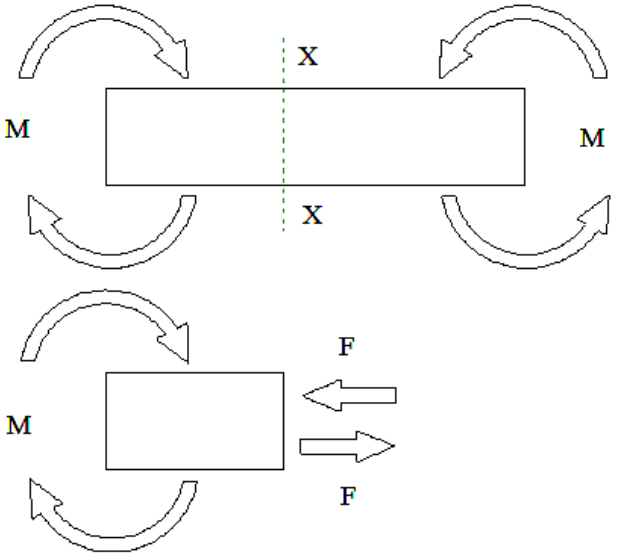

Figure 9. Bending moments creating compressive and tensile stresses.

I. Assumptions with beam theory

Beam theory considers the mechanics of beam like structures from first principals and relies on the following assumptions in relation to any material:

- The microstructure is considered homogeneous and any section of the material to 10^{-3}mm in size is consistent to all elements the same size.
- All components within the material are considered fully bonded. No slippage between components and all joined components behave as the bulk material.
- Materials properties are isotropic and within any given plane or direction of the material will be the same.

When calculating internal stresses and strains further assumptions are:

- The cross section of the beam will remain the same throughout bending without deformation.
- Beam is straight before loading with no predetermined curvature.

- Beam material is linear elastic and obeys Hookes' law as stresses do not exceed the limit of proportionality and remain in the linear elastic region.
- Bending is through the same plane that the applied bending moment or load is applied.
- The cross section of the beam is geometrically symmetrical about a central axis in the same plane as the load.
- Moduli of elasticity in tension and compression are the same
- Stresses are planar and uniformly distributed throughout the cross section.
- The radius of curvature produced from loading is equal across the beam depth.

3.1.7 *Curvature and strain*

Bending moments can be used to calculate internal stresses. These stresses, shown in Figure 9, are both tensile and compressive and it is shown from the analysis of elastic materials that $\sigma_x = E\varepsilon_x = \frac{Ey}{R_c}$ and, $dM_o = \sigma_x y dA$. The sum of all moments is termed the total moment, *M*, where $M = \int \sigma_x y dA$ and substituting for σ_x above, gives, $M = \frac{1}{R_c} E \int y^2 dA$. with $\mathrm{I} = \int y^2 dA$ giving:

$$M = \frac{EI}{R_c} \qquad (2)$$

In response to bending moments, object deformation produces a deflection and subsequent resistive stresses. After bending, the beam section, as shown in Figure 10(a), is transformed to the arc shape of Figure 10(b). The cross-section remains the same, hence straight lines BA and CD remain straight after bending and meet at some point O. Lines such as EF and SN are formed into arcs with a common centre O. Since the top layers are stretched and the bottom layers are compressed there is a layer, the neutral plane, which is neither stretched nor compressed. The lines S'N' and N'N' represent the neutral plane, the line N'N' normal to the plane of bending is known as the neutral axis. The radius of curvature R_c of the arced beam is measured from O to the neutral plane. If θ is the angle in radians of arc

S'N' at O, and the neutral plane remains unchanged in length, so line SN is transformed to arc $S'N' = R_c\theta$.

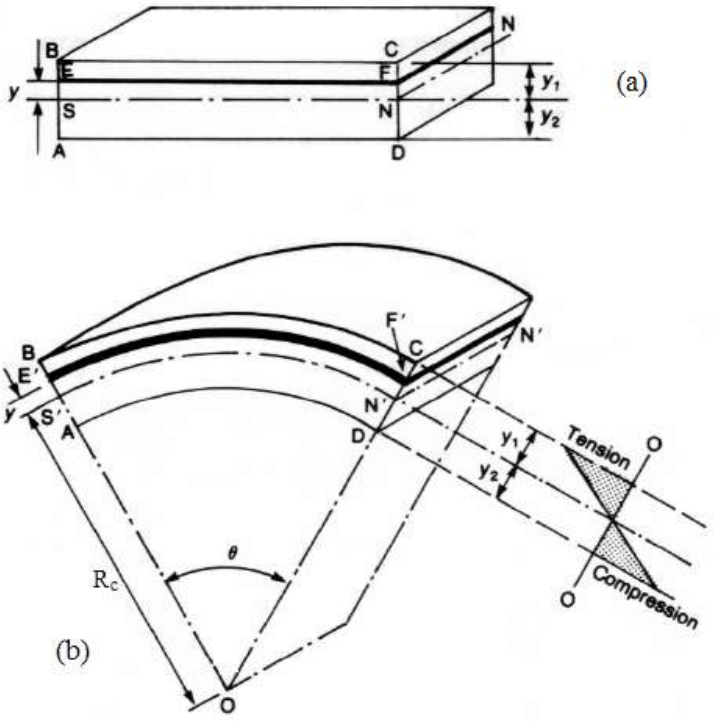

Figure 10. Beam section a) before bending, b) after bending. (After [26]).

To determine changes in length, consider layer EF, distance y from the neutral plane with initial length, $EF = R_c\theta$. After bending EF transforms to, $E'F' = (R_c + y)\theta$. The extension of EF is, $(R_c + y)\theta - R_c\theta = y\theta$, which gives strain in EF $\varepsilon = \dfrac{y\theta}{R_c\theta} = \dfrac{y}{R_c}$.

Stress normal to the beam section in the layer EF, is then given by, $\sigma = E \times \varepsilon = \dfrac{Ey}{R_c}$, or more commonly as $\dfrac{\sigma}{y} = \dfrac{E}{R_c}$.

Since E and R_c are constant for the portion considered, stress varies across the beam depth with the distance from the neutral axis. The distribution of stress across the depth of the beam in Figure 10(b) shows tensile stress being plotted to the left of the base O-O, compressive stress to the right. The maximum stress occurs at the outside surfaces such as AD and BC where y takes its largest values at y_2 and y_1.

3.1.8 *Flexural modulus*

The constant used to evaluate deflection due to bending moments is an elastic constant based on the materials response to an applied load. Youngs' modulus is proportional to direct stress and inversely proportional to the resultant strain of a material when it is subjected to an external tensile load (Figure 6) and may be determined by Equation (1). Elastic modulus gained from flexural loading is from indirect stress or transverse loading with the strain gained from deflection values relative to the neutral axis, as shown in Figure 9, and equated as:

$$E = \frac{\sigma}{\varepsilon} = \frac{F.l^3}{48.I.y} \qquad (3)$$

Although flexural modulus (FM) is an important mechanical property, few studies have been carried out in this area, compared to strength and tensile properties [27]. This is a concern as many structural products would be subjected to more flexural loading than tensile loading during service.

3.2 Composite Materials

Modern-day composites came about in the 1930's and can be attributed to the availability of modern resins and glass fibres. Around this time Douglas Aircraft, (later McDonnell Douglas) in the United States, had demanding designs that pushed the limits of existing materials [28]. The designers were limited by the production of metal moulds used for forming sheets into shaped components. With each new design requiring its own set of moulds the process was expensive and time consuming. Plastic moulds did not withstand the forces produced during the sheet forming process. Glass fibre reinforced phenolic moulds led to glass reinforced moulds becoming the standard for forming prototype parts. Later polyester and epoxy resins became the resin of choice.

Composites were used in structural parts due to metal shortages during World War II. The composites industry strengthened with the development of carbon fibre in the 1960s and aramid fibre in the 1970s. These fibres with superior strength properties improved composite toughness and wear resistance.

In addition to PMCs are metal matrix and ceramic matrix composites. Continuous fibre composites were initially developed exclusively for space and military applications [29, 30]. Short fibre metal and ceramic composites, simpler and cheaper to produce, are often used in automotive and sporting applications [31]. Short fibre reinforced aluminium has found application in drive shafts, diesel engines, and sporting goods such as bicycle components and golf clubs [32].

The mechanical properties of composite materials can be greatly influenced by the orientation of the reinforcement phase. Isotropic properties can be found in particulate composites with uniform distribution and in fibre reinforced composites comprising of short randomly aligned fibres. Anisotropy is often seen in unidirectional continuous and unidirectional discontinuous fibre composites and to the individual layers of multilayered composites.

Elastic modulus, Poisson ratio, tensile and compressive strength, and coefficient of expansion are mechanical properties of composite materials that result from the combined properties of the matrix material, the reinforcement material, and the matrix-reinforcement interactions. Desirable properties for structural materials

depend on the application, for instance, a vaulting pole needs to be as light as possible, must not buckle under maximum load and must only deform elastically. A bicycle needs to have low weight with the frame rigid, and tough enough to withstand the continual loading from the peddling action of the rider [2].

3.2.1 *Particulate Composites*

Particulate composites with random reinforcement phase distributions are a true isotropic composite material. The most widely utilised particulate composite is concrete. It is used for some water born crafts and in the construction of modern sporting facilities.

Aluminium, magnesium and titanium are used for particulate composites. Aluminium is the most prevalent, due to its relative ease of manufacture [1, 2]. Equipment made from these materials include the heads of golf clubs, the 'trucks' associated with high performance skate boards, new extreme sports equipment such as mountain boards and outdoor mountaineering equipment.

PMCs' is an area of composite materials that continues to grow as new developments and new applications are brought to the market [33-36]. Thermoplastic polymers, thermosetting polymers and elastomers are used in sporting equipment. Due to the strength and stiffness of polymers being low compared to metals and ceramics, great benefit is gained from reinforcement. Polymers can be produced using relatively simple processes at reduced processing temperatures and pressures leading to reduced reinforcement degradation compared to metals and ceramics.

The main disadvantages of PMCs are low working temperatures, high thermal expansion coefficients and sensitivity to moisture and radiation. Moisture absorption can also degrade mechanical properties, lower the glass transition temperature and create high internal stresses [30, 36].

Polymers may also be combined with additives to impart specific properties that improve composites. These additives include the following:

- Extenders are added to polymers to increase the bulk volume of expensive polymer resins. They include calcium carbonate, silica, talc and clay. They

may also improve certain mechanical properties such as hardness, wear resistance, thermal conductivity and improve resistance to creep, however, this is often at the expense of strength and ductility [33, 37].

- Stabilisers are added to reduce degradation from ultraviolet radiation and other environmental factors, such as moisture and pH. Carbon black is added to rubber for increased hardness, wear resistance, strength, stiffness and heat resistance. Carbon black also absorbs ultraviolet light limiting UV degradation of rubber [33, 37]. This is of particular benefit to tyre treads and other high wear applications such as the soles of climbing shoes and bicycle brakes. Elastomeric particles may also be added to polymers to improve toughness, vital for resisting the high impact loads often received by sports equipment [33]. Antistatic agents reduce static build up on polymers by attracting moisture to the polymer surface thereby improving the surface conductivity. Flame retardants such as aluminium tri-hydroxide may be used in the manufacture of sportswear and thermal garments, as well as insulation.

3.2.2 *Fibre Reinforced Composites*

I. Fibre interaction

Fibre composite materials gain stiffness from thin fibres capable of transmitting high loads along their length with little resistance to transverse loading. Where the flexural stiffness of single fibres is assumed negligible the fibre transmits load only in tension. The matrix holds the fibres in place, promotes load sharing between fibres and transfers the load from broken fibres to neighbouring intact fibres [38]. The lateral stiffness of the fibres in a composite can therefore be considered equal to that of the matrix. The load in direction of the fibre length is shared between fibre and matrix producing greater global stiffness [39].

Representing heterogeneous materials as homogeneous materials, with isotropic mechanical properties, is considered a disadvantage in that the models may not be suitable for modelling fibre-matrix interactions [40]. Fibre reinforced composites can be characterised by fibre length, volume fraction and direction dependant mechanical properties. Fibre volume fraction is easily controlled by the materials engineer. Fibre length is more problematic when processing methods use

aggressive mixing and feeding mechanisms that cause degradation of fibre length [41]. Mariatti and Chum reported that the number of voids also increases with increase in fibre content [42]. The effect of fibre orientation is less for short fibre reinforcement than for continuous fibre reinforcement. By accounting for all possible reinforcement orientations in a composite, for example with randomly oriented chopped strands, or, with layers of multiaxial woven cloth, anisotropy may be averaged out in favour of isotropic behaviour [27, 43].

II. Fibre-matrix interaction

Fibre matrix interactions are considered very complex [44-48]. Whether continuous fibres or short fibres are used the fibre matrix interaction is an important consideration for composite design. This is due to the large surface area of the reinforcement where the physical interaction at the interface is amplified. The complexity of the interface and problems with accurately predicting the interaction between the fibre and the matrix was the cause of slow progress of composite materials from their conception. Improvement of adhesion did increase the tensile and flexural strength of a composite, but lowered the impact strength and toughness. Methods were devised where surface treatment of fibres enabled superior adhesion, but produced disastrously brittle materials that were in turn rejected as replacements for conventional materials [35].

It is well known that mechanical properties of composite materials are significantly influenced by the interaction between components as the degree of bonding will determine stress transfer between them [35]. Many composites show either or both of the following:

- an interphase (adhesion layer between the components)
- an interface (surface adhesion).

These may be attributed to a chemical interaction often deliberately introduced to bond components and improve material properties. For either case, analysis of the interaction is complex, as, contact regions are often a result of processing, and do not exist as part of individual components [35].

Evaluation of PMCs based on single fibre tests has further proven the dependence

of mechanical properties on bonding [35]. The main disadvantage of many bond tests is the creation of non-uniform stress states near the interface that can initiate debonding [35]. If there is no debonding between components during testing then the test will not be appropriate and may only show the bond is stronger than either component [35]. Measurement of adhesion strength would only be accurate if a uniform stress state could be created over a suitable area. Whether stress concentrations are critical may depend on the ratio of Young's modulus to Poisson ratio [35]. Models based on the theory of adhesives also consider the interphase component but the adhesive has the specific task of bonding components with no dependence on interaction between components to exist [35].

Strong bonding creates efficient load transfer between composite components [35]. Although the bonding needs to be strong to ensure the reinforcement is effective in reinforcing, if too strong it may increase stiffness to the point where it decreases the ability of the matrix to impart ductility and the overall strength and/or toughness of the composite will be reduced [48]. This effect is known as composite brittle fracture, and is cited as the reason for the slow uptake of carbon fibre as a reinforcement material when first introduced in the 1960s [35].

Interfacial adhesion can only be efficiently achieved when the fibre and matrix components are brought into close proximity. Although intimate contact between matrix and fibre is necessary for good adhesion, it does not mean that there is a strong bond, high bond strength may also be gained from extremely smooth surfaces [35]. The maximum contribution to bond strength is considered to be from physicochemical interactions [35].

An important aspect for fibre matrix adhesion is that of wettability, it identifies the ability of a liquid to spread over the surface of a solid. Wettability is measured by the contact angle, ø, between the three phases, solid-gas, gas-liquid and liquid-solid as shown in Figure 11.

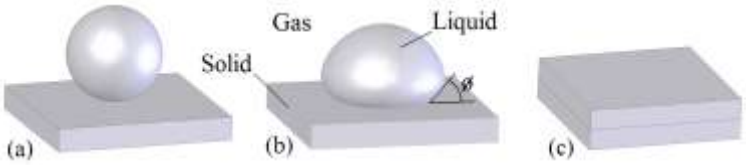

Figure 11. Wetting conditions a) no wetting, b) partial wetting, c) fully wet.

For wetting to occur there must be a reduction of the surface tension at the liquid-solid interface [49]. However wettability is dependent on variables such as, time and temperature of contact, interfacial reactions, and component stoichiometry, surface roughness and polarity. Wettability may also be reduced by chemical reactions, surface in-homogeneity and diffusion of one component into the other [25]. The performance of composites in environments with elevated temperature, high moisture and variable pH levels could also affect the level of wettability or adhesion. As shown in Figure 12 poor wettability can lead to voids in a composite that reduce the mechanical strength and increase stress loading on the matrix.

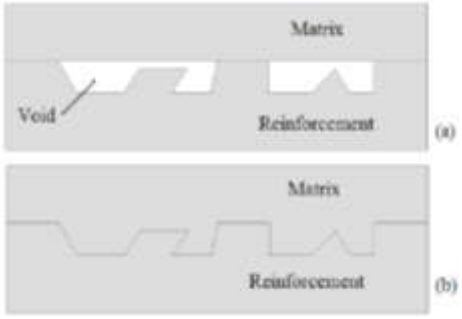

Figure 12. Rugosity of reinforcement with a) poor wetting forming voids, b) good wetting penetrating cavities. (Adapted from [25])

Bonding can take place where there is intimate contact between composite components. The type of bond that forms is dependent on the matrix and reinforcement material, but not on this alone. Bonding mechanisms can be grouped into one of the following forms:

- chemical bonding
- mechanical interlocking
- physio-chemical interactions
- reaction /interfusion.

Interfacial bonds are formed from one or more of the mechanisms at any one time. The bonding mechanism may change during manufacturing or even during service as conditions such as, temperature, load and humidity change [25, 35, 48].

Mechanical bonding is most effective when the rugosity of the fibre is high, this allows for the matrix to penetrate cavities and ridges and to grip the fibres giving

high axial strength. It is also advantageous to have a contraction of the matrix onto the fibre surface to increase the axial strength of the composite by increasing the frictional resistance to give greater load sharing [25, 35, 48].

Physical bonding is considered any form of interfacial bonding with mechanisms involving electrostatic dipolar interactions and hydrogen bonding. For good physical bonding the charged components need to have intimate surface contact. This may be lessened by inclusions, voids and gaseous contaminants [48].

Chemical bonding is covalent, ionic or metallic bonding that forms between functional groups in both the fibre and matrix. The strength of the bonding depends on the number and strength of bonds between the surfaces. Coupling agents such as maealaeic anhydride and silanes are often used to enhance or promote chemical bonding [48, 50].

Reaction or inter-diffusion bonding involves the transport of molecules, atoms, or ions from the reinforcement the matrix or both, to create an interfacial region [25, 35, 48]. For polymer components the surfaces may diffuse matrix molecules into the molecular network of the fibre to form a tangle of molecular chains. The interface region is then considered to vary as a result of factors such as the chosen materials, the process time and temperature [25, 35, 48].

Many methods have been used to quantify the strength of component interactions, these include [44, 48]:

- compressive, flexural and tensile tests
- measurement using laser-Raman spectroscopy
- droplet-debond tests
- fibre pull-out tests
- micro-indentation tests
- fibre fragmentation tests.

This further supports the knowledge that fibre matrix interactions are very complex and can be measured by a method most suitable for end use comparison.

3.2.3 *Multilayer Composites*

Multilayered composites and laminates are widely used in sporting equipment. Laminates consist of material layers joined by an organic adhesive, with many initially developed for the aerospace industry.

Sandwich materials are made up of two or more layers of an outer material laminated with the addition of a central core material. The central core can be in the form of a light weight expanded material or a honeycomb type structure. Generally, neither the outer shell nor the inner core will be particularly strong or rigid, given their physical dimensions, whilst the composite has both of these properties [51].

Another form of multilayered composite, hybrid composites can be classified into two categories, intraply and interply. An intraply hybrid is a mixture of different types of reinforcement within a single reinforcement phase combined within the same matrix, for example woven carbon/aramid cloth in epoxy resin. Interply hybrids are layers of different types of reinforcement within a single composite material, for example a layer of carbon and a layer of glass cloth in polyester resin.

Naik et al cites studies of multilayered hybrids where it was found that tensile failure of composites consisting of brittle reinforcement like carbon is increased when they are hybridised with ductile reinforcement like glass [51]. Called the hybrid effect, it is defined as the positive deviation of a property from the rule of mixtures. Hybrid effects are said to lead to the enhancement of the failure strain and strength properties in excess of that predicted by classical lamination theory and various failure criteria [51].

Reinforcement orientation is considered an important factor in the construction of a multilayered composite. Orientation may be multidirectional in total but the individual laminates are often unidirectional. The individual layers can also be engineered to produce the required mechanical properties for the application [27].

Theory has been adapted and developed for the analysis of multilayered structures. An example is where individual layers are treated as homogeneous, isotropic layers with the section analysed using classical theory for laminated

plates [24]. These theories and equations are not based on new concepts but are essentially the same as those encountered for isotropic materials.

As composites are required to have stability during three dimensional loading, the functionality of any unidirectional composite can be considered limited. The requirement then is to design for multiple layers, with the orientation of the reinforcement phase such that the sum of the multi-ply laminate will provide the properties required by the intended application. This is especially relevant to sporting equipment where the loadings are primarily multi-directional.

3.2.4 *Composites in general*

As engineered materials, composites provide designers with flexibility during the development process. Optimal composite designs are achieved through the use of a variety of component materials, stacking sequences and processing. High performance levels can be gained from uniformly distributed high reinforcement concentrations of high aspect ratio (length/diameter) reinforcement. This conflicts with many mass production processes that often result in complex, unknown reinforcement orientation that can complicate analysis and comparison with model predictions. Hence uncertainty in comparison and interpretation of composites, even when comparing their performance in a range of standard mechanical tests, may occur. It is therefore essential to fully understand the structure-processing-performance relationships of a composite and its components.

Sustainability and environmental factors are often considered when materials selection is being made. This has promoted the use of natural materials as reinforcement in PMCs. Regardless of inherent disadvantages such as moisture uptake, dimensional stability, variability on mechanical properties and bonding problems [6, 38, 50, 52, 53]. Chemical and physical treatments can be used to overcome disadvantages but costs may make this restrictive [54].

Although material properties for many naturally reinforced PMCs are very good, especially specific properties, natural fibre composites and wood cannot compete with glass fibre composites. When accounting for cost, natural fibre composites can have identical or better performance than glass fibre and considerations such as sustainability greatly enhances their competitiveness [55].

4 Theoretical modelling

This chapter investigates modelling composite materials. Component interaction and the approach of other researchers to composite modelling and prediction of and the limitations of current methods are also discussed.

4.1 Mechanical properties

The mechanics of materials are as applicable to composite materials as they are to monolithic materials. However there is the added complexity of component interaction when considering composites. For composites, the algebraic sum of stresses or strains in each component can be used for calculating mechanical properties, only when component interactions do not alter the effect either component would have individually [24].

Two simple models, widely used for determining composite material properties such as, density, elastic modulus and electrical conductivity, are Voigts' iso-strain model, and Reuss' iso-stress model [56]. These models can be represented with the 'slab models' of Figure 13. The difference between the two models is seen in the orientation of the layers relative to the direction of applied loading.

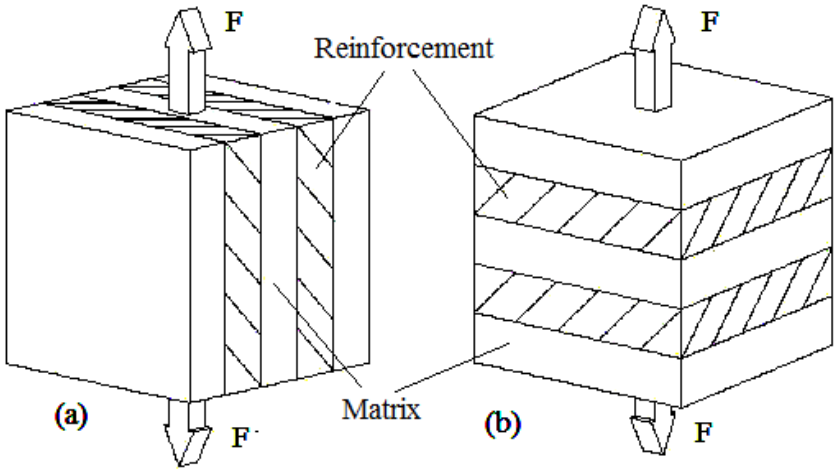

Figure 13. a) Iso-strain model, b) Iso-stress model.

As shown in Figure 13(a) the strain in the loading direction is equal for all components therefore, $\varepsilon_c = \varepsilon_f = \varepsilon_m$. Strain is expressed in terms of tensile stress

and elastic modulus as $\varepsilon = \frac{\sigma}{E}$. Given equilibrium it is shown that stress within the composite is cumulative and dependant on component volume fraction to give $\sigma_c V_c = \sigma_m V_m + \sigma_f V_f$ and therefore, $E_c \varepsilon_c V_c = E_m \varepsilon_m V_m + E_f \varepsilon_f V_f$. For equal strain the composite elastic modulus is determined from:

$$E_c = V_m . E_m + V_f . E_f \qquad (4)$$

When the volume fraction of the reinforcement is high or the matrix modulus is considerably lower than the reinforcements' modulus, the composite modulus can be approximated as $E_c = V_f E_f$. The isostrain model can be graphically represented as shown in Figure 14.

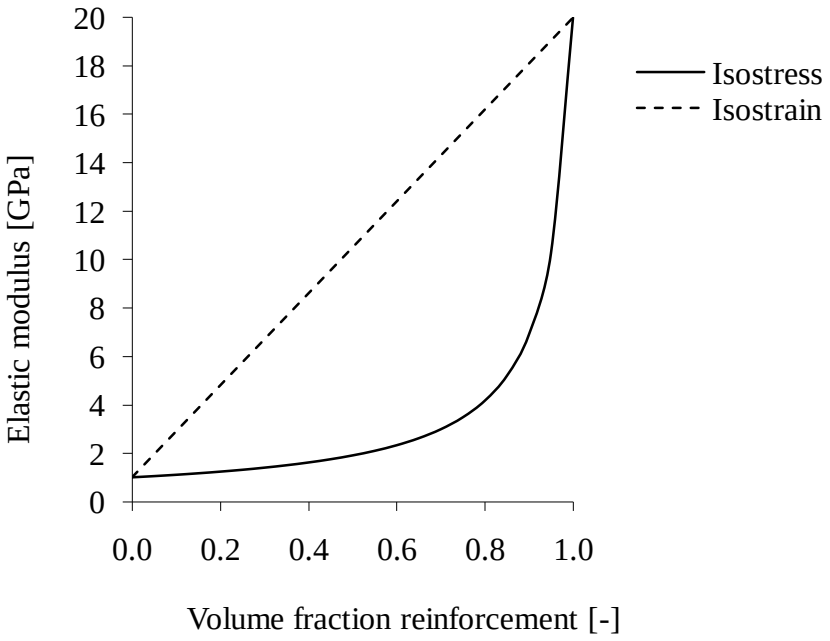

Figure 14. Modulus prediction, a function of reinforcement volume fraction (Em = 1 GPa, Ef = 20GPa).

A transversely applied load (Figure 13(b)) gives the iso-stress model. Stress is equal in all layers, $\sigma_c = \sigma_f = \sigma_m$. Strain is cumulative, ($\varepsilon_c = \varepsilon_f + \varepsilon_m$), and the stress is dependent on the component volume fraction, therefore: $\frac{\sigma_c}{E_c} . V_c = \frac{\sigma_m}{E_m} V_m . + \frac{\sigma_f}{E_f} V_f$. The transverse elastic modulus (Figure 14) can then be determined from Equation 5, and shown in Figure 14:

$$\frac{1}{E_c} = \frac{V_m}{E_m} + \frac{V_f}{E_f} \quad (5)$$

The values obtained using these models are generally considered as indicative only [6] and are often used as upper and lower bounds respectively [27].

A number of researchers [57-63] used methods such as, axial compression, fully constrained plates or three and four point bending to validate their approach to investigation of flexural properties. Table 3 shows an outline for some approaches taken to develop models. The material types range from plain polymers to short fibre reinforced polymers and continuous unidirectional composites. Verification methods range from theoretical proof, to physical experimentation, and, finite element analysis. Some models give reasonable agreement with experimental observations for specific material combinations, while none allow for different material combinations or processing routes [64]. These models are further discussed in Section 4.6.

Table 3. An overview to elastic modulus investigations.

Researcher	**Material Type**	**Verification method**	**Characteristic defined**
GUZ [78]	Carbon/ Epoxy	Theoretical	Elastic modulus
Jacquet [72]	Fibre composite	FEA	Elastic modulus
Beaumont [22]	Glass/ carbon/ Epoxy	Experimental	Elastic modulus
Halpin Tsai [81]	Glass/ polystyrene	Experimental	Tensile modulus
Padawer [80]	Planar reinforced	Experimental	Tensile modulus
Lusis [80]	Planar reinforced	Experimental	Flexural modulus
Crawford [82]	Polymer	Experimental	Flexural modulus

Within a composite, individual components may have linear, non-linear, iso-tropic, anisotropic or orthotropic properties and all adjacent components will interact. To model this complex behaviour within a beam a more adaptable approach is needed and is addressed in the following work.

Modelling approaches, such as those above, are developed with the understanding that fibre and matrix interactions are very complex [35]. The fibre and matrix strain is equal for continuous fibre composites when loading is uniform throughout the fibre length, unlike short fibre reinforcement where the strain

varies across the length of the fibre due to unequal load sharing through the matrix material. The analysis of linear elastic stress of a short fibre composite using the 'shear lag' model was first presented by H.L.Cox and is often the basis of understanding load sharing [39]. The 'shear lag' theory for short fibre composite materials considers high stress areas, such as fibre ends, to be sites where localised interfacial debonding or void formation can occur which may lead to inferior material performance.

The 'shear lag' model considers the transfer of tensile stress from the matrix to the reinforcement through interfacial shear stresses. Figure 15 shows the stresses acting on a fibre section of length L and radius r embedded in a matrix. Under loading the axial tensile stress across the fibre section, σ_f, and the interfacial shear stress, τ_i, acting on the total fibre interfacial area balance the axial tensile stress, σ_f, and the increase in axial tensile stress, $d\sigma_f$, across the fibre section. The tensile and shear stresses must then balance for the static equilibrium condition to equate as $\left(\sigma_f + d\sigma_f\right)r^2\pi = \sigma_f r^2\pi + \tau_i 2r\pi dx$.

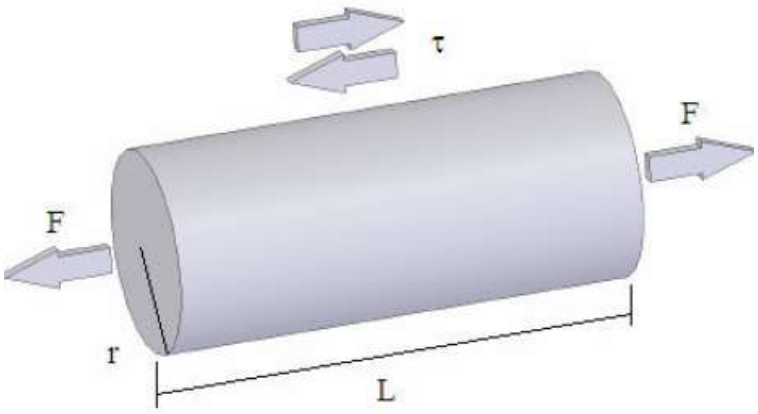

Figure 15. Coxs' shear lag model depicting component interaction.

Multilayer composite models that use material properties from individual components and lack consideration for interaction between adjacent components have generally presented poor results [65]. Ward concludes from anisotropy studies, that the validation of theoretical calculations for elastic properties requires experimental data on carefully controlled samples and, theoretical models that account for the polymer and the reinforcement orientation [66].

In response to this, the compressive and tensile stresses at the neutral axis of a bending beam (Figure 9) are seen to be similar in nature to the interfacial shear stresses between composite components as shown in Figure 15. For this reason it may be possible to account for the complex nature of composite materials, by considering flexural properties, which in turn in will enable the shear stresses to be partially accounted for.

To further support this thinking, the parallel forces seen to balance the bending moments, (Figure 9), and transverse loads, (Figure 10), within a beam produce shear stresses. During bending the shear stresses have a maximum value at the sections neutral axis and distribute through a multilayered section relative to the number of material layers, as shown in Figure 16 [24].

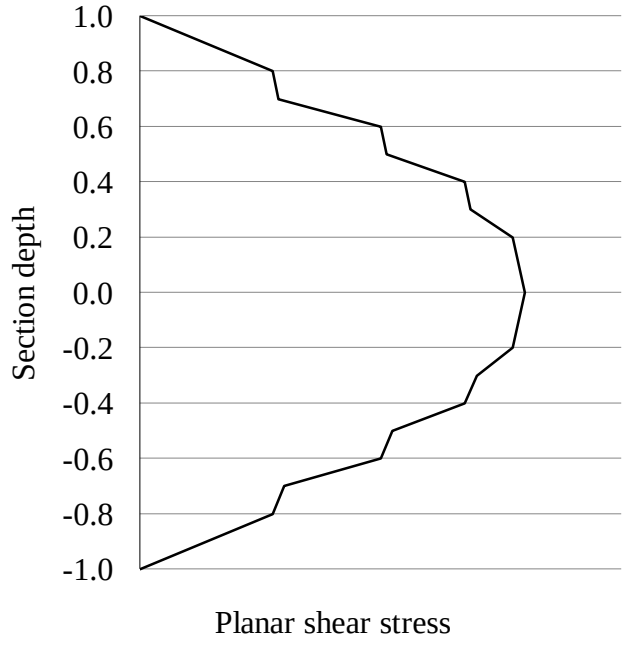

Figure 16. Planar shear stresses within a multilayer section subjected to bending moments [67].

Therefore by considering flexural properties in relation to composite materials previous concerns may be addressed leading to more accurate models

4.2 Assumption and simplification in predictive modelling

Some predictive models are considered simple and elegant while others give complex analytical solutions that are extremely difficult to use [68]. Using simplified geometries, inaccurate component data and not considering component interactions can produce poor results. However, simplistic modelling can in some cases give better resulting data than more sophisticated models because of correct selection of variables [69]. This is especially true with purely fundamental models developed with little or no validation provided [35, 58, 70, 71]. It is also considered that some micro-mechanical models are only useful to define upper and lower boundaries of the investigated mechanical properties, as well as showing characteristic trends [72].

4.2.1 *Theoretical and empirical models*

While there are a number of differences between materials models and equipment models the following limitations can be seen to encompass both:

- Maximum possible packing ratio for reinforcement is dependent on the reinforcement geometry. Fibres being cylindrical have a maximum of near 90%. Although 100% reinforcement is often modelled it is considered that above 80% there is insufficient matrix for practical consideration within a composite [73].

- Many techniques used for modelling make it acceptable to drop specific values from calculations for example non-linear attributes eliminated from bending equations. While this is a typical modelling approach it may reduce accuracy.

- Considering distribution of reinforcement to be homogeneous does not account for irregular distribution through agglomeration or preferential distribution from processing.

- Environmental factors i.e. temperature and humidity, utilised for standard testing regimes are steady state and highly controlled. This is a direct contrast to the conditions most materials are subject to when in use and may not provide an adequate basis for equipment modelling.

- The degree to which matrix and reinforcement interaction is investigated is also of importance.

- Not accounting for reinforcement alignment will limit prediction accuracy as a major advantage of using composite materials is the ability to align reinforcement to maximise mechanical properties.

4.3 Test sample quality issues

Test sample quality is a practical issue controlled by the experimental method. This is a limitation that must be questioned during analytical verification or with empirical derivations. Thermoset and thermoplastic composites may be processed in a number of ways each leading to properties unique to the process method. For example injection moulding will produce reinforcement distribution less homogeneous than casting or compression moulding, and vacuum bagged articles can be produced with more reinforcement than hand lay-up.

Processing methods include:

- casting - material poured/laid into an open mould heated and left to set
- compression moulding - material pressed between hot platens
- extrusion - material forced through a die of predetermined dimensions
- hand lay-up - similar to casting but built up layer by layer
- injection moulded - injecting material melt into a closed die under pressure
- vacuum bagged – casting, compression moulding or hand layup with applied vacuum to remove gas/vapours and further consolidate composite.

The effect of processing method on material properties could be empirically determined.

4.4 Equipment modelling

The use of simplified geometries has permitted successful modelling of many dynamic loading conditions of sports equipment, and even the biomechanical interactions between athletes and equipment [74]. Examples of the simplistic geometric approach include:

An aluminium beam of uniform cross section was used to represent a baseball bat; with the advantage of being simple to measure its physical dimensions. The stiffness was easy to verify and the analysis was done in terms of simple beam theory. The collision dynamics between the bat and ball were subsequently modelled as a uniform beam struck with a ball [75].

A skateboard deck was modelled by considering the deck to behave as a concave shell, under the assumption of pure plate bending. Youngs' modulus and laminate bending stiffness was calculated [74].

A tennis racket was represented as a one dimensional beam (Figure 17), with non-uniform mass distribution [76]. This was modelled using beam theory and the parallel axis theorem for second moment of area: $I_{tr} = I_h - (M + m)h^2$.

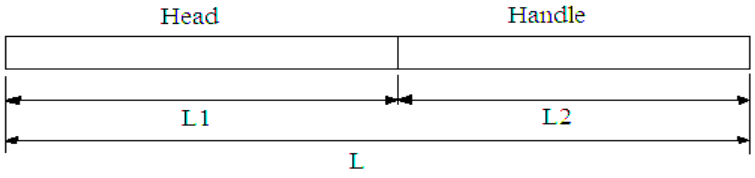

Figure 17. Two segment beam model of tennis racket.

Simplified models such as Figure 18, are widely used. Linkages and cylinders can be used to model any athlete and equipment interactions during equipment use [77].

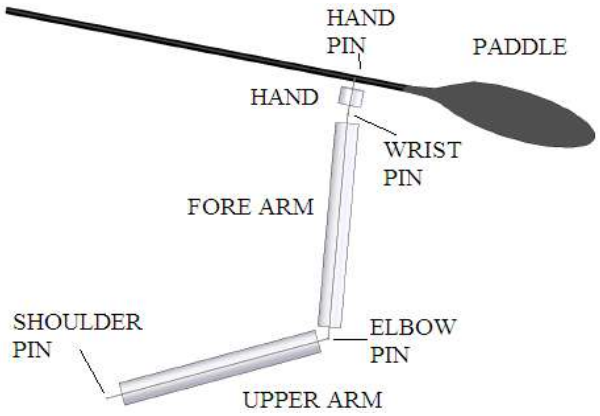

Figure 18. An example of linkages and cylinders used to model dynamic systems, in this case the paddling action.

These approaches indicate that it may be beneficial to use simple representations for modelling equipment. This may also be a suitable approach for the micro-scale modelling of materials where interactions between components lead to changes in mechanical properties.

4.5 Finite element modelling

Finite element modelling is a numerical modelling technique that represents an object as a mesh generated from repeating unit cells (Figure 19). Each unit cell is defined by an equation and is chosen to suit 'in use' conditions and geometry of the object. This equation is applied to each cell and takes into account local variables (such as stresses from adjacent cells) and individual component properties. The resulting system of equations (algorithm) is solved taking account of interaction between adjacent cells. Finite element methods are widely accepted and used to determine the mechanical behaviour of these representative cells [74].

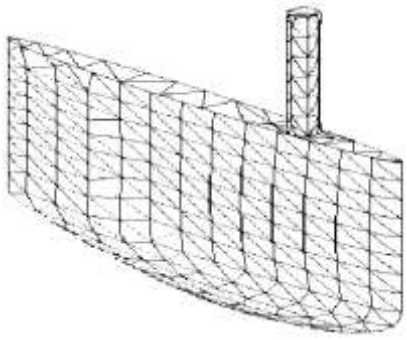

Figure 19. Finite element, mesh generated discretisation.

The repeating unit cells may have a 2D or 3D structure depending on the nature of the problem to be solved and whether the problem can be solved as a shell type structure or a solid structure. Shell elements are used where thickness is small compared to length so that load contributions within the shell thickness may be considered negligible compared to the load contributions affecting the plane of the shell.

The most widely used 2D elements are three-sided, three-noded, triangular elements, or four-sided, four-noded, quadrilateral elements. The nodes are the intersection points of lines as seen in Figure 20(a). 3D elements often use six-sided, four-faced, four-noded, tetrahedral elements, or twelve-sided, six-faced and eight-noded, cubic element (Figure 20(b)). These elements can be given greater accuracy by creating nodes midway between corners as in Figure 20(c).

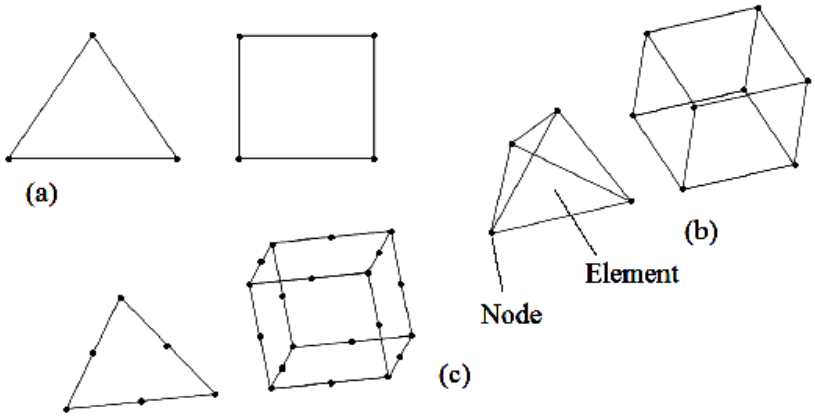

Figure 20. Triangular and quadrilateral based elements for (a) 2D, (b) 3D and (c) higher order, finite computation.

Elements assigned to the matrix, reinforcement or interfacial regions of a composite material allow the components to be assigned their respective mechanical properties. Keeping mathematical complexity within practical computing abilities is a major consideration and is often a limiting factor for the approach to many problems. The polynomial-element (P-element) method used by Pro/Mechanica and Cosmos Works, allows higher order polynomials to solve for otherwise 'poor quality' mesh generation that may otherwise produce inaccuracies or even fail to converge to a solution.

In order to analyse loads on individual elements each is assigned degrees of freedom (DOF). Using a Cartesian co-ordinate system there are three DOF for translational and three DOF for rotational forces. Therefore FEA could be considered a rigorous process sufficient to simulate material models at either the micro-scale or the macro-scale.

4.6 Comparing existing micro-mechanical models

The elastic modulus in bending or, flexural modulus, can be considered one of the most important mechanical properties for structural materials subjected to flexural loading in use [27]. There is often a difference between Youngs' modulus values gained from tensile testing and the values gained from flexural testing which is attributed to shear deformations during bending. By modifying these tests the values should be the same.

Some mathematical models are presented in this section as presented in recent scientific investigations. The findings with respect to PMCs' are shown as Figure 21. The modulus values are considered generic with a relative matrix, $E_m = 1$ and reinforcement, $E_f = 20$.

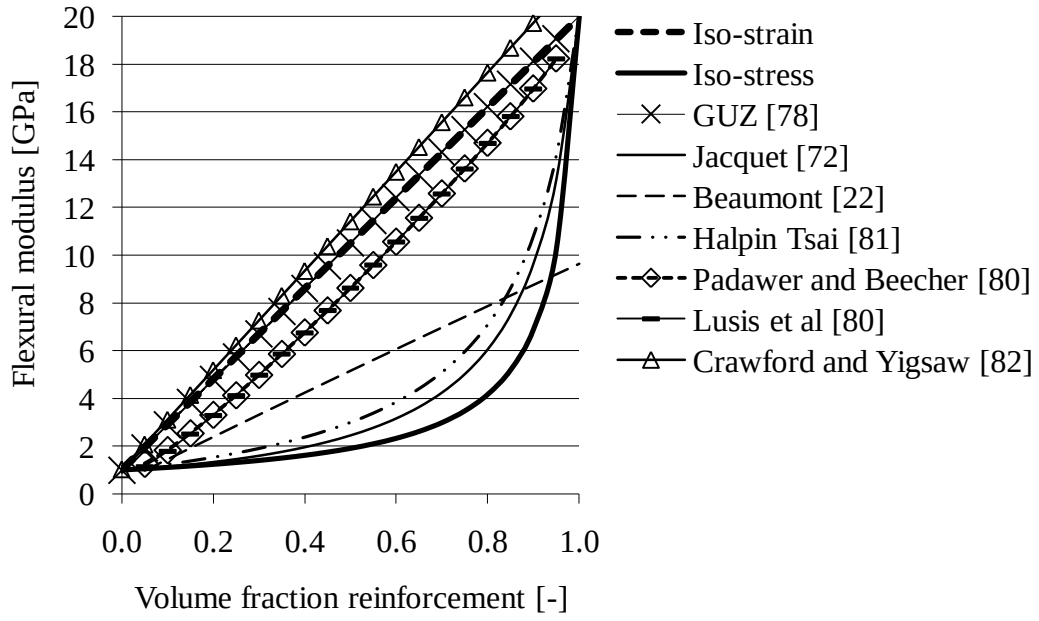

Figure 21. Graphical comparisons of existing models for elastic modulus.

Composite materials in general are not homogeneous; on a micro-scale they are heterogeneous [78]. The heterogeneity of composites can be seen as the presence of numerous homogeneous inclusions in a homogeneous material. Using this analogy Guz proposed the following [78]:

$$E_c = V_m E_m + V_f E_f + \frac{4 G_m V_m V_f \left(\nu_f - \nu_m\right)^2}{1 + V_f \left(1 - 2\nu_m\right) + V_m \left(1 - 2\nu_f\right) \left(G_m / G_f \right)} \qquad (6)$$

According to Smith, a model for elastic modulus should ensure position, thickness and symmetry of the layers about midplane is presented [79]. The elastic modulus for a multilayered material, with a given volume fraction of reinforcement, is the same regardless of the position, thickness, or symmetry of the layers about the mid-plane [79]. However, when a multilayered material is subject to bending, the distribution of the reinforcement is critical and the rule of mixtures cannot be used as it does not take layer configuration into account. Smith used the graphical method of Figure 22 to represent symmetrical and unsymmetrical layered systems. This allows comparisons of flexural modulus where upper and lower bounds produced an envelope within which any given configuration value would fall [79].

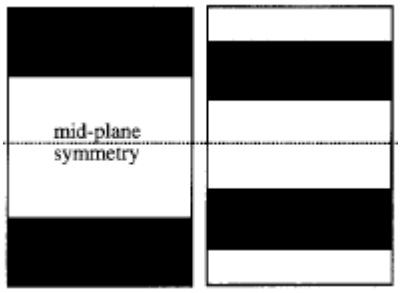

Figure 22. A layered system used to determine FM efficiencies [79].

Using the rule of mixtures Jacquet et al considered a composite in terms of basic cells, shown in Figure 23. The horizontal and vertical components of the composite cell are used to describe the composite elastic modulus in part and presented as Equation (7) [72].

$$E_H = E_f \cdot \sqrt{V_f} + E_m(1-\sqrt{V_f})$$
$$E_V = \frac{E_f}{\sqrt{V_f}} + \frac{E_m}{1-\sqrt{V_f}} \qquad (7)$$

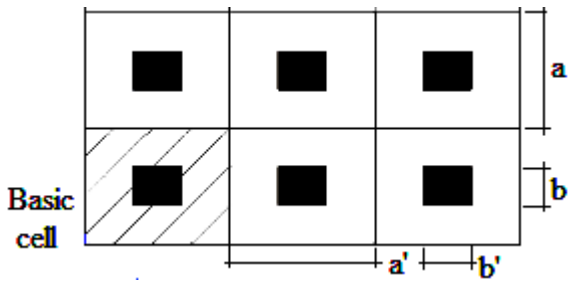

Figure 23. The basic cells with the shaded region showing the composite. The reinforcement is shown dark and the matrix light.

From Equation (7) it is proposed that the elastic modulus of the composite as a whole is calculated from Equation (8):

$$E_c = \frac{E_f . E_m}{E_m + \dfrac{E_f (1-\sqrt{V_f})}{\sqrt{V_f}}} + (1-\sqrt{V_f})E_m \qquad (8)$$

Investigating micromechanical theory of deformation within polymer composite materials, Beaumont considered the behaviour of composite materials [64]. Due to size and scale differences of the components the interactions in composite materials are considered only a sub-element of the overall design process. The modulus was estimated using a rule of mixtures and, presented as Equation (9) [64]. Although Smith considers that for layered systems subject to bending the layer configuration is critical and so the mixture rule cannot be used [Smith, 1999 #129].

$$E_L = \left(\frac{n_m a_m E_m + n_f a_f E_f}{2(b+d)} \right) \qquad (9)$$

Halpin Tsai developed Equation (10) for prediction of elastic modulus, similar to work presented by Meddad and Fisa and appears to be based on the iso-strain model, cited in [80] and [81]. They used the number of layers and layer thickness for reinforcement only.

$$E = E_f \frac{1 + ABV_m}{1 - BV_m} \quad A = \frac{2}{n_f a_f} \quad B = \frac{\dfrac{E_m}{E_f} - 1}{A + \dfrac{E_m}{E_f}} \qquad (10)$$

Investigating how polymer content and reinforcement interaction effects composite modulus, Verbeek presented Equations (10-11) as A, developed by Padawer and Beecher, and B, developed by Lusis et al. [80].

$$E = \mu V_f E_f + V_m E_m \qquad (11)$$

where $A \rightarrow \mu = 1 - \left(\dfrac{\tanh(n)}{n} \right)$, $B \rightarrow \mu = 1 - \left(\dfrac{\ln(n+1)}{n} \right)$ and $n = \dfrac{1}{n_f a_f} \left(\dfrac{G_m V_f}{E_f V_m} \right)^{\frac{1}{2}}$.

Crawford and Yigsaw considered strain related effects in flexural testing and present an adaptation of classical beam theory $E = \frac{L^3 m}{4bd^3}$ for calculating elastic modulus [82].

$$E = \frac{L^3 m}{4bd^3}\left[1 + 3(1 + 0.5v)\left(\frac{d}{l}\right)^2\right] \quad (12)$$

Some of these approaches to the prediction of elastic modulus are based on shear lag models and classical beam theory. None however account for transverse loading effects, critical for validating predicted elastic modulus values. Pure bending, that accounts for transverse effects, can be achieved using flexural methods.

5 Modelling applications

In this Chapter micromechanical models are developed to predict the flexural modulus for fibre reinforced PMCs. Three approaches are presented based on the conditions of perfect bonding, non-adhesion and partial adhesion. Finally composites are modelled using CAD and the three predictive approaches are used to provide pre-processing data necessary in virtual simulation.

5.1 Developing a micro-mechanical model

In order to define mechanical properties of any equipment an appropriate geometrical description is needed. When considering flexural modulus to represent in use loading conditions it would be necessary to have the geometrical representation in a form most suitable for this. Considering PMC materials we can interpret Figure 24 as discrete layers of reinforcement and matrix. If we consider this layered structure to represent a beam then one could use classical beam theory for analysing the elastic modulus.

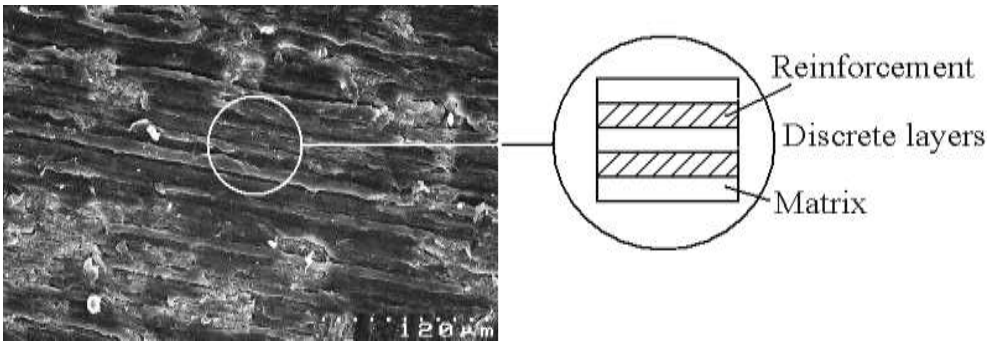

Figure 24. SEM micrograph section of PMC with layered simplification.

5.1.1 *The elemental approach*

The geometrical description of Figure 24 could be considered to be a repeating unit of the micro-structure of a composite if it were scaled according to actual reinforcement dimensions. Otherwise it may be suitable to represent the whole of an artefact in a simplistic form. A limitation of this analogy is that it only represents fibre reinforced composites, although it may also be similar for other planar reinforcements.

I. Multilayered structure constraints

When considering the discrete layers of a multilayered structure a combination of the parallel axis theorem and classical beam theory can be used to analyse the element, in terms of its second moment of area.

The model element is defined as symmetrical around a central polymer layer. Therefore the neutral axis will be fixed in the central polymer layer regardless of the number of plies stipulated in the model. In the model, k is defined as the number of plies, where one ply consists of 4 layers. A ply is defined as one fibre and one polymer layer placed on each side of the central layer. It is seen that the first ply will consist of five layers, with a central polymer layer and each subsequent ply consisting of four layers. The total number of layers n is then defined as $n = 4k + 1$. The number of fibre layers and matrix layers are now determined in terms of k as $n_f = 2k$, and $n_m = 2k + 1$.

As seen in Figure 25 the packing arrangement of the reinforcement will determine the maximum reinforcement fraction for a PMC (Appendix I). Where reinforcement is represented by cylinders (fibres) or spheres (particles) Figure 25(a) shows hexagonal packing which gives a maximum of 91% reinforcement and Figure 25(b) shows square packing which gives a maximum of 79% reinforcement. At these maximums there is not total encapsulation of the fibre. If encapsulation requires matrix to a thickness of 10% of the reinforcement diameter then a maximum fraction would be 82% for hexagonal packing and 71% for square packing. Considering the above in regard to the encapsulation of fibres it is considered here to be impractical to predict for greater than 80% reinforcement.

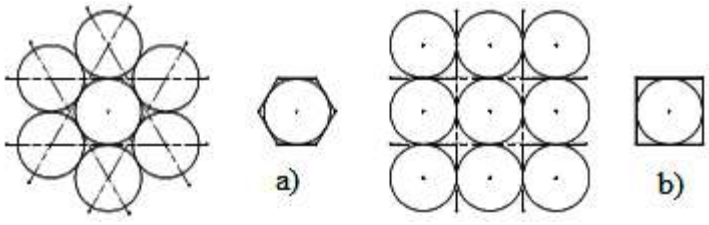

Figure 25. Fibre packing (a) hexagonal (b) square packing.

II. Fundamental equations.

Classical beam theory gives the equation $E.I = M.R_c$ for static equilibrium. During three point bending (Figure 26), where the radius of curvature for the homogeneous composite beam and the discrete layered simplification is assumed equal, bending moments will also be equal. This allows use of the equation $E_c.I_c = E_L.I_L$ to determine the modulus. The fundamental equation for composite modulus is then calculated as:

$$E_C = \frac{E_L.I_L}{I_C} \tag{13}$$

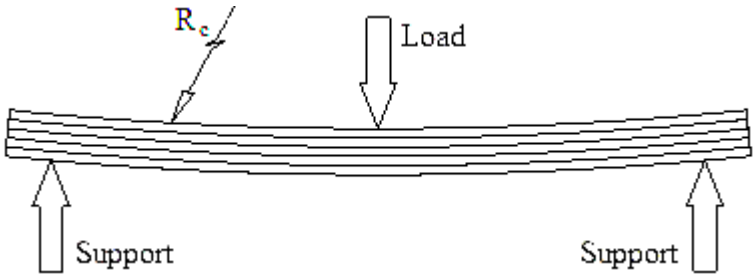

Figure 26. Three point bending of multilayered beam section.

Expressions for second moment of area are required for the composite beam, I_C, and the multilayered beam, I_L. It is also assumed that the composite is homogeneous so $I_C = \frac{b.d^3}{12}$.

In order to determine the second moment of area for multilayered beams, it is necessary to account for both the reinforcement and matrix modulae. The equivalence method can be used to determine an equivalent cross sectional area for the beam by using the modulae ratio *R*, defined as [83]:

$$R = \frac{E_f}{E_m} \tag{14}$$

The total second moment of area, I_L, is then the sum of the matrix and reinforcement components with account for the modulae ratio:

$$I_L = I_f + \frac{I_m}{R} \tag{15}$$

Geometrically, this has the effect of reducing the matrix layer width, b, and the cross section then becomes the equivalent section shown in Figure 27. The multilayer element can then be analysed using a single value for elastic modulus, equal to that of the reinforcement modulus.

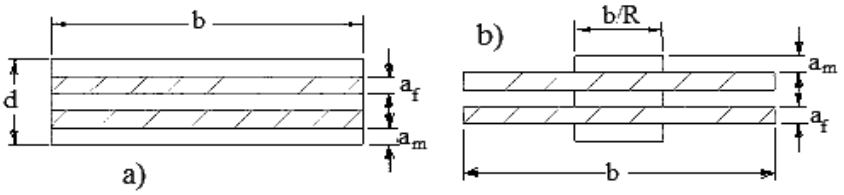

Figure 27. Multilayer models, a) Multilayer section, b) Equivalent section.

III. Component volume fraction

To produce a model that is capable of predictions for any volume fraction it is essential to relate layer thickness to volume fraction. This will allow the number of individual layers and the volume fraction to be adjusted independently.

The total number of layers, n, is the sum of the matrix and reinforcement layers given by $n = n_m + n_f$. The total section depth, d, is equal to the sum of all layer depths as seen in Figure 27. Assuming there are no voids within the composite components or between the composite layers the depth is calculated as

$$d = a_m.n_m + a_f.n_f \qquad (16)$$

The layer thickness for each component layer can be determined from Equation (14) to give the thickness of any matrix layer, as $a_m = \frac{d - a_f.n_f}{n_m}$, and the thickness of any reinforcement layer, as $a_f = \frac{d - a_m.n_m}{n_f}$.

The total composite volume, can be expressed as $V = (a_m.b.l)n_m + (a_f.b.l)n_f$. Considering equal conditions by accounting for the volume fraction of the component gives, $V = \frac{(a_m.b.l)n_m}{V_m} = \frac{(a_f.b.l)n_f}{V_f}$ and so:

$$a_m = \frac{a_f.n_f.V_m}{V_f.n_m} \qquad (17)$$

and

$$a_f = \frac{a_m.n_m.V_f}{V_m.n_f} \tag{18}$$

Equations (15) and (16) form general equations for matrix and reinforcement layer thickness and given, $d = \frac{a_f.n_f}{V_f} = \frac{a_m.n_m}{V_m}$ yields, $a_m = \frac{d.V_m}{n_m}$, and $a_f = \frac{d.V_f}{n_f}$

IV. The layered composite model.

The initial approach to this problem was to determine a general equation for second moment of area for the element with the layers indicated (5, 9…∞) over the possible range of reinforcement volume fractions (0 - 1).

The second moment of area of any layer with a regular rectangular section, about its own neutral axis, OO, is:

$$I_{OO} = \frac{b.a^3}{12} \tag{19}$$

When accounting for perfect adhesion within a multilayered section the neutral axis of individual layers are transformed to a single neutral axis, XX, for all layers, (Figure 28).

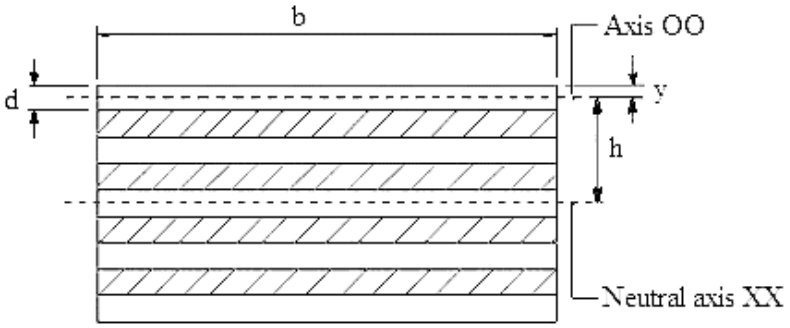

Figure 28. Layerwise approach to the theorem of parallel axis.

The total second moment of area of the layered beam is the sum of the second moment of area of each individual layer about the neutral axis, XX:

$$I_{XXL} = \sum_{1}^{i-k} I_{XXfi} + \frac{1}{R}\sum_{1}^{i-k} I_{XXmi}$$

The parallel axis theorem is used to determine the second moment of area for individual layers about the neutral axis [18]. From the theory the second moment of area of any section (layer) about axis OO parallel to the neutral axis XX is:

$$I_{XX} = I_{OO} + Ah^2 \qquad (20)$$

From equation (18) the second moment of area of any layer, i, around the beams neutral axis is $I_{XXi} = I_{OOi} + Ah_i^2$.

Distance h_i being the distance between any layers' neutral axis, OO, and the beams neutral axis, XX, as shown in Figure 28. Therefore h_i is a function of reinforcement volume fraction and total number of layers.

The second moment of area of an individual layer around OO can be expressed using Equation (17), for reinforcement layers as $I_{OOfi} = \frac{b.a_f^3}{12}$, and matrix layers as $I_{OOmi} = \frac{b.a_m^3}{12.R}$.

5.1.2 *The perfect adhesion case*

In this model it is assumed that every fibre is fully embedded in matrix and that the adhesion between them is perfect. The element must then be chosen such that the number of layers in the model is representative of the composite.

Selecting one matrix layer and one fibre layer would not represent encapsulated fibres about a central matrix layer. Representing the model with an infinite number of layers would give a homogeneous material, where the composite modulus is simply a weighted average of each component. Even though the number of layers is expected to be large, it cannot be infinite, since the fibres are present as discreet layers in the composite and represent the heterogeneous microstructure.

I. The second moment of area

To determine the overall second moment of area for the composite element, the reinforcement layers and matrix layers are considered separately. The total second moment of area for all reinforcement or matrix layers is the sum of the individual

layers second moment about the beams neutral axis.

If the second moment of area for the reinforcement layer, *i*, around its own neutral axis is I_{XXi} and the distance from neutral axis to the beams neutral axis is h_{fi} then the total second moment of area for the reinforcement fraction is:

$$I_{rein} = \sum_{i=1}^{k} (I_{XXi} + A_f h_{fi}^{\ 2}) \tag{21}$$

The distance between the i_{th} layers' neutral axis and the beams neutral axis can then be expressed in terms of the layer number, *i*, the reinforcement thickness, a_f, and the polymer layer thickness, a_m, to give $h_{fi} = \frac{1}{2}(2k-1)(a_m + a_f)$ and $h_{mi} = k(a_m + a_f)$, with $1 \le i \le k$.

Equation (21) can be rewritten as $I_{rein} = \sum_{i=1}^{k} I_{XXi} + \sum_{i-1}^{k} A_f h_{fi}^{\ 2}$, where $\sum_{i=1}^{k} I_{XXi} = n_f \left(\frac{b a_f^{\ 3}}{12} \right)$. Substituting for a_f and n_f gives $\sum_{i=1}^{k} I_{XXi} = \frac{bd^3}{12} \frac{V_f^{\ 3}}{4k^2} = I_C \Gamma_f$

and $\sum_{i-1}^{k} A_f h_{fi}^{\ 2} = \sum_{i-1}^{k} \left(2ba_f h_{fi}^{\ 2} \right)$. Because a_f is constant it can be removed from the summation to give $\sum_{i-1}^{k} A_f h_{fi}^{\ 2} = 2ba_f \sum_{i-1}^{k} h_{fi}^{\ 2}$. Now it is shown that $\sum_{i-1}^{k} h_{fi}^{\ 2} = \frac{(a_m + a_f)^2}{4} \left[\frac{k}{3}(2k-1)(2k+1) \right]$ and $(a_m + a_f)^2 = d^2 \left[\frac{(2k-1)(2k+1)}{(2k)^2 (2k+1)^2} \right]$,

therefore $\sum_{i-1}^{k} \left(2ba_f h_{fi}^{\ 2} \right) = \frac{bd^3}{12} \left[V_f (2k + V_f)^2 \frac{(2k-1)}{(2k)^2 (2k+1)} \right] = I_C \Lambda_f$.

The total second moment of area for the fibre fraction now becomes

$$I_{rein} = \sum_{i=1}^{k} I_{XXi} + \sum_{i-1}^{k} A_f h_{fi}^{\ 2} = I_C \left(\Gamma_f + \Lambda_f \right) \tag{22}$$

A similar analysis is followed for the matrix layer with the total second moment of area for the matrix layers: $I_{matrix} = \sum_{j=1}^{k} (I_{XXj} + A_m h_{mj}^{\ 2})$. After manipulation, as shown in Appendix II, the total second moment of area for the matrix becomes:

$$I_{matrix} = \sum_{j=1}^{k} I_{XXj} + \sum_{j-1}^{k} A_m h_{mj}{}^2 = I_C\left(\Gamma_m + \Lambda_m\right) \qquad (23)$$

Using the equivalent section method the total second moment of area for the model element is then calculated from equations (13), (22) and (23) as:

$$I_L = \frac{I_C}{R}\left(\Gamma_m + \Lambda_m\right) + I_C\left(\Gamma_f + \Lambda_f\right) = I_C\left[\frac{\left(\Gamma_m + \Lambda_m\right)}{R} + \left(\Gamma_f + \Lambda_f\right)\right] \qquad (24)$$

II. Flexural modulus

From equation (13), (14) and (24) the composite flexural modulus can be determined as:

$$E_{PB} = E_m\left(\Gamma_m + \Lambda_m\right) + E_f\left(\Gamma_f + \Lambda_f\right) \qquad (25)$$

Where $\Gamma_m = \dfrac{V_m{}^3}{(2k+1)^2}$, $\qquad \Lambda_m = \left[V_m\left(2k + V_f\right)^2 \dfrac{(k+1)}{k(2k+1)^2}\right]$,

$\Gamma_f = \dfrac{V_f{}^3}{4k^2}$, $\qquad \Lambda_f = \left[V_f\left(2k + V_f\right)^2 \dfrac{(2k-1)}{(2k)^2(2k+1)}\right]$.

Equation (25) is accessible from the accompanying CD as the Java executionable file ‘Perfect bonding model’ (Appendix III).

The calculated flexural modulus values for a generic composite having mechanical properties as set out in Table 4, are plotted as Figure 29.

Table 4. Mechanical specifications for generic composite components.

Material	**Diam.**	**Density**	**Elastic mod.**	**Poisson**
	[mm]	[g/cm^3]	[Gpa]	[-]
Matrix	n/a	1.00	1.00	0.40
Reinforcement	0.025	2.00	20.00	0.25

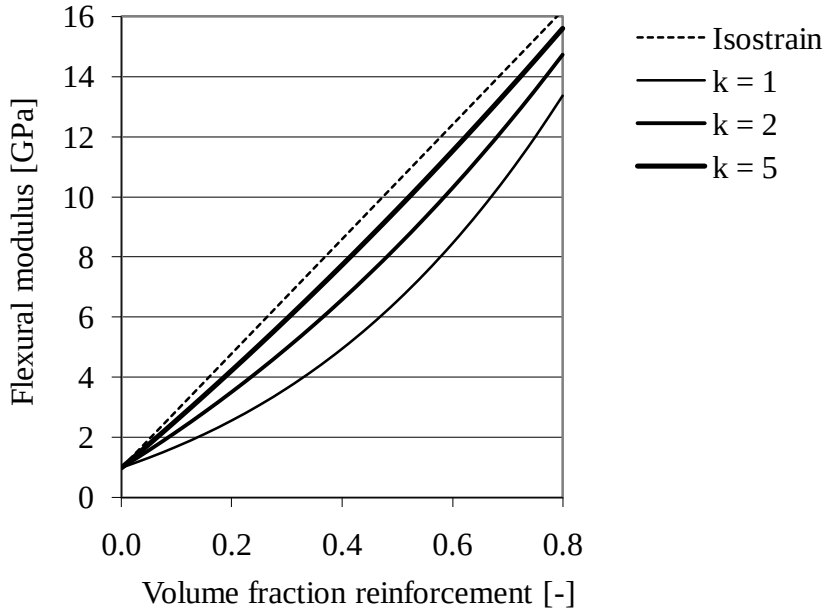

Figure 29. Modulus values calculated from perfect bonding model.

5.1.3 *The no adhesion case*

The second case considers no bonding between the composite components.

I. The second moment of area

Determining the overall second moment of area for a composite with no adhesion between layers, the reinforcement layers and matrix layers are considered separately. When determining the second moment of area of individual layers the parallel axis theorem is no longer used and each layers second moment is calculated about its own neutral axis. The total second moment of area for all reinforcement or matrix layers would be the sum of the individual layers second moment about their own neutral axis [84].

If the second moment of area for the reinforcement layer around its own neutral axis is I_{XXi} then the total second moment of area for the reinforcement fraction is $I_{rein} = \sum_{i=1}^{k} I_{XXi}$. Where $\sum_{i=1}^{k} I_{XXi} = n_f \left(\frac{b a_f{}^3}{12} \right)$ and substituting for a_f and n_f gives $\sum_{i=1}^{k} I_{XXi} = \frac{b d^3}{12} \frac{V_f{}^3}{4k^2} = I_C \Gamma_f$.

The total second moment of area for the reinforcement fraction is therefore:

$$I_{rein} = I_C \Gamma_f \tag{26}$$

A similar analysis is followed for the matrix layer with the total second moment of area for the matrix layers $I_{matrix} = \sum_{j-1}^{k} I_{XXj}$. Where $\sum_{j=1}^{k} I_{XXj} = n_m \left(\frac{b a_m^{\ 3}}{12} \right)$ and substituting for a_f and n_f we get $\sum_{j=1}^{k} I_{XXj} = \frac{bd^3}{12} \frac{V_m^{\ 3}}{(2k+1)^2} = I_C \Gamma_m$. The total second moment of area for the matrix fraction becomes:

$$I_{matrix} = I_C \Gamma_m \tag{27}$$

By considering the equivalent section method, the total second moment of area for the non-adhesion element is then calculated by substitution of equations (26) and (27) into equation (15) to give the formula:

$$I_{FS} = \frac{I_C \Gamma_m}{R} + I_C \Gamma_f = I_C \left[\frac{\Gamma_m}{R} + \Gamma_f \right] \tag{28}$$

II. Flexural modulus

Considering no-adhesion and defining I_C in terms of the elastic modulus of the reinforcement the composite flexural modulus is calculated from Equation (13) by substituting for Equations (14) and (28) to produce:

$$E_{FS} = E_m \Gamma_m + E_f \Gamma_f \tag{29}$$

As with the previous model, Equation (29) and the mechanical properties in Table 4, are used to produce a series of curves representative of the flexural modulus of any rectangular layered section having a matrix and reinforcement component. Equation (29) is accessible from the accompanying CD as the Java executionable file ‘No adhesion model’ (Appendix III). These values are plotted as Figure 30.

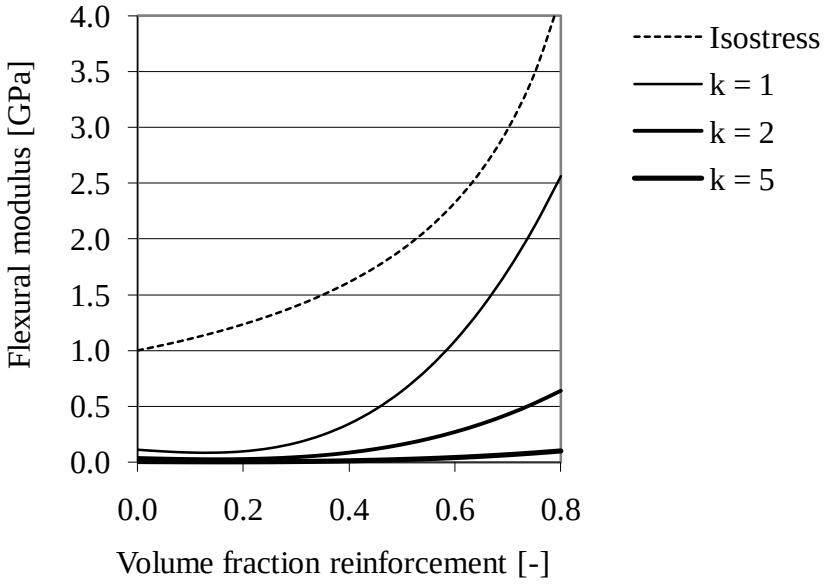

Figure 30. Modulus values calculated from the no adhesion model.

5.1.4 *The partial adhesion case*

A partial adhesion model should predict values that fall between that of the perfect adhesion model and the no-adhesion model.

I. The second moment of area

From comparison between the perfect adhesion case (Equation 25), and the no-adhesion case (Equation 29), it can be seen that the parameters Λ_m and Λ_f drop out of the equation for no-adhesion. Λ_m and Λ_f can then be considered a function of the degree of adhesion between layers while Γ_m and Γ_f represent the contribution of each individual layer. An empirical factor, C_A the coefficient of adhesion is therefore incorporated to account for bonding to give:

$$I_{PA} = I_C\left[\frac{\left(\Gamma_m + C_A\Lambda_m\right)}{R} + \left(\Gamma_f + C_A\Lambda_f\right)\right] \qquad (30)$$

From observation the coefficient of adhesion is considered to have a value of one for perfect adhesion and zero for no-adhesion.

II. Flexural modulus

The composite flexural modulus, E_{PA}, is determined from equation (13) by substituting for equations (14) and (30) to produce:

$$E_{PA} = E_m\left(\Gamma_m + C_A\Lambda_m\right) + E_f\left(\Gamma_f + C_A\Lambda_f\right) \quad (31).$$

Equation (31) is accessible from the accompanying CD as the Java executionable file 'Partial adhesion model' (Appendix III). These values are plotted as Figure 31 and Figure 32.

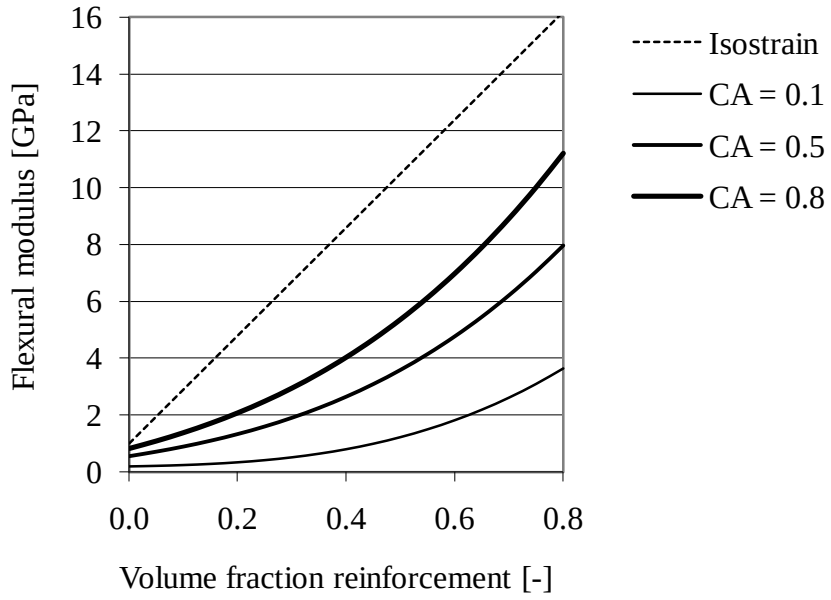

Figure 31. Modulus values calculated from partial adhesion case 1 @ k=1.

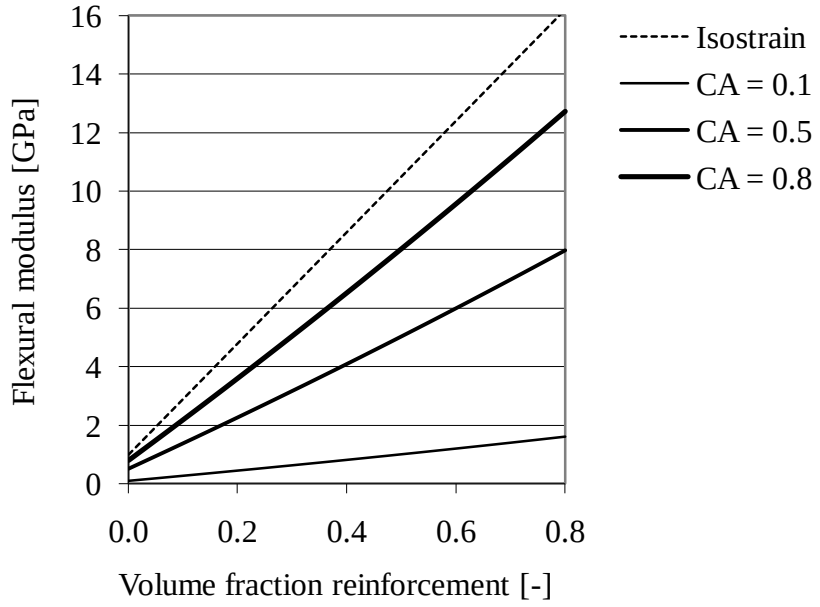

Figure 32. Modulus values calculated from partial adhesion case 1 @ k=10.

5.2 Computer Aided Modelling

The most common modelling technique for industry applications is prototyping. Prototypes as full scale working models are made to enable field testing and monitor dynamic changes to give deterministic results. In order to move from the physical to the virtual testing realm the method of modelling must be rigorous. Considering modelling systems the micro-mechanical models previously developed cover static, probabilistic and symbolic models but do not allow for changing conditions. If CAD models are produced and simulated loads applied, using FEA, dynamic, probabilistic and iconic categories are accounted for allowing realistic predictions [36]. This section presents solids modelling indicating how virtual design may be affected.

5.2.1 *Solids modelling*

Three approaches can be used to model a fibre reinforced beam. The iconic model, (Figure 33(a)), with fibres represented as cylindrical rods encapsulated in the matrix. The semi-iconic model, (Figure 33(b)), is a layered approach with each layer representing fibre or matrix respectively and is symbolic of the micro-mechanical models previously presented. The analog model, (Figure 33(c)), with composite properties does not account for individual components.

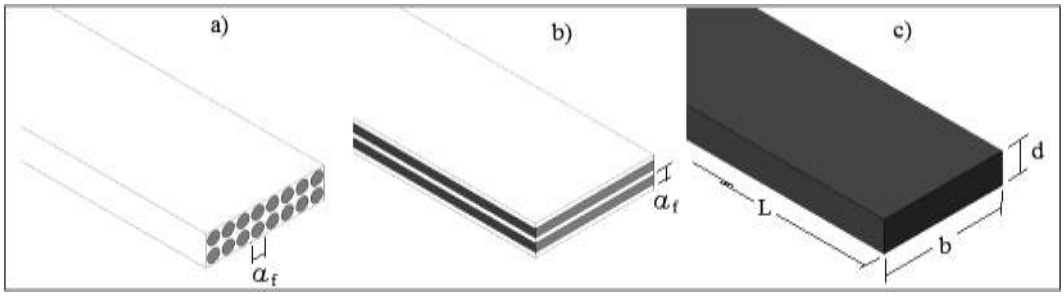

Figure 33. Solids models of beam. a) Iconic, b) semi-iconic and c) analog.

When a CAD model is geometrically symmetrical it can be created as a partial model to reduce file size and complexity. However, where simulation of the whole artefact is required and loading is not symmetrical the use of simplified models is not possible.

5.3 FEA Simulation

Computer simulation of composite models is presented in this section using COSMOSworks. After initial attempts at simulation using the iconic CAD model it was found that complexity of the model prevented simulation. It can be seen in Table 5 that the file size of the iconic model is larger than that of the semi-iconic model even though the semi-iconic element is 50% larger dimensionally.

Table 5. Pre-processing data for the composite models.

Model		Iconic	Semi-iconic	Analog
a_f	[mm]	0.0250		
d		0.060	0.092	
L		0.960	1.467	
b		0.240	0.367	
Element size		0.013	0.019	0.046
CAD file size		211KB	123KB	47KB
Pre-pro file size		15.1MB	10.5MB	0.8MB
Element count		70870	49236	2877

5.3.1 *Simulation 1: The elemental approach*

This approach uses the semi-iconic model by presenting the repeating units of Figure 34, for simulation. Element dimensions are chosen based on reinforcement size, in this case a value of 25µm is used to account for the fibre diameter. The volume fraction and arbitrary k values allow calculation of the element thickness. Width and length of the element are gained from using the physical description, set out in the ASTM D790 standard, b = 4d and L = 4b (Table 6).

Figure 34. CAD element models used for simulation.

Table 6. Dimensions for semi-iconic element models (Appendix IV).

a_f	[mm]	0.025			
V_f		0.1		0.5	
k		1	5	1	5
a_m	[mm]	0.150	0.205	0.017	0.023
d		0.50	2.50	0.10	0.50
L		8.00	40.00	1.60	8.00
b		2.00	10.00	0.40	2.00

I. Pre-processing

Pre-processing involves meshing the CAD model, applying restraints, choosing component modulus values and defining loading conditions. Some of the pre-processing data from this approach is shown as Table 7.

Table 7. Semi-iconic element data (Appendix V).

	V_f	0.1		0.5	
Pre-processing	k	1	5	1	5
	Element size [mm]	0.14	0.48	0.02	0.09
	DOF	191829	581175	124971	415332
	Load [N]	0.10	0.10	0.10	0.10
Simulation	Deflection [mm]	0.04	0.01	0.04	0.01
	E_{sim} [Gpa]	6.31	7.86	31.87	33.59

II. Simulation

On successful completion of the pre-processing the simulation/analysis is run to determine the material response to loading.

III. Modulus determination

From the data of Table 7 composite modulus values for each simulated volume fraction are determine. Modulus data is back calculated from Equation (32) and illustrated as Figure 35.

$$E_{sim} = \frac{5}{4}\frac{L^3}{bd^3}\frac{F}{y} \tag{32}$$

E_{sim} = modulus of elasticity in bending from simulation.

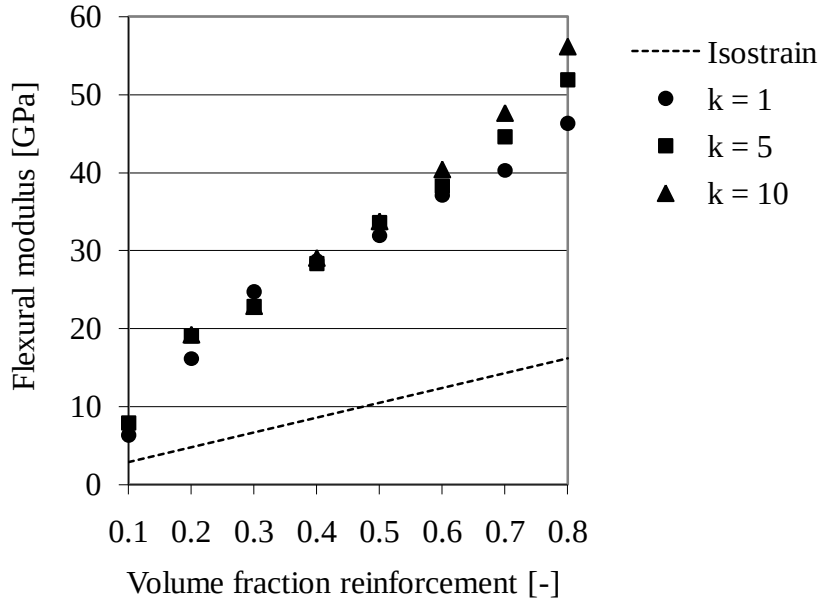

Figure 35. Modulus values for simulated semi-iconic composite element

5.3.2 *Simulation 2: The analog approach*

The solids model presented in this approach are greatly simplified and are identical for each composite material, regardless of the volume fraction of reinforcement.

I. Pre-processing

Material properties are predicted with the micro-mechanical models defined earlier. Table 8 gives pre-processing data that is identical for all models using this approach.

Table 8. Analog pre-processing and simulation data (Appendix VI).

Element size		1.6 mm			
DOF		15657			
V_f		0.1		0.2	
		E_{Pb}	**E_{PA}**	**E_{Pb}**	**E_{PA}**
Modulus	**[Mpa]**	1622.1	894.5	2514.7	1333.8
Load	**[N]**	0.1		0.1	
Deflection	**[mm]**	0.005	0.009	0.003	0.006
Load	**[N]**	10.0		10.0	
Deflection	**[mm]**	0.522	0.946	0.336	0.634

II. Simulation

The modulus values were predicted using the developed micro-mechanical models for conditions of perfect bonding (E_{PB}) and partial adhesion (E_{PA}). On successful completion of the pre-processing the simulation is run to determine the material response to the loading conditions. Simulation was successfully completed for all analog solids models with some load/deflection data set out in Table 8.

III. Modulus determination

From the load/deflection data of Table 8 back calculation using Equation (32) was needed to obtain the composite modulus for the simulated generic composite. The modulus data is shown in Figure 36.

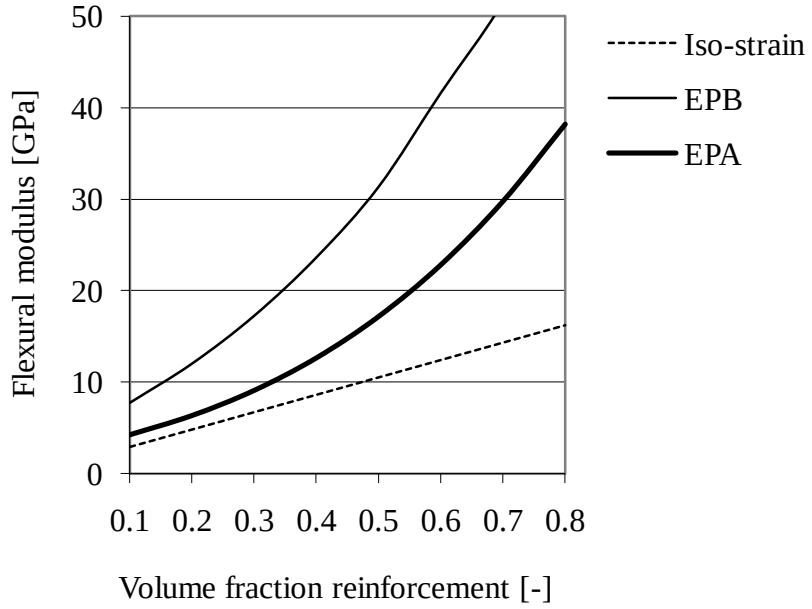

Figure 36. Analog modulus plotted from simulation result.

The FEA of a generic composite using the solid models demonstrated here provides an indication of how simulation can be used to compare any given solids modelling approach to another. The requirement for mechanical properties such as elastic modulus to complete simulation is addressed in this case by the use of the micro-mechanical models developed earlier. However, there is the need for validation to determine the accuracy of the simulation in regard to the material system in question.

6 Experimental

This chapter presents the processing and test equipment and the methods followed for validation of the models presented in Chapter 5. All processing and testing equipment is shown in Appendix VII.

6.1 Standard testing regimes

The component materials of Table 9 were batched to form the composites of Table 10. Two repeats for each composite batch were tested.

Table 9. Composite components and samples.

Material	Identifier	Note	Density	Tens mod
			[g/cm3]	[Gpa]
Wood fibre (Pine Softwood)	W_f	1-5 mm	1.40	15.00
Glass fibre (Cratec 101C)	G_f	6 mm	2.60	78.50
Carbon fibre (Panex 33)	C_f	8 mm	1.81	228.00
LLDPE (Bynel 4125)	M_B	>200C	0.93	0.414
PP/ Glass fibre (Aplax)	B_A	$0.3V_f$	1.10	4.14
PA66/ Carbon fibre (Duralon)	B_D	$0.33V_f$		

Table 10. Test sample values.

Batch	Identifier	Vol. fraction fibre (V_f)	Section depth (d)	Span ratio (l/d)
1	M_B/ W_f	0.0 - 0.6	3.2	16
2	M_B/ G_f	0.0 - 0.6	3.2	16
3	M_B/ C_f	0.0 - 0.6	3.2	16
4	B_A	0.3	3.2	16
5	B_D	0.33	3.2	16

6.1.1 *Methodology*

Sample preparation

Each batch (Table 10) was compounded in the twin screw extruder using a 10mm diameter strand die. The temperature profile varied from 120^{o}C at the feed to 210^{o}C at the die with a screw speed of 150 rpm.

The extrudite was granulated after compounding with an 8mm screen and dried at 50^{o}C for 72 hours.

The granulated extrudite was injection moulded to form the appropriate test pieces. Temperature ranged from 150^{o}C at the feed to 210^{o}C at the nozzle with a screw speed of 150 rpm.

Three point bend test

Following ASTM D790 [85], six samples for each composite batch were tested. The two beam supports and the loading head were 16mm diameter. A cross head speed of 2.0mm/min was used.

Tensile test

Following ASTM D638 [86], six samples for each composite batch were tested. A cross head speed of 2.0mm/min was used.

Compression test

Following ASTM D695 [87], six samples for each composite batch were tested. A cross head speed of 1.3mm/min was used.

6.2 Product testing

As part of the model verification commercial products were tested with the materials and product specifications as shown in Table 11. Product testing is also consistent to what may be expected from a commercial manufacturing process.

Table 11. Product data and identifiers.

Material	Identifier	Geometry	Vol. fraction fibre (V_f)	Span ratio (l/d)
PP/Glass fibre (Aplax)	B_A	Blade	0.3	16
PA66/Carbon fibre (Duralon)	B_D	Blade	0.33	16
ADR256 Epoxy/Hemp fibre	S_H	Shaft	0.25	~16
SP Epoxy/Glass fibre	S_G	Shaft	0.55	~16
SP Epoxy/Carbon fibre	S_C	Shaft	0.6	~16

6.2.1 *Methodology*

Sample preparation

Test specimens were cut from flat uniform sections of commercial paddle blades using the bandsaw to dimensions prescribed in ASTM D790.

Shaft samples were cut from the paddle-shafts to lengths of 600mm.

Bend test for paddle blade specimens

Using ASTM D790 six samples of each paddle blade were tested with one repeat.

Bending test for paddle-shafts

Four samples of each paddle-shaft type were tested using the paddle-shaft bend jig, (Appendix VII, Figure A66c)). A test span of 450mm was used which gave an approximate span ratio of 16.

Each shaft was loaded to give 1mm deflection, unloaded and rotated 60 degrees to give six data points. The 1mm deflection was assumed to be within the elastic limit for the shaft and allowed multiple readings without adverse affect. Rotation accounted for any seam effects of the shaft, a result of the manufacture process.

7 Discussion and results

7.1 Elastic modulus

Linear elastic materials obey Hookes' law and when loaded the strain is directly proportional to the stress. The constant of proportionality is the modulus of elasticity (or Young's modulus). These values are determined depending not on load but on the materials response to load. Response under load is important for sporting equipment and where loading characteristics can be pre-determined the composite designed to maximise performance [88].

The stress-strain relations of many plastics do not conform to Hooke's law across their elastic range but deviate at low stress limits. Applying the term "modulus of elasticity" to describe the stiffness or rigidity of a plastic can then be questioned as the exact stress-strain characteristics are dependent on rate of stressing, temperature and load history. Modulus predictions are also said to be more consistent than predictions of failure behaviour in spite of the mechanisms involved appearing more complex than those for mechanical strength [65].

Where the material has the same modulus in tension and compression the use of either tensile or flexural tests will produce the same results for elastic modulus [89]. A tensile test will provide a pure stress situation from tensile forces and the compressive test will provide a pure stress situation from compressive forces. A flexural test, however, is a product of both tensile and compressive forces and hence a more complex stress regime.

Although it may be expected that flexural and tensile tests produce similar results this is often not the case for composite materials. It is not unusual for the value from flexural testing to be different from the value for the same material tested with tensile or compressive tests [90]. At small L/d ratios a bending beam is expected to be subjected to high shear stress at the neutral axis. At progressively larger L/d ratios the shear is said to minimise and outer fibres increase resistance to bending provided the compressive resistance is great enough [90].

The compressive, flexural and tensile elastic modulus values for carbon, glass and wood fibre reinforced LLDPE were calculated, from the experimental results, and

are presented in Figure 37, Figure 41 and Figure 43.

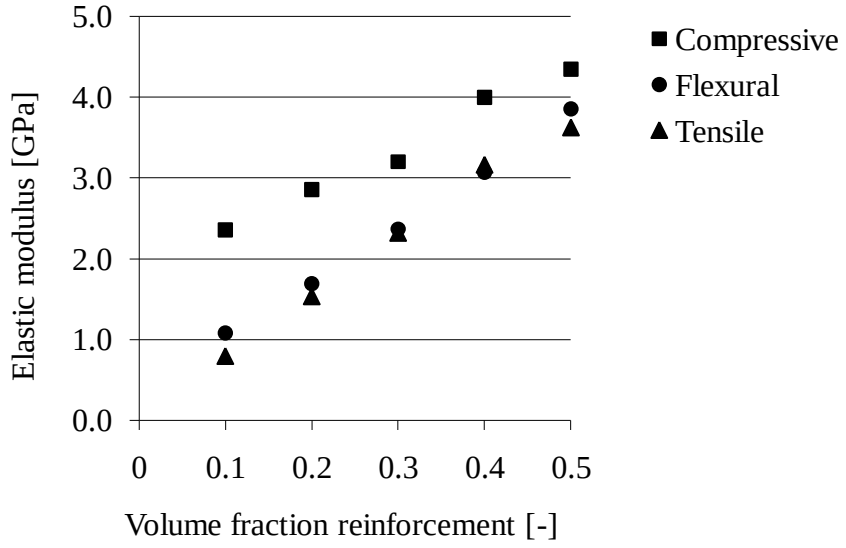

Figure 37. Modulus values for Wood fibre/LLDPE.

As set out in Chapter 6 the test conditions were constant for all tests with the samples conditioned for 24hrs prior to testing.

The values for wood fibre/LLDPE (Figure 37) are similar for the tensile and flexural condition with the compressive values greater. Although this is not the expected result inspection of the test samples (Figure 38) does show failure on the surface of the sample that was in tension during bending when the deflection was great.

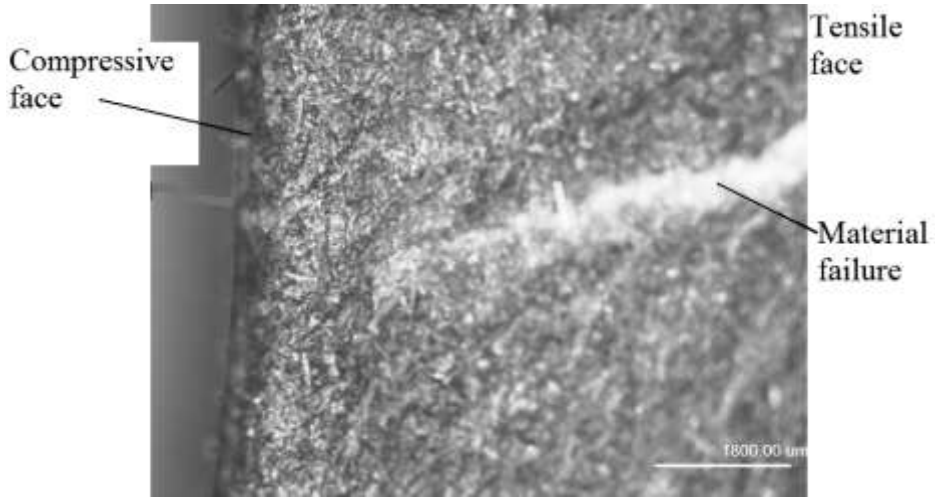

Figure 38. Failure shown on wood fibre composite of bend sample.

The higher compressive value could be further accounted for by considering the wood fibre morphology shown in Figure 39. Wood fibres have an irregular shape

and tend to a quasi-random orientation. This quasi-random orientation can reduce the ability of fibres to load share during tensile loading with little if any reduction during compressive loading. It can also be seen from Figure 39 that there are un-bonded regions about the fibres that contribute to a weaker composite structure.

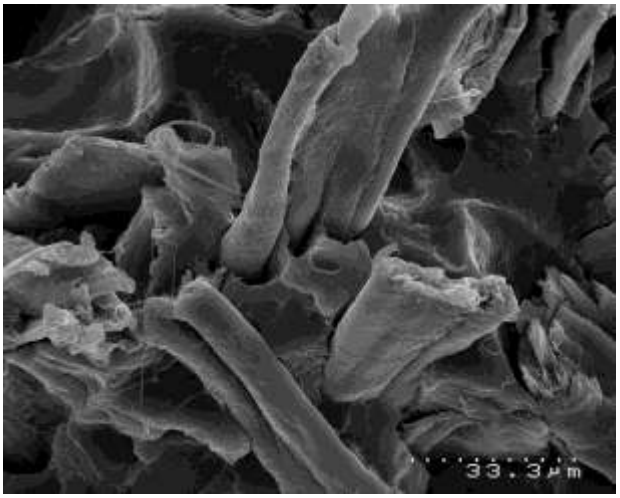

Figure 39. Wood fibre/LLDPE micrograph.

This unconventional result may be further accounted for when considering Figure 40. It is seen that there is agglomeration of the fibres which reduces preferential distribution essential for load sharing between fibres. Agglomeration also reduces the aspect ratio of the reinforcement which can dramatically affect the tensile properties of a composite. The agglomerated fibres tend to become little better than a filler material capable of increasing compressive properties while reducing the tensile properties to below that of the neat polymer.

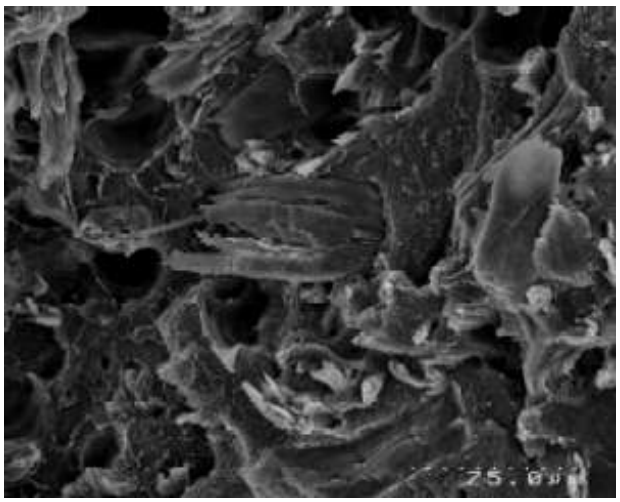

Figure 40. Wood fibre agglomeration micrograph.

The modulus values for glass fibre/LLDPE (Figure 41) differ for all tests, as expected. The tensile and flexural modulus values have a greater increase than the compressive modulus values. The tensile modulus values do tend to be greater than the flexural modulus and considerably greater than the compressive modulus.

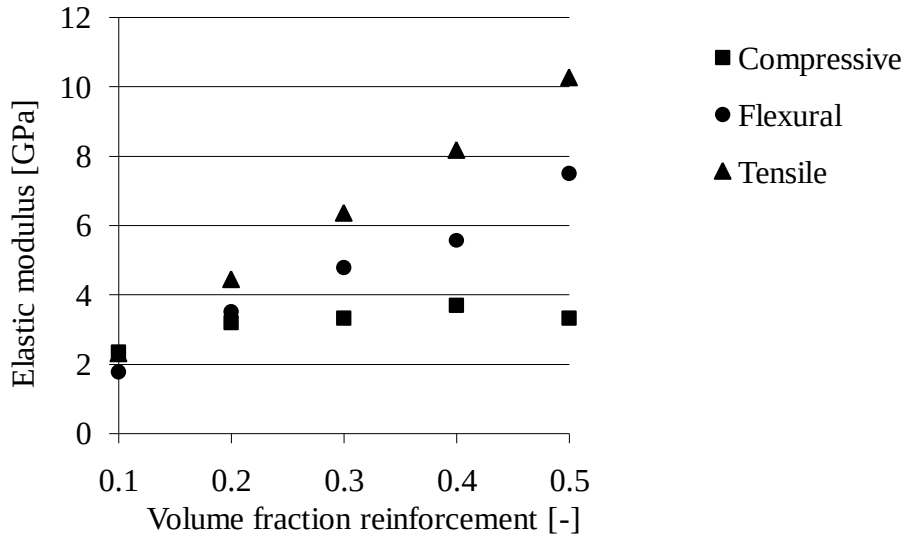

Figure 41. Modulus values for Glass fibre/LLDPE.

From inspection of the flexural test samples, (Figure 42), it is seen that when the sample deflection was great, failure occurred on the face of the bending test sample that was in tension. This may indicate that the compressive strength is greater than the tensile strength in contrast to the modulus values that show tensile modulus value above the compressive value.

Figure 42. Failure shown on glass fibre composite bend sample.

The carbon fibre/LLDPE samples, (Figure 43), give a similar trend to the glass-fibre samples. Tensile and flexural modulus values show a greater increase than the compressive modulus values. Carbon fibre is known to be optimally suited for tensile applications as opposed to compressive. It is also seen from inspection of the flexural test specimens that when the samples were loaded to break the failure occurred on the face of the bending test sample that was in tension. This once again may indicate that the compressive strength is greater than the tensile strength at large deflections.

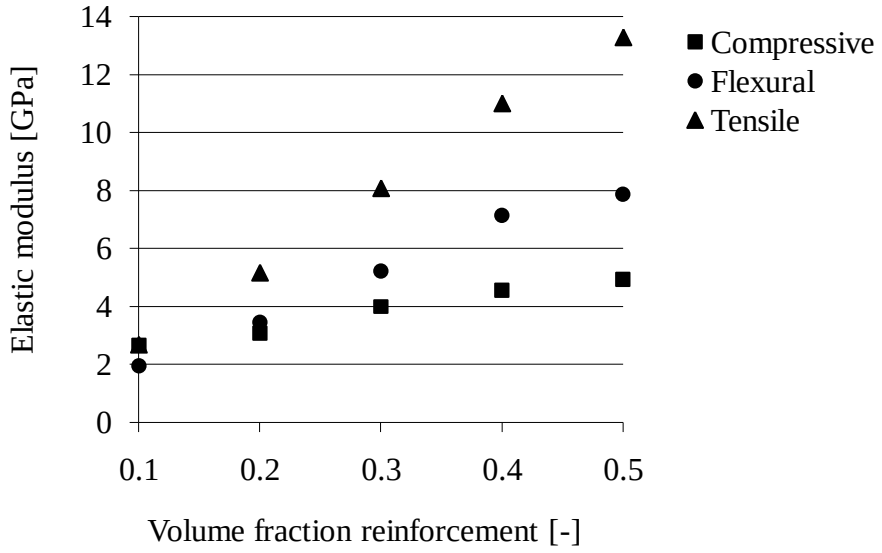

Figure 43. Modulus values for Carbon fibre/LLDPE.

The Aplax and Duralon paddle material (Table 12) show a similar trend when compared to the other materials. This indicates that the fibres are used to greater advantage with the materials under tensile loads. The modulus value obtained for the Duralon carbon paddle material, over the LLDPE carbon samples, under tensile conditions, indicates that the Duralon may be optimised for interfacial adhesion making full use of the superior tensile properties of carbon fibre.

Table 12. Modulus values from testing of paddle blade materials.

		Tensile	**Compressive**	**Flexural**
	Vf	**[Mpa]**		
Ba	0.3	7073	2455	4823
Mb/Gf	0.3	6364	3333	4790
Bd	0.33	22965	7162	8845
Mb/Cf	0.3	8084	4000	5225

The micrographs of Figure 44 and Figure 45 show comparison between the Duralon and the carbon fibre reinforced LLDPE. It can be seen that the Duralon shows intimate contact between components indicating superior bonding. The LLDPE/ carbon has less contact indicated by the apparent non-contact regions about the fibres.

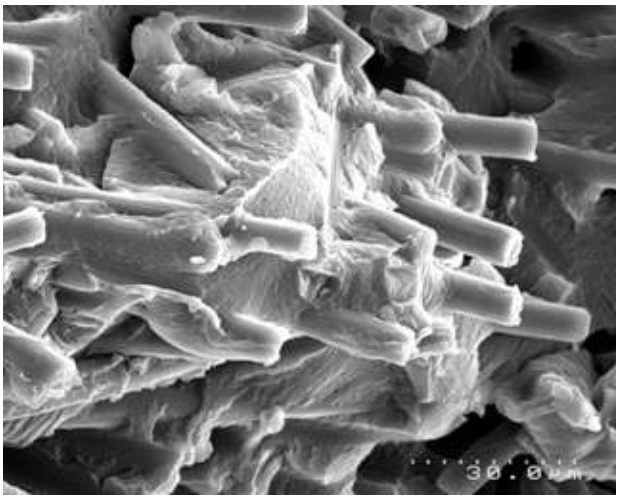

Figure 44. Duralon carbon fibre blade material showing superior adhesion.

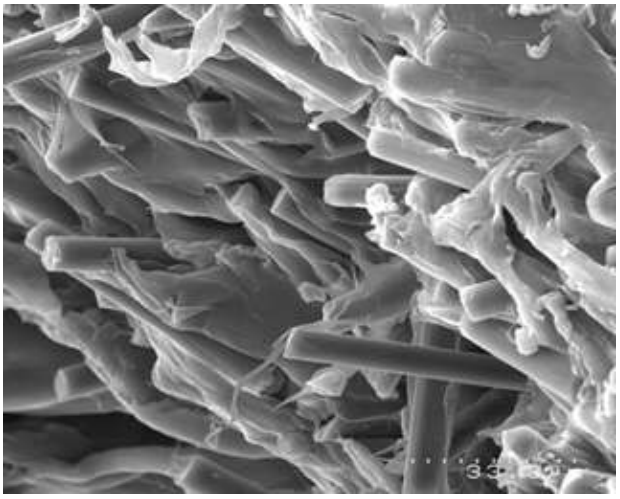

Figure 45. LLDPE/ carbon composite samples showing debonding.

7.2 Micromechanical models

Although the geometry is often very complex as seen in Figure 46, the fibre reinforcement and the encapsulating matrix create a layered structure. Simple beam theory may be used to analyse the composite by calculating the second moment of area of the geometry with respect to any number of layers, as appropriate for the given composite.

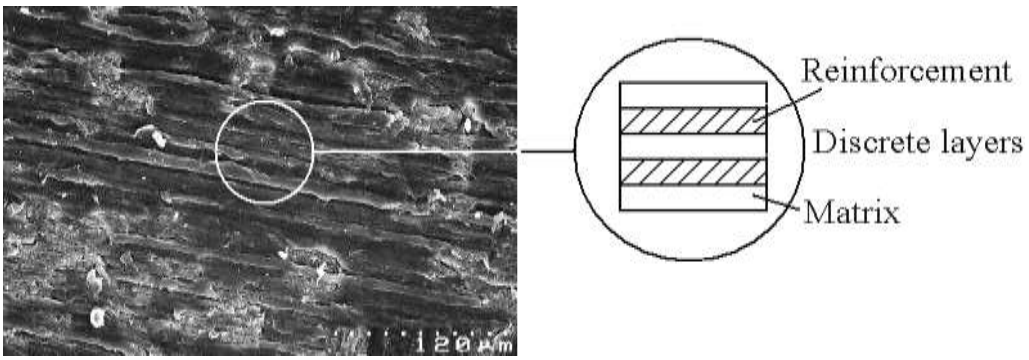

Figure 46. Micrograph section of PMC with layered simplification.

7.2.1 *Perfect bonding model*

This model considers every fibre to be fully embedded in matrix and that the bonding between phases is perfect.

Considering wood fibre composites (Figure 39) the fibres are not uniform and not cylindrical, but are flattened, irregular and hollow, partly as a result of processing.

From Figure 47 it can be seen that the k=1 (1 ply or 5 layers) PB model shows good agreement with experimental. The departure in accuracy above 40 vol% fibre is possibly from inadequate matrix encapsulation of the fibres.

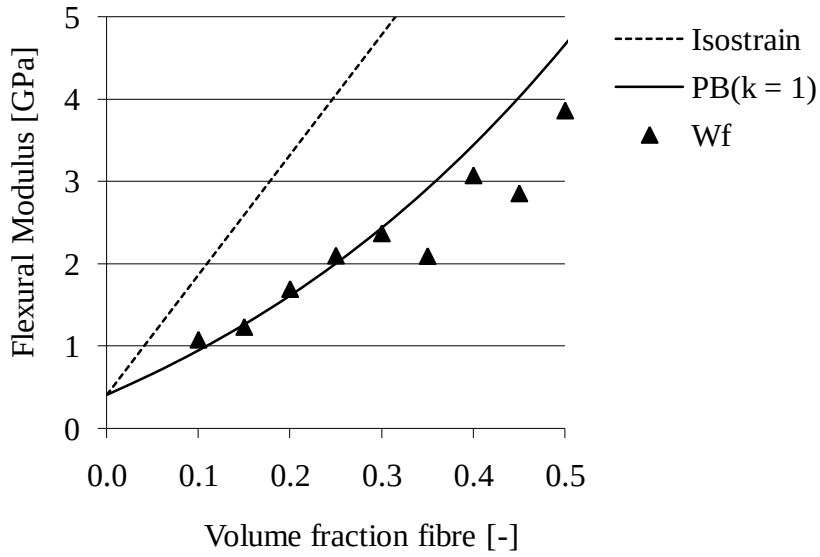

Figure 47. Wood fibre/LLDPE plot for perfect bonding model and values obtained from experimental.

Glass fibres have a regular geometry even after processing as shown in Figure 48. The rough surface of the glass fibre indicates mechanical bonding would be improved.

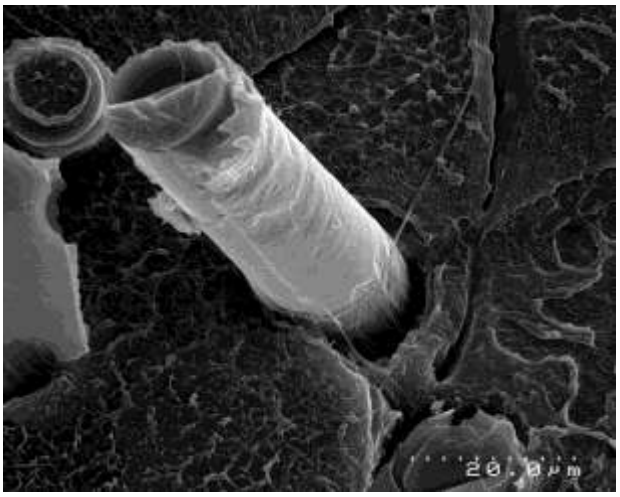

Figure 48. Glass fibre/ LLDPE micrograph.

Predictions for glass fibre/epoxy samples shown in Figure 49 show good agreement with k=1 PB model. At 50 vol% fibre the prediction is slightly higher, possibly due to fibre agglomeration not allowing the matrix material to completely wet each fibre.

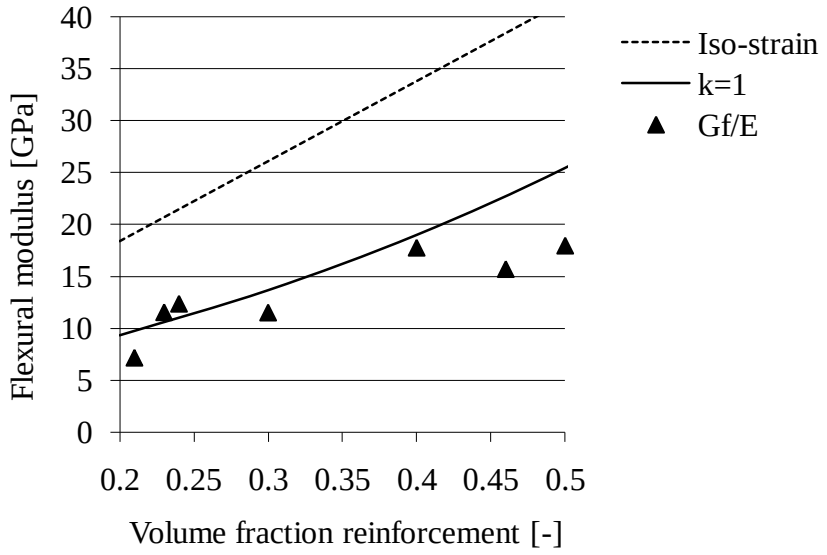

Figure 49. Glassfibre/Epoxy plot for the PB model and experimental values.

Glass fibre/LLDPE samples show different characteristics. Looking at Figure 50, it is seen that the k=1 PB model does not show good agreement with the experimental results.

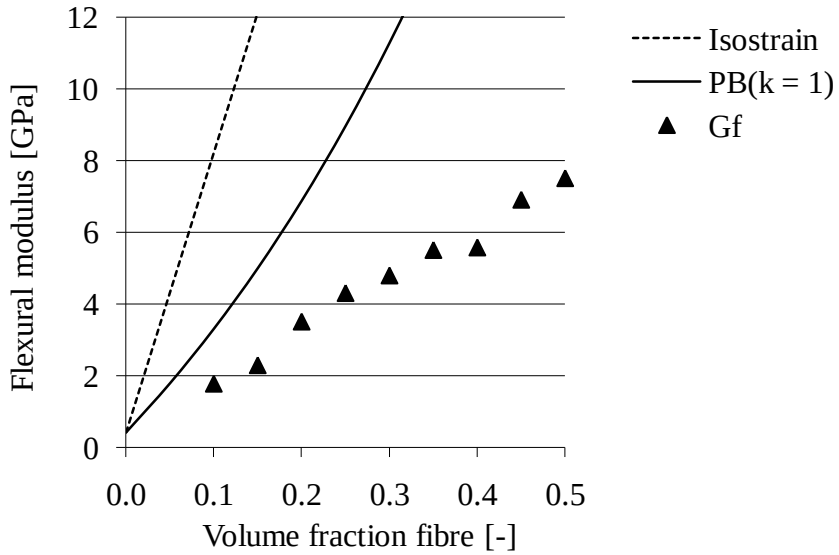

Figure 50. Glassfibre/LLDPE plot for the PB model and experimental values.

The carbon fibres, shown in Figure 51, are regular in shape with a longitudinally grooved surface appearance, showing little adhesion to the matrix.

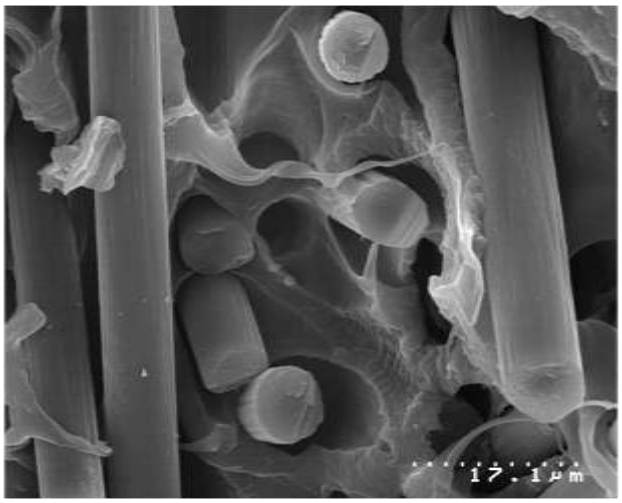

Figure 51. Carbon fibre/ LLDPE composite micrograph.

The predicted values for the carbon fibre/LLDPE using the perfect bonding model are not in agreement with the practical results as shown in Figure 52. The smooth appearance of the fibres and clear separation between fibres and matrix indicates that adhesion is poor.

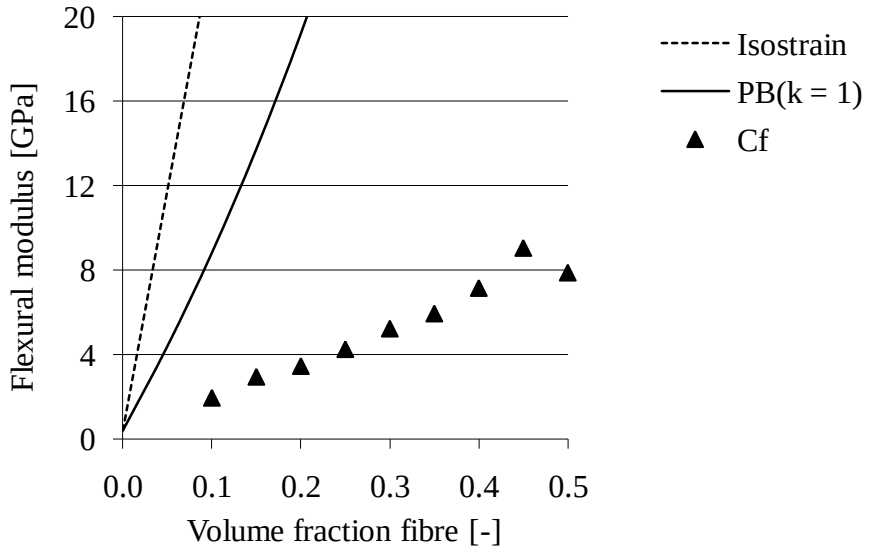

Figure 52. Carbonfibre/LLDPE plot for PB model and experimental values.

From the various composites tested, it is clear that in all cases the five layer model gave the best results although the results themselves where only in agreement for the wood fibre/LLDPE and the glass fibre/epoxy materials. This is somewhat unexpected since a large, but not infinite, number of layers would be more representative of the heterogeneous structure of the material. Five layers may be considered valid, but, it is expected that when refinements to the model are made the number of layers in the model would increase.

Although the wood fibres are seen to be irregular they do have surface structure conducive to good mechanical bonding. The glass fibres, although regular in geometry, have some surface irregularity that could also aid mechanical adhesion. Fibre agglomeration, within the composite systems, is probably due to the bundled nature of the reinforcing fibres in their raw state. No process was used to break apart the reinforcement fibre bundles to reduce agglomeration. Similar differences are seen for the carbon fibre which could explain the validation results. The carbon fibres were received with no coupling agents and nothing was done to improve the bonding with the LLDPE.

7.3 Frictionless model

The most prominent assumption with the PB approach is that of perfect adhesion. The contrasting case considers the discrete layers but disregards adhesion between components. It is not expected that this model would provide any relevance to the experimental data, but it increases understanding of the bonding component of the base model.

Bynel LLDPE is manufactured with functional groups to aid adhesion with reinforcement. To illustrate the effect of interfacial bonding regular moulding grade LLDPE was used as comparison. From the experimental data, shown in Figure 53, it was shown that the perfect bonding prediction is accurate when the functional LLDPE is used. The values obtained using the regular LLDPE/wood fibre is intermediate to that predicted by the perfect bonding and the frictionless model. As expected, the reduction in adhesion lowers the modulus value with this example typical of how poor bonding results in weaker mechanical properties.

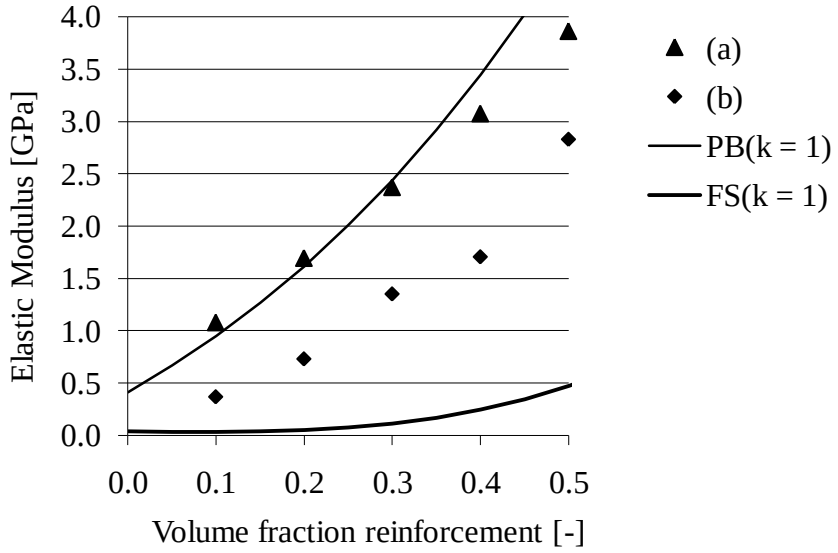

Figure 53. Modulus data shown for wood fibre reinforced a) Functional LLDPE and b) Regular LLDPE.

Values from the regular LLDPE/glass fibre and Bynel LLDPE/glass fibre composites (Figure 54) show that neither model is accurate and values fall between the PB and FS models. Glass fibres are known to show poor bonding with thermoplastics confirming that PB is an unrealistic expectation in the model.

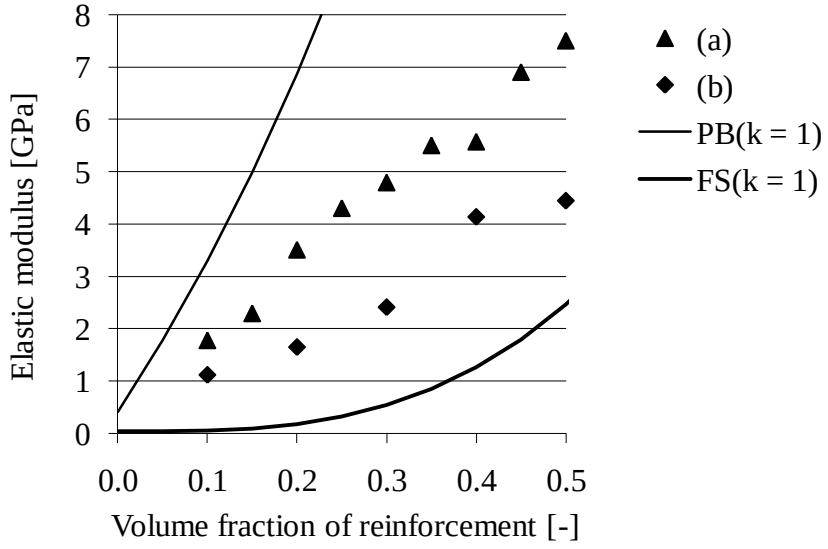

Figure 54. Modulus data shown for a) Functional matrix and b) Regular matrix with glass fibre reinforcement.

The LLDPE/carbon fibre composite (Figure 55) shows closer agreement with the frictionless prediction model than that of the perfect bonding model. This is an indication of poor bonding between the matrix and reinforcement components.

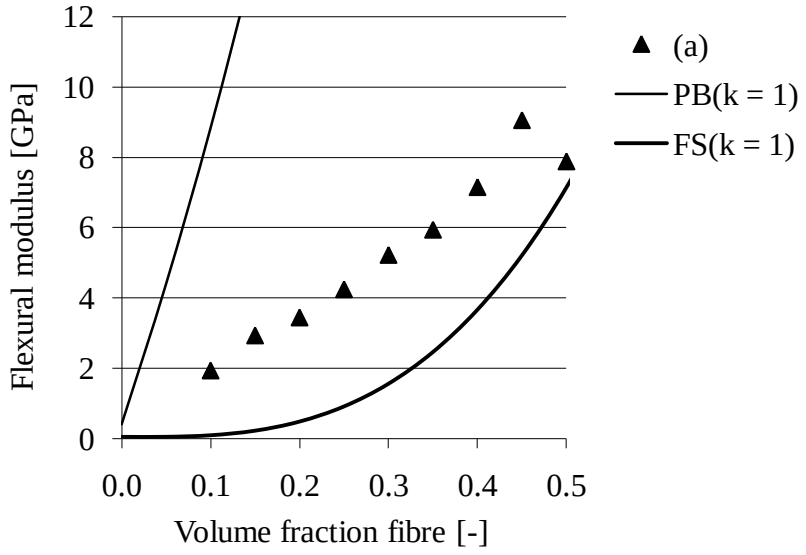

Figure 55. The frictionless model validated using experimental data from a) Bynel LLDPE/Carbon fibre samples.

The results, shown above, indicate the need to account for interfacial adhesion in modelling.

7.4 Partial adhesion model

By analysing the models, $E_{PB} = E_m(\Gamma_m + \Lambda_m) + E_f(\Gamma_f + \Lambda_f)$ for perfect bonding and $E_{FS} = E_m\Gamma_m + E_f\Gamma_f$ for the frictionless stack, it is proposed that the terms Λ_m and Λ_f are representative of the degree of adhesion between the matrix and reinforcement components.

The partial adhesion model, $E_{PA} = E_m(\Gamma_m + C_A\Lambda_m) + E_f(\Gamma_f + C_A\Lambda_f)$, incorporates a bonding coefficient, C_A, which may vary from zero to one. In order to fit the model to the wood fibre/ LLDPE composite, as seen in Figure 56, the interfacial coefficient will be 0.9 to validate the model when k=1 and 0.5 to validate the model when k=10.

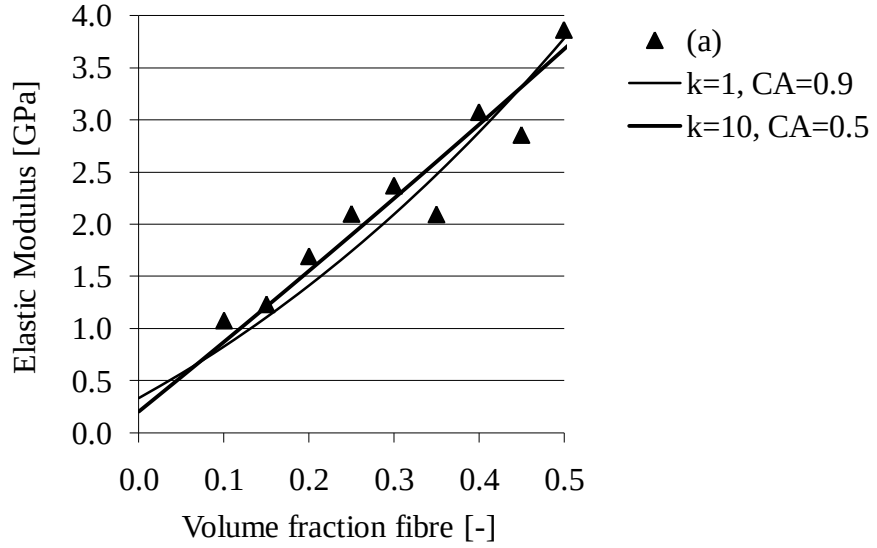

Figure 56. Predictions for Bynel LLDPE/Wood fibre, a) Experimental.

The results, shown as Figure 57, give good agreement with both predictive curves. The prediction, when k = 10 and C_A = 0.2 shows agreement through the whole range, while when k = 1 when C_A = 0.5 agreement is with the lower fractions only.

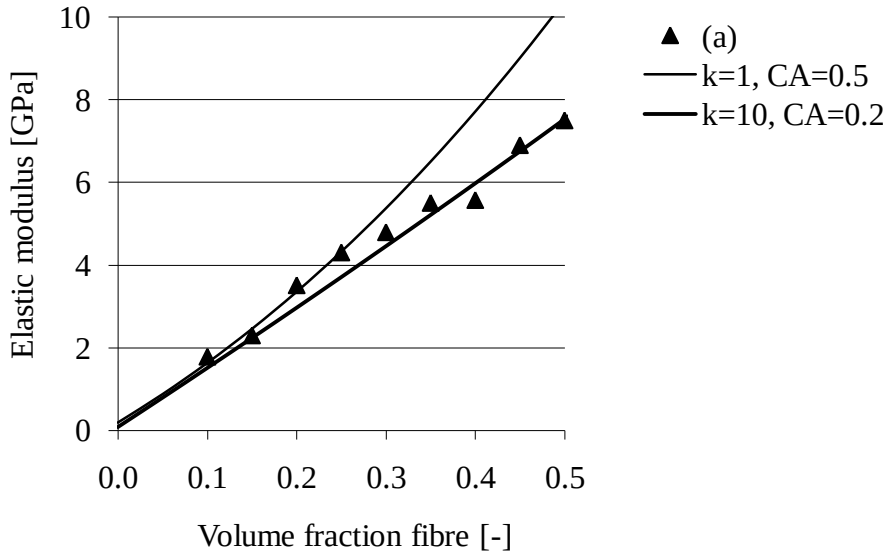

Figure 57. Predictions for Bynel LLDPE/Glass fibre, a) Experimental.

It is seen from Figure 58 that the predictions for the LLDPE/carbon fibre composite do not show agreement but do present an upper and lower limit from the k= 1 and k= 10 models considering C_A= 0.1. This reconfirms the previous observation that interfacial adhesion for the carbon fibre/ LLDPE composite system is very poor.

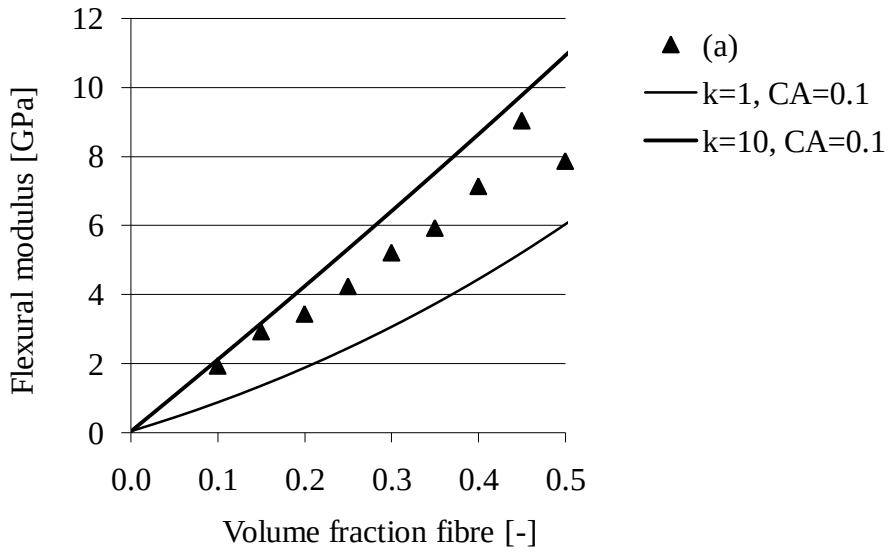

Figure 58. Predictions for Bynel LLDPE/Carbon fibre, a) Experimental.

From this section it can be concluded that accurate prediction is possible, using the partial adhesion model, providing an appropriate bonding coefficient is used. While it is possible to manipulate the partial adhesion model by changing the adhesion coefficient the basis for doing so must be proven. The adhesion coefficient is an indication of the interfacial strength between the matrix and reinforcement. If we consider the maximum adhesion value within a composite to be the lesser of the matrix or the reinforcement ultimate shear stress then it should be possible to find the ideal C_A value for any given system. The lower shear value will generally be from the matrix with its inherent low strength and high toughness.

To validate the selection of the C_A values, Table 13 shows effective shear values relative to the C_A. These values may be determined by considering the maximum shear stress at $C_A = 1$, and the minimum or zero effective shear, at $C_A = 0$. It has been reported that interfacial shear values for glass fibre PMCs' are approximately 40MPa. Although this would correspond to a $C_A = 0.5$ it is seen, from Figure 57, that a $C_A = 0.2$ is more accurate for the glass fibre/ LLDPE composite.

Table 13. Effective shear values from the given coefficient of adhesion.

Max. Tens	27.8 MPa
Max. Shear	69.6 Mpa
CA	**Effective shear**
0	0
0.1	6.96
0.2	13.92
0.3	20.88
0.4	27.84
0.5	34.8
0.6	41.76
0.7	48.72
0.8	55.68
0.9	62.64
1	69.6

All of the samples were made using the same injection moulding process and even though there were some differences in the processing parameters of the materials, this cannot be considered to have a major impact on the composite samples. The most obvious difference is seen to be the modulus ratio (Table 14). It is known that, as the modulus ratio increases the predictive ability of mechanical models is reduced [49]. This is due to stress concentrations at the edges (ends) as a load response. The stress concentrations are greater given a greater modulus ratio. It is reported that the stress concentrations cause component adhesion to fail at loads far below what the individual materials would characteristically fail under [49].

Table 14. Modulus ratio for each composite.

Material	**Modulus ratio**	
LLDPE/Wood fibre	15.0/0.414	36
LLDPE/Glass fibre	78.5/0.414	190
LLDPE/Carbon fibre	228/0.414	551

Processes, such as injection moulding, produce a transient melt-flow; this tends to produce poor fibre distribution and matrix impregnation in comparison to a process such as, compression moulding [41, 91]. As seen, with the wood fibre/ LLDPE composite, fibre agglomeration reduces dispersion of the fibres through the matrix and will lower mechanical properties [41]. Although agglomeration will reduce the dispersion of the fibres it may be considered that the orientation of

the agglomerates will reduce any preferential orientation due to processing in favour of a more uniform distribution [43].

Poor matrix impregnation is even more pronounced at high fibre fractions and will have a greater impact on mechanical properties although fibre agglomeration will be less noticeable. Their mechanical properties will still, however, be inferior, compared to long fibre unidirectional composites.

7.5 Practical application to sports equipment

Table 15 shows data for the kayak-paddle shafts that were tested. The calculated flexural modulus values differ from the predicted values attained from the perfect bonding model. This indicates that the interfacial adhesion for the hemp fibre shafts and carbon fibre shafts are less than ideal and that the interfacial adhesion for the glass fibre shafts are greater than that expected using the perfect bonding model with a k value of one.

Table 15. Data from paddle shaft flexural testing.

Shaft type	V_f	ν	ρ	Load	Modulus [Gpa]				
				[N]	Exp.	PB	PA	C_A	k
Hemp/Epoxy	0.25	0.34	1.21	50	2.30	5.74	2.30	0.3	3
Glass/Epoxy	0.55	0.27	1.98	100	32.50	26.89	32.50	0.8	18
Carbon/Epoxy	0.60	0.20	1.45		67.42	94.05	67.64	0.5	8

The partial adhesion model can be adapted to fit the experimental results as shown in Table 15 values for k and C_A. As a means to validate selection of the adhesion coefficient values we can use effective shear values as shown in Table 13. This would however require some validation in the form of empirical data.

It was noted also that failure for all of the shafts occurred on the side of the shaft that was in compression during the bend test. This compressive failure mode was not seen in the original composite beam samples and indicates that the beam cross section may have a bigger effect than initially thought.

Maximum fibre loading is used in equipment to capitalise on high specific properties. At high loadings fibres directly contacting each other can bend, break or misalign relative to any preferential orientation. Bent or misaligned fibres will yield more easily than aligned fibre when compressed due to buckling. During a tensile test bent or misaligned fibres could realign as the strain increases [41]. With flexural testing, the samples are subjected to both tensile and compressive forces where bent or misaligned fibres would alter the response of the composite as discussed. These concerns will be a barrier to predictive modelling even with the most stringent quality control in many composite test specimens.

7.6 The virtual design approach

CAD models may be extremely complex when considering composite materials and structures. The external structure will often span several dimensional scales, for example, the carbon paddle shaft length may be 500mm, the wall thickness 1.1mm, and the reinforcement fibre diameter 7.2µm. The number of individual parts within a direct 3D solids model of this shaft would be in the hundreds of thousands. These CAD files may also require translation into a suitable format for simulation within a FEA environment. The interaction between components must be specified and may include bonded parts, frictional conditions and material variations throughout the section. Computation files become very large and the computing power required to adequately handle the files becomes unrealistic. These considerations support the analog approach to simulation; in order to effectively do this, however, suitable mechanical data is required.

7.6.1 *Computer Simulation*

Based on the analog modelling approach, simulation of beams and cylinders during three point bending is investigated using CosmosWorks.

7.6.2 *Model specifications*

Analog models of paddle shafts were created in Solidworks using the test sample dimensions and materials properties given in Table 16.

Table 16. Paddle shaft specifications.

Material	**Shaft OD**	**Shaft thickness.**	**Fibre diam.**	**Density**	**Elastic mod.**	**Poisson**
	mm			**[g/cm^3]**	**[Gpa]**	**[-]**
SP Epoxy	N/A			1.22	3.17	0.35
ADR 246 Epoxy				1.14	3.38	0.35
Hemp fibre	28.0	3.33	0.050	1.40	25.00	0.30
Glass fibre	27.9	1.25	0.015	2.60	73.00	0.20
Carbon fibre	27.6	1.10	0.008	1.61	235.00	0.10

7.6.3 *Pre-processing*

Analysis time depends on the type and number of elements, the number of nodes, the node displacements, and the accuracy required of the analysis. The small size of the reinforcement, in comparison to the full shaft, increases the number of elements, the degrees of freedom and the file size, and highlights the preference for simplified models. This will be a concern for any composite material.

7.6.4 *Simulation*

Using analog CAD models, (Section 5.2), flexural loading of the paddle-shafts was simulated (Figure 59). The composite elastic modulus values needed for simulation were calculated using the micromechanical models for perfect bonding (E_{Pb}) and partial adhesion (E_{PA}).

Figure 59. Virtual shaft testing using COSMOSWorks.

7.6.5 *Simulation of loaded test samples*

Because the analog approach is used the sample geometry (Table 17) does not account for the composite components as individual materials. The flexural modulus values for simulation of the composites, in Table 18, are determined from the predictive models for perfect bonding (PB) and partial adhesion (PA).

Table 17. Analog beam model dimensions and pre-processing data.

Beam dimensions	**[mm]**	(b) 12.5 x (d) 3.2 x (l)51.4
Element size		1.6
DOF		15657
Load	**[N]**	1.0

Table 18. Predicted modulus from PA and PB.

Reinforcement	V_f	ν	ρ	PB [Gpa]	PA [Gpa]	CA	k	PA [Gpa]	CA	k
Wood fibre	0.1	0.44	0.98	0.95	0.86	0.9	1	0.50	0.5	1
	0.2	0.42	1.02	1.62	1.46			0.84		
	0.3	0.41	1.07	2.44	2.21			1.28		
	0.4	0.39	1.12	3.45	3.13			1.85		
	0.5	0.38	1.17	4.67	4.25			2.57		
Glass fibre	0.1	0.43	1.10	3.30	1.51	0.2	10	0.70	0.5	1
	0.2	0.40	1.26	6.87	2.97			1.52		
	0.3	0.38	1.43	11.30	4.46			2.69		
	0.4	0.35	1.60	16.70	5.98			4.34		
	0.5	0.33	1.77	23.20	7.53			6.60		
Carbon fibre	0.1	0.42	1.02	8.83	2.12	0.1	10	0.96	0.1	1
	0.2	0.38	1.11	19.20	4.25			2.35		
	0.3	0.35	1.19	32.00	6.42			4.60		
	0.4	0.31	1.28	47.80	8.65			8.07		
	0.5	0.28	1.37	66.80	10.90			13.10		

In Figure 60 it can be seen that the deflection values from the experimental are well matched to the simulation data for both the PA and PB models, using C_A = 0.9 and k = 1.

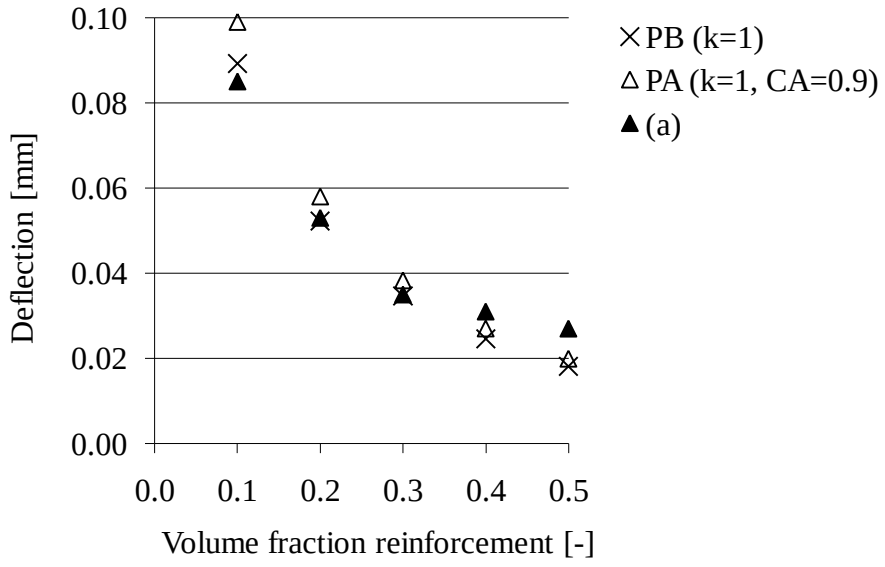

Figure 60. Wood fibre composite simulation data, a) experimental values.

The simulation process used solid mesh elements and the FFE iterative solver, considered suitable for this type of problem [92]. The direct sparse solver and the FFE plus iterative solver could also be used in this case, but it was found that the only effect was to increase the simulation time. Direct solvers are considered for materials with different modulae of elasticity in the same problem and should therefore only be considered for the iconic or semi-iconic models. The FFE plus solver should only be considered for problems with more than 100,000 DOF, this case was less than 16,000 DOF.

The simulation results for the glass fibre composites, (Figure 61), show good agreement with the PA model given $C_A = 0.2$ and $k = 10$. It was found that the assumption of perfect bonding is inappropriate although the trend is similar. This would indicate that the adhesion between the components is not ideal and that the interfacial stresses may be increased due to the differences in modulae.

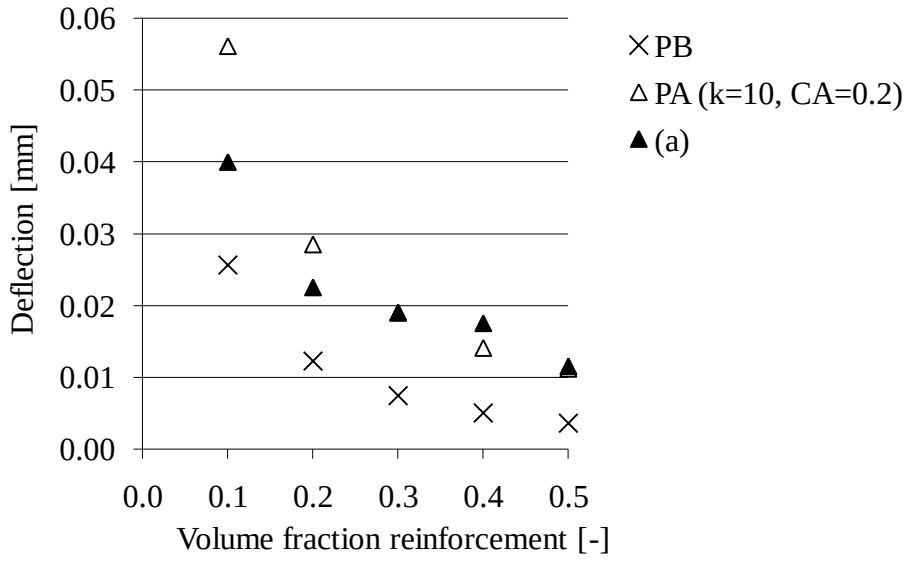

Figure 61. Glass fibre composite simulation data, a) experimental values.

The carbon fibre composites gave similar results to the glass fibre composite, (Figure 62). The PB model produced results far below the experimental values. The results infer that the composite itself has poor interfacial bonding. Using the PA model proved most reliable using $C_A = 0.1$ and $k = 10$.

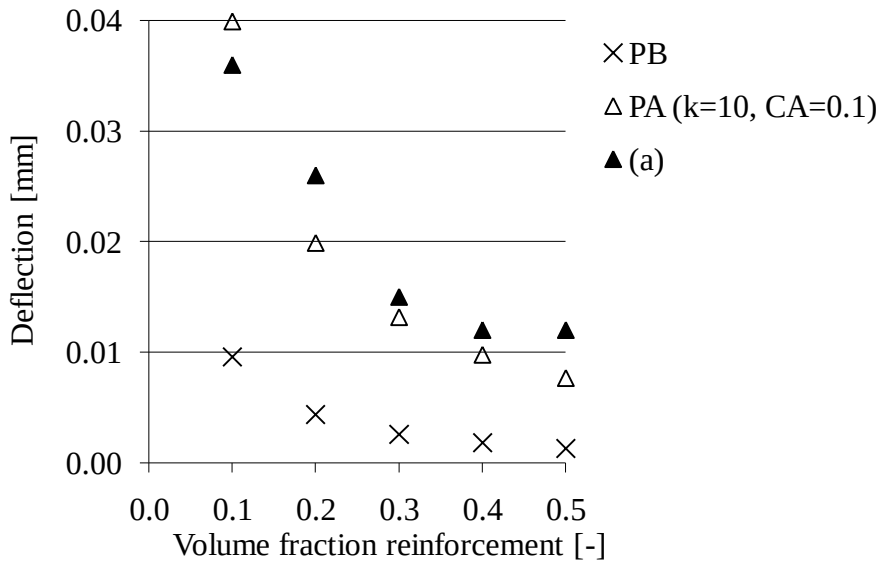

Figure 62. Carbon fibre composite simulation data, a) experimental values.

7.6.6 *Simulation of loaded shaft samples*

Solid models of commercially manufactured composite paddle-shafts were produced and simulated under three point bending. The response to loading, of the simulated shafts, is compared to the experimental values gained from the actual shafts and shown in Table 19.

Table 19. Shaft deflection values from experimental and simulated loading.

Shaft type	Deflection [mm]				
	Exp.	PB	PA	CA	k
Hemp/Epoxy	2.20	0.92	2.31	0.5	1
Glass/Epoxy	0.86	0.77	0.63	0.5	1
Carbon/Epoxy	0.50	0.25	0.35	0.1	1

The simulation data for the shafts does not correspond well with the experimental results. The hemp/epoxy shaft is most closely simulated with a deflection value within 5% of the experimental value at $C_A = 0.5$. The glass/epoxy shaft is closely simulated by the PB modulus value to 10% with the PA model requiring a $C_A = 0.5$. The carbon/epoxy shaft has simulation within 16% with the PA value at $C_A = 0.5$ indicating that the adhesion is poor for the given modulus properties of the reinforcement.

The results for the paddle-shafts do not provide the intended accuracy. The main difference between the paddle-shafts and the ASTM test samples is the reinforcement. The hemp, glass and carbon reinforcement used for construction of the shafts were all woven cloth with continuous fibres oriented at 0^o and 90^o to the shaft axis to account for bending and torsional effects. It would also be expected that the composite systems used in production of the glass fibre and carbon fibre shafts would be chosen to capitalise on optimum compatibility for their purpose. This is not the case for the hemp fibre shaft where the system itself is by no means idealised to give maximum performance.

It was also noted that the side of the shaft in compression failed first during the bend tests. This was not seen with the original test samples where the side in tension failed.

8 Conclusions

The sport and leisure industry in New Zealand has the potential to become a major user of composite materials and could benefit from development of appropriate virtual design and manufacturing strategies. Use of virtual engineering methods to find faults, explore alternatives, and optimise product performance before detailed design or prototyping could greatly improve preproduction efficiencies. This approach could also encompass strategies that include materials design in order to benefit equipment development.

Solids' modelling was used to produce analog models of fibre reinforced composite materials that portrayed behavioural characteristics of a composite but not the physical characteristics of the individual components. The analog approach has lead to significant reductions in file size but required material properties for further design verification.

The mechanical properties of individual reinforcement and matrix components are well documented, either in general literature or from manufacturers' data. However, mechanical properties for composites are not as well documented. This presented a problem that was addressed with the use of micro-mechanical modelling.

Perfect bonding, no-adhesion and partial adhesion micro-mechanical models were developed. With regard to the mechanical properties of composite materials the interfacial adhesion showed to be the most important factor. Of the three models the partial adhesion model was proven to be the most adaptable. The partial adhesion model accounted for adhesion between components by considering an 'effective shear value' at the interface. Validation of the models was done by flexural testing injection moulded samples of glass, wood and carbon short fibre reinforced polyethylene.

It was possible to manipulate the partial adhesion model by changing the adhesion coefficient and the number of plies and it was found that it can be successfully done by relating the shear strength of the matrix material, to the adhesion coefficient, termed the effective shear value.

It was shown that the adhesion coefficient range was 0.1 for carbon fibre, 0.5 for glass fibre to 0.9 for the wood fibre composites. It was concluded that the adhesion coefficient is crucial and it is recommended that further work is to be done to validate effective shear values by empirical means. This would enable the partial adhesion model to predict elastic modulus values based on the materials and processing methods used for manufacture of sporting equipment.

The elastic modulus values determined from the partial adhesion model were used in FEA simulation of paddle shafts. The predictive data was adapted for simulation from the initial validation. The adhesion coefficient range was 0.1 for carbon fibre, 0.5 for glass fibre and 0.5 for the hemp fibre composite shafts. Although the simulation required empirical adjustments to improve the results it was shown that the unadjusted values gave improvements over mechanical properties taken from reference texts or mixture rules.

The simulation functionality within many CAD packages has long been considered a design aid suitable for comparison of known systems and not suitable for unknown systems. From this work it has been shown that CAD functionality can be extended, with the use of a simple predictive model, to assist in materials design by eliminating complex geometries, reducing pre-processing time and minimising simulation time.

.

References

1. Katsanis, D. and S.M. Grove. *Design and prototype manufacture of a bicycle frame.* in *The 1st International Conference on the Engineering of Sport*. 1996. Sheffield, united Kingdom.

2. Easterling, K.E., *Advanced Materials for Sports Equipment*. 1993, London: Chapman and Hall.

3. Hendry, M.A. and M. Hubbard. *Effects of rod taper on fly casting performance*. in *The 4th International Conference on the Engineering of Sport*. 2002: Blackwell Science.

4. Carreira, R.P., Q.H. Ly, and G. Lagante. *A Bicycle Frame Finite Element Analysis: Standard Tests and Common Cycling Situations Simulation*. in *The 4th International Conference on the Engineering of Sport*. 2002: Blackwell Science.

5. Stanbridge, K., R. Jones, and S. Mitchell, *The effect of shaft flexibility on junior golfers performance*. 2003, Loughborough University. p. 18.

6. Herrera-Franco, P.J. and A. Valadez-Gonza´lez, *Mechanical properties of continuous natural fibre-reinforced polymer composites.* Composites: Part A: Applied Science and Manufacturing, 2004. **35**: p. 339–345.

7. McCauley, C.J., ed. *Machinerys Handbook*. 26th ed. 2000, Industrial Press inc.: New York. 571-577.

8. Statistics New Zealand. *New Zealand Business Demographic Statistics At February 2005*. [Web page] 2005 February 2005 [cited 2006 5 March]; Available from: http://www2.stats.govt.nz/domino/external/pasfull/pasfull.nsf/7cf46ae26dcb6800cc256a62000a2248/4c2567ef00247c6acc2570bd000fb33a?OpenDocument.

9. MarketNewZealand.com. *Sports equipment industry profile*. 2002 [cited 2006 6 April]; Available from: http://www.marketnewzealand.com/MNZ/aboutNZ/sectors/14368/13159.aspx.

10. van Aalst, I., D. Kazakov, and G. McLean, *SPARC Facts '97-'01*. 1997, SPARC.

11. ubd.co.nz online business directory. *NZ Business*. [Keyword search, Sports equipment] 2006 [cited 2006 6 March]; Available from: http://www.ubd.co.nz/.

12. ubd.co.nz online business directory. *NZ Exports and Imports*. [Keyword search, Sports equipment] 2006 [cited 2006 6 March]; Available from: http://www.nzexporters.co.nz/search/directory_search.asp?Action=S.

13. yellowpages.co.nz. *Sporting Goods in New Zealand*. [Keyword search, Sports Equipment New Zealand.] 2006 [cited; Available from: http://www.yellowpages.co.nz/Pages/Search/Results/Cached/0,2837,a6001_b6216_c1531_l0_m0,00.html.

14. Moxson, V.S. and F.H. Froes, *Fabricating Sports Equipment Components via Powder Metallurgy*. Journal of Materials Science, 2001. **53**(4): p. 39.

15. Desbordes, M., *Empirical Analysis of the Innovation Phenomena in the Sports Industry*. Technology Analysis & Strategic Management, 2002. **14**(4): p. 481-498.

16. Kodama.H and Maeda.Y, *Development of Large-Scale Composite Masts for the Americas Cup Racing Yachts*, in *Comprehensive Composite Materials*, A. Kelly, C. Zweben, and e. al, Editors. 2000, Elsevier Science Ltd, UK: Oxford. p. 451-457.

17. McConnell, V.P., *Applications of composites in sporting goods*, in *Comprehensive Composite Materials*, A. Kelly, C. Zweben, and e. al, Editors. 2000, Elsevier Science Ltd., UK: Oxford. p. 787-809.

18. Hosking, A.K. and M.R. Harris, *Applied Mechanical Design*. Third ed. 1997, Victoria: H&H Pubishing. lots.

19. Crabb, H., C, *The Virtual Engineer: 21st century product development*. 1998, Dearborn: Society of Manufacturing Engineers. 166.

20. Lemon, J., *The Value of Simulation-Driven Design.*, in *ANSYS Solutions*. 2005. p. 29-32.

21. Stickler, P.B. and M. Ramulub, *Parametric analyses of stitched composite T-joints by the finite element method.* Materials and Design, 2002. **23**: p. 751–758.

22. Beaumont, P.W.R. and H. Sekine, *Physical Modelling of Engineering Problems of Composites and Structures.* Applied Composite Materials, 1999. **7**: p. 13–37.

23. McDowell, D.L., *Foreword.* Journal of Computer-Aided Materials Design: Special Issue: Design of Heterogeneous Materials, 2004. **11**: p. 81-83.

24. Tuttle, M.E., *Structural analysis of composite materials.* 2004, Washington: Marcel Dekker Inc. 0-8247-4717-8.

25. Chawla, K.K.E., *Composite Materials, Science and Engineering.* Vol. Second. 1998, New York: Springer-Verlag.

26. Hannah, J. and M.J. Hillier, *Applied Mechanics*. Third metric ed. 1995, Essex: Longman Scientific & Technical. 448.

27. Shao-Yun, F., H. Xiao, and Y. Chee-Yoon, *The flexural modulus of misaligned short fiber reinforced polymers.* Composites Science and Technology, 1998. **59**: p. 1533 - 1542.

28. Strong, B., *In the Beginning.* Composites, 1996: p. 9-15.

29. Clarke, J.L., ed. *Structural Design of Polymer Composites. Eurocomp Design Code and Handbook.* 1 ed. 1996, E & FN Spon: London. 751.

30. Dept. of Defense USA, ed. *The Composite Materials Handbook MIL-17, Polymer Matrix Composites: Materials, Usage, Design and Analysis.*, ed. A. International. Vol. 3. 2002.

31. Jenkins, M., *Advanced materials and sporting performance.* Interdisciplinary Science Reviews, 2002. **27**(1): p. 61-66.

32. Ewart, P.D. and K.P. Pickering. *Sports Equipment Development; Materials, Design and the Future*. in *Young People, Sport and Physical Activity: Healthy Futures?* 2004. Hamilton NZ.

33. Kelly, A., *Concise Encyclopedia of Composite Materials*. Revised ed, ed. A. Kelly. 1994: Elsevier Science. 349.

34. Higgins, R.A., *Properties of Engineering Materials*. 2Rev ed. 1995, London: Edward Arnold. 495.

35. Harris, B., *Engineering Composite Materials*. Second ed. 1999, Cambridge: The University Press, UK.

36. Dieter, G.E., *Engineering Design. A Materials and Processing Approach*. 3RD ed. 2000, Singapore: McGraw-Hill Book Co.

37. Dominghaus, H., *Plastics for Engineers. Materials, Properties, Applications.* 1993: Hanser.

38. Luo, S. and A.N. Netravali, *Interfacial and mechanical properties of environment-friendly "green" composites made from pineapple fibers and poly(hydroxybutyrate-co-valerate) resin.* Journal of Materials Science, 1999. **34**: p. 3709-3719.

39. Cox, H.L., *The elasticity and strength of paper and other fibrous materials.* British Journal of Applied Physics, 1951. **3**: p. March.

40. Goda, T., et al., *Finite element analysis of a polymer composite subjected to a sliding steel asperity: Part I Normal fibre orientation.* Journal of Materials Science, 2002. **37**: p. 1575 – 1583.

41. Thomason, J.L. and M.A. Vlug, *Influence of fibre length and concentration on the properties of glass fibre-reinforced polypropylene: 1. Tensile and flexural modulus.* Composites: Part A, 1995. **27**: p. 477-484.

42. Mariatti, M. and P.K. Chum, *Effect of Resin:Fiber Ratio on the Properties*

of Glass Fiber Reinforced Plastic Composites. International Journal of Polymeric Materials, 2004. **54**: p. 975-984.

43. Rakow, J.F. and A.M. Waas, *The Effective Isotropic Moduli of Random Fibrous Composites, Platelet Composites, and Foamed Solids.* Mechanics of Advanced Materials and Structures, 2003. **11**: p. 151-173.

44. Ashbee, K., *Fundamental Principles of Fiber Reinforced Composites*. 1993: Technomic Publishing co. 424.

45. Folkes, M.J. and S.T. Hardwick, *The mechanical properties of glass/polypropylene mutilayer laminates.* Journal of Materials Science, 1990. **25**: p. 2598-2606.

46. Haboussi, D., D. Helene, and L. Jean, *Proposal of refined interface models and their application for free-edge effect.* Composite Interfaces, 2001. **Vol. 8,**(No. 1,): p. pp. 93–107.

47. Lutz, M.P. and R.W. Zimmerman, *Effect of the Interphase Zone on a Bulk Modulus of a Particulate Composite.* Journal of Applied Mechanics, 1996. **63**: p. 855-861.

48. Matthews, F.L. and R.D. Rawlings, *Composite materials: Engineering and science*. 1999, Cambridge: Woodhead Publishing Limited. 470.

49. Sharpe, L.H., *The Interphase of Adhesion.* Journal of Adhesion, 1971. **4**: p. 51-64.

50. Neamul Alam, S., *The Characterisation of Natural Fibres and their Interfacial and Composite Properties*, in *Materials Engineering*. 2004, Waikato: Hamilton. p. 109.

51. Naik, N.K. and e. al, *Impact response and damage tolerance characteristics of glass-carbon/ epoxy hybrid composite plates.* Composites: Part B, 2001. **32**: p. 565-574.

52. Aziz, S.H. and M.P. Ansell, *The effect of alkalization and fibre alignment on the mechanical and thermal properties of kenaf and hemp bast fibre composites: Part 1 – polyester resin matrix.* Composites Science and Technology, 2003. **64**: p. 1219-1230.

53. Haijun, L. and M.S. Mohini, *High Stiffness Natural Fiber-Reinforced Hybrid Polypropylene Composites.* Polymer-Plastics Technology and Engineering, 2003. **Vol. 42**(No. 5): p. pp. 853–862.

54. Sebe, G., et al., *RTM Hemp Fibre-Reinforced Polyester Composites.* Applied Composite Materials, 2000. **7**: p. 341-349.

55. d'Almeida, J.R.M., *Analysis of Cost and Flexural Strength Performance of Natural Fiber-Polyester Composites.* Polymer-Plastics Technology and Engineering, 2001. **40**(2): p. 205–215.

56. MATTER Project Team. *Materials Science on CD-ROM*. [CD-ROM] 1998 [cited; Version 2.1:[

57. O'Brien, T.K. and R. Kruegar, *Analysis of ninety degree flexural tests for characterisation of composite tensile strength.* 2001, US Army Research Laboratory: Hampton.

58. Arnautov, A.K. and Y.M. Tarnopol'skii, *Longitudinal Flexure as a Method for Determining the Flexural Strength of Composite Materials.* Mechanics of Composite Materials., 2004. **40**(1): p. 17-28.

59. Gorik, A.V., *Theoretical and Experimental Deformation Parameters of Composite Beams with account of Deplanation of Cross section in Bending.* Mechanics of Composite Materials, 2003. **39**(1): p. 57-64.

60. Heger, J. *Combined Tensile-Bending Load Simulation of the Notched Thick Wall Multi-Layer Laminate Composite used for Aircraft Body Building.* [Web Site Industry Paper.] [cited 2002 15 June 2002]; Available from: http://www.ansys.com/industry/aerospace/conference_papers/heger3.html.

61. Hou, J.P. and G. Jeronimidis, *Bending stiffness of composite plates with delamination.* Composites: Part A: Applied science and manufacturing, 1999. **31**: p. 121-132.

62. Vipulanadan, C. and S. Mebarkia, *Flexural strength, toughness, and fracture properties of polyester composites.* Journal of Applied Polymer Science, 1993. **50**(7): p. 1159-1168.

63. Hsueh, C.-H., *Youngs modulus of unidirectional discontinuos-fibre composites.* Composites Science and Technology, 2000. **60**: p. 2671-2680.

64. Blanc, M. and M. Touratier, *Modelling Elastic and Thermoelastic Thick Multilayered Composites by a New Constrained Discrete Layer Approach.* Mechanics of Advanced Materials and Structures, 2005. **13**: p. 95-114.

65. Crookston, J.J., A.C. Long, and I.A. Jones, *A summary review of mechanical properties prediction methods for textile reinforced polymer composites.* Journal of Materials, Design and Applications, 2004. **219**(L2): p. 91-109.

66. Ward, M., *Mechanical anisotropy of highly oriented polymers.* Journal of Computer-Aided Materials Design, 1996. **4**: p. 43-52.

67. Alfano, G., et al., *MITC finite elements for laminated composite plates.* International Journal for Numerical Methods in Engineering., 1999. **50**: p. 707-738.

68. Hong-Yuan, L. and M. Yiu-Wing, *An appraisal of composite interface mechanics models and some challenging problems.* Composite Interfaces, 1998. **6**(4): p. 343-362.

69. Hobbs, S.Y., *Predicting the Flexural Rigidity of Thermoplastic Structural Foams.* Journal of Cellular Plastics, 1976. **12**(5): p. 258-263.

70. Golas, J., et al., *On an approach to the solution of the bending problem for laminated plates.* Mechanics of Composite Materials, 2002. **38**(3): p. 253-262.

71. Liu, D. and X. Li. *Analysis of Composite Laminates with a Generalised Zigzag theory.* in *The American Society for Composites. Ninth technical Conference.* 1994.

72. Jacquet, E., F. Trivaudey, and D. Varchon, *Calculation of the Transverse Modulus of a Unidirectional Composite Material and of the Modulus of an Aggregate: Application of the Rule of Mixtures.* Composites Science and Technology, 1998. **60**: p. 345-350.

73. Sims, G.D., et al., *Glass Fiber Reinforced Plastics--Properties*, in *Comprehensive Composite Materials*. 2000, Pergamon: Oxford. p. 151-197.

74. Endruweit, A. and P. Ermanni, *Experimental and numerical investigations regarding the deformation-adapted design of a composite flex slalom skateboard.* Sports Engineering, 2002. **5**: p. 141–154.

75. Cross, R., *Impact of a ball with a bat or racket.* American Journal of Physics, 1999. **67**(8): p. 692-702.

76. Cross, R., *Customising a tennis racket by adding weights.* Sports Engineering, 2001. **4**(8): p. 1-14.

77. Suzuki, S., S.J. Haake, and B. Heller. *Skill Analysis of the Wrust Release in Golf Swing to Utilise Shaft Elasticity*. 2005. Tokyo: Australasian Sports Technology Alliance.

78. Guz, I. and Y. Rushchitskii, *Comparison of Mechanical Properties and Effects in Micro and NanoComposites with Carbon Fillers (Carbon Microfibers, Graphite Microwhiskers, and Carbon Nanotubes).* Mechanics of Composite Materials, 2004. **40**(3).

79. Smith, D.J. and P.G. Partridge, *Flexural stiffness envelopes for planar multilayered systems containing two dissimilar materials.* IMechE Proc Instn Mech Engrs, 1999. **213**(Part L): p. 1-20.

80. Verbeek, C.J.R., *The Youngs' modulus of compression moulded LLDPE-phlogopite composites*, in *Dept. of Chemical Engneering*. 2001, Unversity of Pretoria: Pretoria. p. 100.

81. Meddad, A. and B. Fisa, *Filler-matrix debonding in glass bead-filled polystyrene.* Journal of Material Science, 1997. **32**: p. 1177-1185.

82. Crawford, R.J. and Y. Yigsaw, *A study on the effect of test variables on the flexural modulus of plastics.* Journal of Materials Science Letters,

1983(3): p. 171-176.

83. Gere, J.M. and S.P. Timoshenko, *Mechanics of Materials*. Third ed. 1993: Chapman and Hall.

84. Vable, M., *Chapter 6: Symmetric Bending of Beams*, in *Mechanics of Materials*, M. Vable, Editor. 2002, Oxford University Press: USA. p. 6-(1-37).

85. ASTM D 790, *Standard test method for flexural properties of unreinforced and reinforced plastics and electrical insulating materials*, in *ASTM materials standards*, ASTM Committee D-20 and D. Subcommittee, Editors. 2003.

86. ASTM D 638, *Standard test method for tensile properties of unreinforced and reinforced plastics and electrical insulating materials*, in *ASTM materials standards*, ASTM Committee D-20 and D. Subcommittee, Editors. 2004.

87. ASTM D 695, *Standard test method for Compressive Properties of Rigid Plastics*, in *ASTM materials standards*, ASTM Committee D-20 and D. Subcommittee, Editors. 2002.

88. Vinson, J.R. and R.L. Sierkowski, *The behaviour of structures composed of composite materials*. 1986, Dordrecht, The Netherlands: Martinus Nijhoff Publishers.

89. Jones, R.M., *Apparent Flexural Modulus and Strength of Multimodulus Materials.* Journal of Composite Materials, 1976. **10**: p. 342-351.

90. Sideridis, E. and G.A. Papadopoulos, *Short-Beam and Three-Point-Bending Tests for the study of Shear and Flexural Properties in unidirectional-Fiber- Reinforced Epoxy Composites.* Journal of Applied Polymer Science, 2003. **93**: p. 63–74.

91. Thomason, J.L., *The influence of fibre length and concentration on the properties of glass fibre reinforced polypropylene: 5. Injection moulded long and short fibre PP.* Composites: Part A, 2002. **33**: p. 1641–1652.

92. Corp., S.R.A., *COSMOS Education Edition*. 2006.

Appendices.

Appendix I

Fibre packing limits:

In order to be able to produce a model that is capable of predictions for any volume fraction it is essential to relate layer thickness to volume fraction. This will allow the number of individual layers and the volume fraction to be adjusted independently.

There is however a theoretical level for volume fraction about which the matrix will not encapsulate the reinforcement. The closest packing arrangement is the hexagonal packing of Figure A63 (a) and the square packing of Figure A63(b).

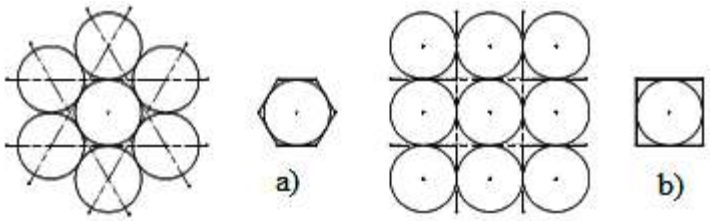

Figure A63. Reinforcement packing limits. a) Hexagonal, b) Square.

Considering the packing arrangements of both configurations the maximum theoretical values for volume fraction can be calculated as follows:

$V_f = \frac{A_f}{A_T}$, given $A_f = \pi.r^2$

$A_H = 3.464.r^2$, for hexagonal packing and $A_S = 4.r^2$ for square packing.

$$V_{fH} = \frac{A_f}{A_H} = \frac{\pi.r^2}{3.464.r^2} = \frac{\pi}{3.464} \quad \therefore \quad V_{fH} = 0.907 \approx 0.9 .$$

and $$V_{fS} = \frac{A_f}{A_S} = \frac{\pi.r^2}{4.r^2} = \frac{\pi}{4} \quad \therefore \quad V_{fS} = 0.785 \approx 0.8 .$$

Appendix II

Matrix determination:

Where n = number of layers (5, 9, 13...) then k is the number of plies (where five layers make the first ply, and four layers the second, and subsequent plies.) $n = 4k + 1$. The number of fibre and matrix layers can be determined in terms of k as $n_f = 2k$ and $n_m = 2k + 1$. The thickness of individual layers can be determined from: $a_f = \frac{V_f d}{n_f}$ and $a_m = \frac{V_m d}{n_m}$.

To determine the overall second moment of area for the composite, the fibre layers and matrix layers are considered separately. When determining the second moment of area of each individual layer the parallel axis theorem is used to transform each layers second moment around its own neutral axis to that of the beams', Figure 28. For that the distance from the beams neutral axis to that of the individual layers is needed. This distance is a function of k, and is defined as $h_f = \frac{1}{2}(2k-1)(a_m + a_f)$ and $h_m = k(a_m + a_f)$.

A similar analysis to that given in section 5.1 for the fibre layer is followed for the matrix layer. The total second moment of area for the matrix layers is $I_{mstrix} = \sum_{j-1}^{k}(I_{xxj} + Ah_{mj}{}^2)$. This can be written as $I_{matrix} = \sum_{j-1}^{k} I_{xxj} + \sum_{j-1}^{k} Ah_{mj}{}^2$.

Furthermore: $\sum_{j-1}^{k} I_{xxj} = n_m\left(\frac{ba_m{}^3}{12}\right)$. Substituting for a_m and n_m to give: $\sum_{j-1}^{k} I_{xxj} = \frac{bd^3}{12}\frac{V_m{}^3}{(2k+1)^2} = I_C\Gamma_m$ and $\sum_{j-1}^{k} Ah_{mj} = \sum_{j-1}^{k}\left(2ba_m h_{mj}{}^2\right)$.

Where a_m is constant and can be removed from the summation to give: $\sum_{j-1}^{k} Ah_{mj} = 2ba_m \sum_{j-1}^{k} h_{mj}{}^2$.

Now it can be shown that $\sum_{j-1}^{k} h_{mj}{}^2 = \frac{2(a_m + a_f)^2}{(2k+1)}\left[\frac{k}{6}(2k+1)(k+1)\right]$ and as $(a_m + a_f)^2 = d^2\left[\frac{(2k-1)(k-1)}{(2k)^2(2k+1)^2}\right]$ this gives:

$$\sum_{j-1}^{k}\left(2ba_m h_{mj}{}^2\right) = \frac{bd^3}{12}\left[4V_m\left[(2k+1)-V_m\right]^2\frac{k(k+1)}{(2k)^2(2k+1)^2}\right] = I_C\Lambda_m .$$

The total second moment of area for the matrix fraction now becomes: $I_{matrix} = \sum_{j-1}^{k} I_{xxj} + \sum_{j-1}^{k} Ah_{mj}{}^2 = I_C\Lambda_m .$

Appendix III

The following files will be found on the accompanying CD located inside the back cover.

Java runtime environment download.

Java executionable files for micro-mechanical models.

Example files for micro-mechanical models.

Source codes for micro-mechanical models.

Appendix IV

Dimensions for semi-iconic element models:

Material	V_f	Generic			Wood fibre			Glass fibre			Carbon fibre		
a_f mm		0.0250			0.0500			0.0130			0.0072		
k		1	5	10	1	5	10	1	5	10	1	5	10
n_m		3	11	21	3	11	21	3	11	21	3	11	21
	0.1												
a_m mm		0.150	0.205	0.214	0.300	0.409	0.429	0.078	0.106	0.111	0.043	0.059	0.062
d mm		0.500	2.500	5.000	1.000	5.000	10.000	0.260	1.300	2.600	0.144	0.720	1.440
L mm		8.00	40.00	80.00	16.00	80.00	160.00	4.16	20.80	41.60	2.30	11.52	23.04
b mm		2.00	10.00	20.00	4.00	20.00	40.00	1.04	5.20	10.40	0.58	2.88	5.76
	0.2												
a_m mm		0.067	0.091	0.095	0.133	0.182	0.190	0.035	0.047	0.050	0.019	0.026	0.027
d mm		0.250	1.250	2.500	0.500	2.500	5.000	0.130	0.650	1.300	0.072	0.360	0.720
L mm		4.00	20.00	40.00	8.00	40.00	80.00	2.08	10.40	20.80	1.15	5.76	11.52
b mm		1.00	5.00	10.00	2.00	10.00	20.00	0.52	2.60	5.20	0.29	1.44	2.88
	0.3												
a_m mm		0.039	0.053	0.056	0.078	0.106	0.111	0.020	0.028	0.029	0.011	0.015	0.016
d mm		0.167	0.833	1.667	0.333	1.667	3.333	0.087	0.303	0.607	0.048	0.168	0.336
L mm		2.67	13.33	26.67	5.33	26.67	53.33	1.39	4.85	9.71	0.77	2.69	5.38
b mm		0.67	3.33	6.67	1.33	6.67	13.33	0.35	1.21	2.43	0.19	0.67	1.34
	0.4												
a_m mm		0.025	0.034	0.036	0.050	0.068	0.071	0.013	0.018	0.019	0.007	0.010	0.010
d mm		0.125	0.625	1.250	0.250	0.750	1.500	0.065	0.195	0.390	0.036	0.108	0.216
L mm		2.00	10.00	20.00	4.00	12.00	24.00	1.04	3.12	6.24	0.58	1.73	3.46
b mm		0.50	2.50	5.00	1.00	3.00	6.00	0.26	0.78	1.56	0.14	0.43	0.86
	0.5												
a_m mm		0.017	0.023	0.024	0.033	0.045	0.048	0.009	0.012	0.012	0.005	0.007	0.007
d mm		0.100	0.500	1.000	0.200	0.500	1.000	0.052	0.130	0.260	0.029	0.072	0.144
L mm		1.60	8.00	16.00	3.20	8.00	16.00	0.83	2.08	4.16	0.46	1.15	2.30
b mm		0.40	2.00	4.00	0.80	2.00	4.00	0.21	0.52	1.04	0.12	0.29	0.58
	0.6												
a_m mm		0.011	0.015	0.016	0.022	0.030	0.032	0.006	0.008	0.008	0.003	0.004	0.005
d mm		0.083	0.417	0.833	0.167	0.333	0.667	0.043	0.087	0.173	0.024	0.048	0.096
L mm		1.33	6.67	13.33	2.67	5.33	10.67	0.69	1.39	2.77	0.38	0.77	1.54
b mm		0.33	1.67	3.33	0.67	1.33	2.67	0.17	0.35	0.69	0.10	0.19	0.38
	0.7												
a_m mm		0.007	0.010	0.010	0.014	0.019	0.020	0.004	0.005	0.005	0.002	0.003	0.003
d mm		0.071	0.357	0.714	0.143	0.214	0.429	0.037	0.056	0.111	0.021	0.031	0.062
L mm		1.14	5.71	11.43	2.29	3.43	6.86	0.59	0.89	1.78	0.33	0.49	0.99
b mm		0.29	1.43	2.86	0.57	0.86	1.71	0.15	0.22	0.45	0.08	0.12	0.25
	0.8												
a_m mm		0.004	0.006	0.006	0.008	0.011	0.012	0.002	0.003	0.003	0.001	0.002	0.002
d mm		0.063	0.313	0.625	0.125	0.125	0.250	0.033	0.033	0.065	0.018	0.018	0.036
L mm		1.00	5.00	10.00	2.00	2.00	4.00	0.52	0.52	1.04	0.29	0.29	0.58
b mm		0.25	1.25	2.50	0.50	0.50	1.00	0.13	0.13	0.26	0.07	0.07	0.14

Shaded values outside of acceptable parameters.

Appendix V

Semi-iconic element pre-processing and simulation data:

Material	V_f	Generic			Wood fibre			Glass fibre			Carbon fibre		
a_f mm		0.0250			0.0500			0.0130			0.0072		
k		1	5	10	1	5	10	1	5	10	1	5	10
n_m		3	11	21	3	11	21	3	11	21	3	11	21
	0.1												
a_m mm		0.150	0.205	0.214	0.300	0.409	0.429	0.078	0.106	0.111	0.043	0.059	0.062
elements		63943	193725	N/A unable to pre-process.	58093	N/A unable to pre-process.		62304	175631		35108	161045	
mesh mm		0.140	0.480		0.180			0.048	0.212	0.500	0.030	0.118	0.300
F N		0.100	0.100		0.100			0.010	0.100	1.000	0.001	0.010	0.100
y mm		0.041	0.007		0.026			0.005	0.008	Unable to sim	0.001	0.001	Unable to sim
E Gpa		6.31	7.86		4.92			10.88	12.99		15.38	20.31	
	0.2												
a_m mm		0.067	0.091	0.095	0.133	0.182	0.190	0.035	0.047	0.050	0.019	0.026	0.027
elements		57569	162573	320788	48890	161337	N/A unable to pre-process.	48133	162250	272781	49604	161462	244814
mesh mm		0.041	0.210	0.410	0.090	0.410		0.024	0.107	0.240	0.013	0.059	0.140
F N		0.100	0.100	1.000	0.100	0.100		0.010	0.100	1.000	0.001	0.010	0.100
y mm		0.022	0.005	0.027	0.034	0.006		0.006	0.010	0.048	0.001	0.001	0.006
E Gpa		23.53	19.01	19.26	7.45	7.90		15.62	19.27	20.46	19.73	26.73	29.79
	0.3												
a_m mm		0.039	0.053	0.056	0.078	0.106	0.111	0.020	0.028	0.029	0.011	0.015	0.016
elements		43907	163474	347618	36087	149984	N/A unable to pre-process.	43242	162173	272127	39992	177267	245073
mesh mm		0.030	0.140	0.270	0.060	0.290		0.016	0.071	0.160	0.009	0.039	0.090
F N		0.100	0.100	1.000	0.100	0.100		0.010	0.100	1.000	0.001	0.010	0.100
y mm		0.031	0.007	0.034	0.040	0.007		0.008	0.012	0.057	0.001	0.002	0.008
E Gpa		24.72	22.79	22.92	9.60	10.66		19.28	24.31	26.01	24.88	31.97	35.48
	0.4												
a_m mm		0.025	0.034	0.036	0.050	0.068	0.071	0.013	0.018	0.019	0.007	0.010	0.010
elements		46037	148299	295288	43147	163120	219755	42642	136880	267703	35340	148957	245427
mesh mm		0.022	0.110	0.220	0.045	0.210	0.500	0.012	0.059	0.120	0.007	0.030	0.070
F N		0.100	0.100	1.000	0.100	0.100	1.000	0.010	0.100	1.000	0.001	0.010	0.100
y mm		0.036	0.007	0.035	0.044	0.008	0.036	0.008	0.011	0.062	0.001	0.002	0.008
E Gpa		28.60	28.33	29.09	11.60	13.22	14.06	23.85	35.20	31.61	32.38	38.82	42.84

Shaded values outside of acceptable parameters.

Material	V_f	Generic			Wood fibre			Glass fibre			Carbon fibre		
a_f mm		0.0250			0.0500			0.0130			0.0072		
k		1	5	10	1	5	10	1	5	10	1	5	10
n_m		3	11	21	3	11	21	3	11	21	3	11	21
	0.5												
a_m mm		0.017	0.023	0.024	0.033	0.045	0.048	0.009	0.012	0.012	0.005	0.007	0.007
elements		41657	138444	349306	45448	163608	293210	35391	177094	245225	25944	164160	245522
mesh mm		0.018	0.090	0.160	0.035	0.170	0.350	0.009	0.042	0.100	0.006	0.024	0.045
F N		0.100	0.100	1.000	0.100	0.100	1.000	0.010	0.100	1.000	0.001	0.010	0.100
y mm		0.040	0.008	0.038	0.047	0.008	0.039	0.009	0.014	0.064	0.001	0.002	0.009
E Gpa		31.87	33.59	33.77	13.71	15.24	16.36	27.68	35.14	38.69	42.25	46.81	52.07
	0.6												
a_m mm		0.011	0.015	0.016	0.022	0.030	0.032	0.006	0.008	0.008	0.003	0.004	0.005
elements		44253	162331	319701	35349	162824	294593	29297	148735	268318	32324	162612	243133
mesh mm		0.014	0.070	0.140	0.029	0.140	0.290	0.008	0.038	0.080	0.005	0.020	0.045
F N		0.100	0.100	1.000	0.100	0.100	1.000	0.010	0.100	1.000	0.001	0.010	0.100
y mm		0.041	0.008	0.038	0.049	0.008	0.039	0.009	0.014	0.062	0.001	0.002	0.008
E Gpa		37.05	38.24	40.42	15.64	18.42	19.63	34.56	43.76	47.49	46.66	58.10	65.04
	0.7												
a_m mm		0.007	0.010	0.010	0.014	0.019	0.020	0.004	0.005	0.005	0.002	0.003	0.003
elements		33798	162729	317787	49736	161495	246408	30250	177282	245539	27500	148204	237348
mesh mm		0.013	0.060	0.120	0.024	0.120	0.270	0.007	0.024	0.070	0.004	0.018	0.040
F N		0.100	0.100	1.000	0.100	0.100	1.000	0.010	0.100	1.000	0.001	0.010	0.100
y mm		0.045	0.008	0.038	0.046	0.008	0.036	0.008	0.013	0.057	0.001	0.002	0.007
E Gpa		40.25	44.54	47.65	19.28	22.13	24.90	44.55	55.09	60.44	71.05	77.20	85.20
	0.8												
a_m mm		0.004	0.006	0.006	0.008	0.011	0.012	0.002	0.003	0.003	0.001	0.002	0.002
elements		50886	177295	346054	56033	175890	317916	41167	177009	270958	51796	161834	246965
mesh mm		0.011	0.050	0.100	0.021	0.100	0.210	0.006	0.026	0.060	0.003	0.015	0.034
F N		0.100	0.100	1.000	0.100	0.100	1.000	0.010	0.100	1.000	0.001	0.010	0.100
y mm		0.044	0.008	0.036	0.046	0.008	0.035	0.006	0.011	0.050	0.001	0.001	0.006
E Gpa		46.28	51.88	56.16	22.04	26.95	29.24	61.35	73.96	79.42	79.69	108.65	119.13

Appendix VI

Analog pre-processing and simulation data:

Element size		1.6 mm							
DOF		15657							
V_f		0.1		0.2		0.3		0.4	
		E_{Pb}	E_{PA}	E_{Pb}	E_{PA}	E_{Pb}	E_{PA}	E_{Pb}	E_{PA}
Modulus	[Mpa]	1622	895	2515	1334	3606	1907	4935	2648
Load	[N]	0.1		0.1		0.1		0.1	
Deflection	[mm]	0.0052	0.0095	0.0034	0.0063	0.0023	0.0044	0.0017	0.0032
Load	[N]	10.0		10.0		10.0		10.0	
Deflection	[mm]	0.522	0.946	0.336	0.634	0.234	0.443	0.171	0.319
E_{sim}	Mpa	7763	4281	12041	6385	17270	9134	23646	12686
V_f		0.5		0.6		0.7		0.8	
		E_{Pb}	E_{PA}	E_{Pb}	E_{PA}	E_{Pb}	E_{PA}	E_{Pb}	E_{PA}
Modulus	[Mpa]	6542	3590	8465	4768	10744	6214	13419	7962
Load	[N]	0.1		0.1		0.1		0.1	
Deflection	[mm]	0.0013	0.0024	0.0010	0.0018	0.0008	0.0014	0.0006	0.0011
Load	[N]	10.0		10.0		10.0		10.0	
Deflection	[mm]	0.129	0.235	0.097	0.177	0.079	0.136	0.063	0.106
E_{sim}	Mpa	31357	17212	41605	22858	51550	29810	64410	38227

PB at k = 1, PA at k = 1 and CA = 0.5.

Appendix VII

Processing and test Equipment:

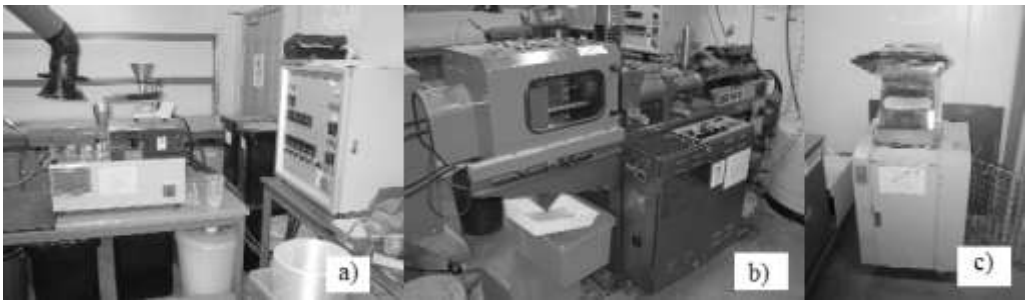

Figure A64. a) Thermo Prism TSE 16 TC twin screw extruder (TEx), b) Dr Boy 15kN Injection moulder (IM), c) Castin triblade granulator (CG).

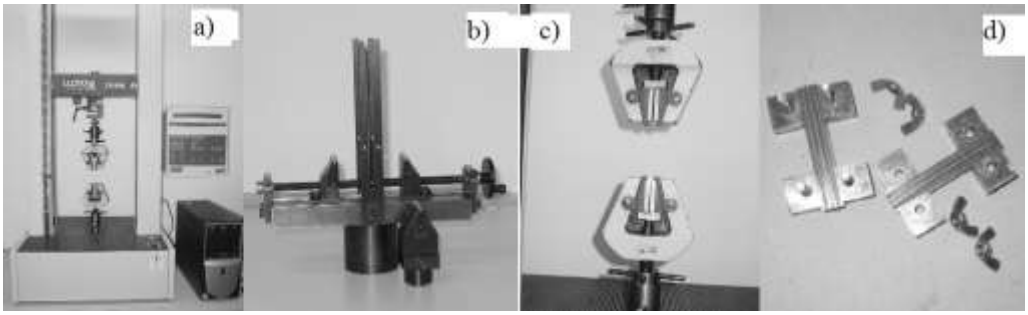

Figure A65. a) Lloyd LR30C universal testing instrument (UT) b) Three point bend apparatus, c) Tensile test grips, d) Compression support jig.

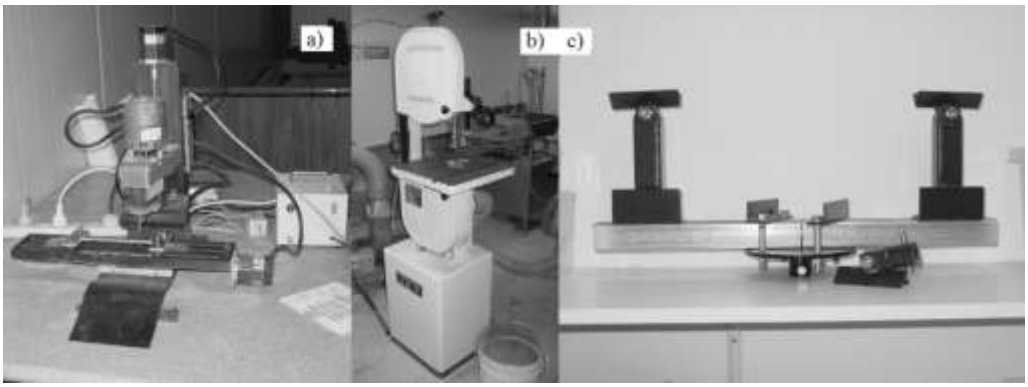

Figure A66. a) MaxNC milling machine, b) Band saw, c) Paddle-shaft bend jig.